

STATUS OF THESIS

Title of thesis

THE EFFECTS OF SILICA SAND (SiO₂) AND ZIRCONIA (ZrO₂) ON THE MECHANICAL AND THERMAL PROPERTIES OF THE PRESSURELESS SINTERED Al₂O₃-SiO₂-ZrO₂ COMPOSITE

I MEBRAHITOM ASMELASH GEBREMARIAM

hereby allow my thesis to be placed at the Information Resource Center (IRC) of Universiti Teknologi PETRONAS (UTP) with the following conditions:

1. The thesis becomes the property of UTP
2. The IRC of UTP may make copies of the thesis for academic purposes only.
3. This thesis is classified as


Confidential

Non-confidential

If this thesis is confidential, please state the reason:

The contents of the thesis will remain confidential for _____ years.

Remarks on disclosure:



Signature of Author

Permanent address: _____

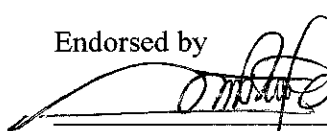
Addis Ababa University

Ethiopia

P.O.Box: 254

Date : 27/05/2013

Endorsed by



Signature of Supervisor

DR OTHMAN MAMAT
Associate Professor
Mechanical Engineering Program
UNIVERSITI TEKNOLOGI PETRONAS
Bandar Seri Iskandar, 31750 Tronoh
Perak Darul Ridzuan, Malaysia.

Name of Supervisor

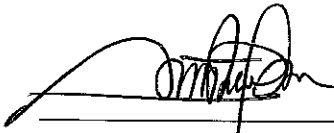
Assoc. Prof. Dr. Othman Mamat

Date : 27/5/2013


UNIVERSITI TEKNOLOGI PETRONAS
THE EFFECTS OF SILICA SAND (SiO₂) AND ZIRCONIA (ZrO₂) ON THE
MECHANICAL AND THERMAL PROPERTIES OF THE PRESSURELESS
SINTERED Al₂O₃-SiO₂-ZrO₂ COMPOSITE

by
MEBRAHITOM ASMELASH GEBREMARIAM


The undersigned certify that they have read, and recommend to the Postgraduate Studies Programme for acceptance this thesis for the fulfillment of the requirements for the degree stated.

Signature:  **DR OTHMAN MAMAT**
Associate Professor
Mechanical Engineering Programme
UNIVERSITI TEKNOLOGI PETRONAS
Bandar Seri Iskandar, 31750 Tronoh
Perak Darul Ridzuan, Malaysia.

Main Supervisor: Associate Professor Dr. Othman Mamat

Signature:  **Dr. Faiz Ahmad**
Associate Professor
Mechanical Engineering Department
Universiti Teknologi PETRONAS
Bandar Seri Iskandar, 31750 Tronoh
Perak Darul Ridzuan, Malaysia

Co-Supervisor: Associate Professor. Dr. Faiz Ahmad

Signature:  **Ir. Dr. Masri Baharom**
Head of Department/Associate Professor
Department of Mechanical Engineering
Universiti Teknologi PETRONAS
Bandar Seri Iskandar, 31750 Tronoh,
Perak Darul Ridzuan, Malaysia

Head of Department: Ir. Dr. Masri Baharom

Date: 30/5/13

THE EFFECTS OF SILICA SAND (SiO_2) AND ZIRCONIA (ZrO_2) ON THE
MECHANICAL AND THERMAL PROPERTIES OF THE PRESSURELESS
SINTERED Al_2O_3 - SiO_2 - ZrO_2 COMPOSITE

by

MEBRAHITOM ASMELASH GEBREMARIAM

A Thesis

Submitted to the Postgraduate Studies Programme

as a Requirement for the Degree of

DOCTOR OF PHILOSOPHY

MECHANICAL ENGINEERING

UNIVERSITI TEKNOLOGI PETRONAS

BANDAR SERI ISKANDAR,

PERAK

APRIL 2013

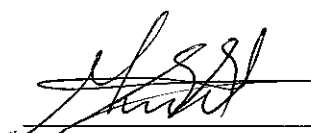
DECLARATION OF THESIS

Title of thesis THE EFFECTS OF SILICA SAND (SiO₂) AND ZIRCONIA (ZrO₂) ON THE MECHANICAL AND THERMAL PROPERTIES OF PRESSURELESS SINTERED Al₂O₃-SiO₂-ZrO₂ COMPOSITE

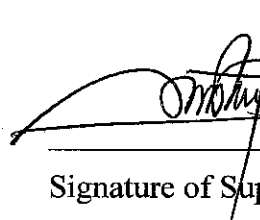
I MEBRAHITOM ASEMELASH GEBREMARIAM

hereby declare that the thesis is based on my original work except for quotations and citations which have been duly acknowledged. I also declare that it has not been previously or concurrently submitted for any other degree at UTP or other institutions.

Witnessed by



Signature of Author



DR OTHMAN MAMAT
Associate Professor
Mechanical Engineering Programme
UNIVERSITI TEKNOLOGI PETRONAS
Bandar Seri Iskandar, 3150 Tronoh
Perak Darul Ridzuan, Malaysia.

Signature of Supervisor

Permanent address: _____
Addis Ababa University, Ethiopia:
P.O.Box: 254

Name of Supervisor
Assoc. Prof. Dr. Othman Mamat

Date : 27/05/2013

Date : 27/5/2013

DEDICATION

To Fretana and my father Asmelash Gebremariam

ACKNOWLEDGEMENTS

I would like to deeply thank my supervisor Assoc. Prof. Dr Othman Mamat for his unconditional support, guidance and understanding, continuous support throughout my work. He encouraged me to investigate the topic of this work which I found it very interesting. His guidance throughout my study thought me to become an independent researcher, which may be of more value. I would like to thank also my co-supervisor Assoc. Prof. Dr. Faiz Ahmad for his support during my research work.

~~Special thanks go to Mechanical Engineering Materials laboratory technologists~~ Mr. Anuar, Mr. Mahfuz, Mr. Irwan, and Mr. Paris and Mr. Faisel for their help in executing my experiments. I also thank Universiti Teknologi PETRONAS for the financial support during my whole study through the Graduate Assistantship (GA) scheme.

I am indebted to my friends in UTP for their continuous support and the brainstorming discussions which I strongly believe that what I have learned from them during the study period is worthy to articulate for problem solving.

Finally, my greatest thanks go to my parents who shaped me with their never ending patience.

Mebrahitom Asmelash

April, 2013.

ABSTRACT

The research work presents an investigation on the pressureless sintering, microstructure and mechanical properties of three component ceramic composite material consisting of alumina, silica and zirconia for structural applications. The effect of each component composition on the physical and mechanical properties was studied. Mechanical properties including fracture toughness, flexural strength, and hardness at ambient temperature were determined and thermal shock resistance properties up to 950°C were also investigated. These properties were compared among the monolithic Al₂O₃, Al₂O₃-ZrO₂ (AZ) and Al₂O₃-SiO₂-ZrO₂ (ASZ) composites. The microstructure of sintered, thermal shocked and fractured surface states was investigated using FESEM and AFM. A three phase microstructure was adopted with a composition of 70% by weight of alumina, 10% by weight of silica and 20% by weight of zirconia. The reinforcements of the SiO₂ and ZrO₂ contributed in improving the mechanical properties of the composite. The sintered composite was mainly consisted of a highly crystallized form of alumina, mullite and zirconia phases. The fracture toughness of the composites were measured using Indentation Fracture (IF) method, and an average value of 0.86 MPa.m^{1/2}, 1.75 MPa.m^{1/2}, and 2.39 MPa.m^{1/2} for the Al₂O₃, AZ and ASZ composites respectively. A significant increase in the toughness was realized by the inclusion of the ZrO₂ and SiO₂ oxides. The inclusions of the reinforcement underwent phase transformation under stress as well as by making an interlocking three phase composite. It was observed that the fracture mode was mainly intercrystalline for the sintered Al₂O₃ and AZ composite but for the ASZ, it was mainly transcrystalline. In addition to the formation of mullite due to the reaction of silica and alumina, silica was shown to act as a transient liquid phase sintering aid that reduced the sintering temperature of the Al₂O₃-SiO₂-ZrO₂ composite to 1450~1500°C from 1650~1700°C. Dilatometric measurements show that SiO₂ additions increased the densification rate during the intermediate stage relative to the

monolithic alumina samples. The ASZ composites possessed the highest thermal shock resistance than the monolithic alumina and AZ, with a critical temperature difference (ΔT_C) being 430°C. Such superior thermal shock resistance was attributed to the improvement of the fracture toughness by three components composite system and the availability of mullite (silica) phase as reinforcement. The main conclusion from the results in this work indicated that the identified optimum mix of Al_2O_3 matrix with SiO_2 and ZrO_2 reinforcement show an improved room temperature mechanical and the thermal shock resistance than the monolithic Al_2O_3 and binary Al_2O_3 - ZrO_2 composites.

ABSTRAK

Kerja penyelidikan membentangkan satu siasatan di tanpa tekanan beban pensinteran, mikrostruktur dan sifat-sifat mekanikal tiga komponenbahan komposit seramik mengandungi alumina, silica dan zirkonia untuk permohonan struktur. Dengan satu peningkatan dalam jumlah kedua dan fasa ketiga, kadar pemecahan menjadi lebih stabil, dan menolak membiakkanrekahan semasa permohonan kuasa luaran. Sifat-sifat mekanikal termasuk keliatan patah, kekuatan lenturan, dan kekerasan di suhu ambient telah ditentukan dan ciri-ciri rintangan kejutan haba sehingga 950°C juga disiasat. Ciri-ciri ini telahdipertandingkan antara Al_2O_3 monolitik, $\text{Al}_2\text{O}_3\text{-ZrO}_2$ (AZ) dan $\text{Al}_2\text{O}_3\text{-SiO}_2\text{-ZrO}_2$ (ASZ) komposit. Mikrostruktur tersinter, terma terkejut dan mematahkan negeri-negeri permukaan disiasat menggunakan FESEM and AFM.

Tiga fasa telah diterima dengan satu komposisi 70% oleh beratalumina, 10% oleh berat silica dan 20% oleh berat zirkonia. Pengukuhan SiO_2 and ZrO_2 menyumbang dalam meningkatkansifat-sifat mekanikal rencam. Tersinter rencam terutamanya mengandungi bentuk yang amat terhablur alumina, mulit dan fasa-fasa zirkonia. Keliatan patah komposit diukur menggunakan Indentation Fracture (IF) kaedah, dan satu nilai purata $0.86 \text{ MPa}\cdot\text{m}^{1/2}$, $1.75 \text{ MPa}\cdot\text{m}^{1/2}$, dan $2.39 \text{ MPa}\cdot\text{m}^{1/2}$ untuk Al_2O_3 , komposit AZ and ASZ masing-masing. Satu kenaikan signifikan dalam keliatan telah disedari oleh kemasukan ZrO_2 and SiO_2 oksida. Memasukkan peneguhan menjalani penjelmaan fasa di bawah tekanan sertadengan membuat satu saling mengunci tiga fasa. Ia adadiperhatikan bahawa ragam patah terutamanya antara habluran untuk tersinter rencam Al_2O_3 and AZ kecuali ASZ, ia terutamanya transcrystalline. Tambahan kepada pembentukan mulit disebabkan tindak balas silica dan alumina, silica telah ditunjukkan melakonkan satu fasa cecair fana pensinteran bantuan yang mengurangkan pensinteran suhu rencam $\text{Al}_2\text{O}_3\text{-SiO}_2\text{-ZrO}_2$ kepada 1450~1500°C. Ukuran-ukuran Dilatometric menunjukkan bahawa pencampuran-pencampuran SiO_2 menambah kadar penumpatan semasa peringkat pertengahan relatif kepada contoh-

contoh alumina monolitik. ASZ komposit mempunyai rintangan kejutan haba tertinggi aripada alumina monolitik dan AZ, dengan perbezaan suhu genting menjadi 430°C. Rintangan kejutan haba hebat sedemikian ada dianggap berpunca daripada peningkatan keliatan patah oleh penghalusan bijian dan ketersediaan fasa mulit sebagai peneguhan. Kesimpulan utama dari keputusan-keputusan dalam tugas ini menunjukkan bahawa penghalusan bijian matriks Al_2O_3 disebabkan tiga komponen ada satu kaedah berpotensi untuk meningkatkan suhu bilik mekanikal dan rintangan kejutan haba alumina berpangkalan komposit.

In compliance with the terms of the Copyright Act 1987 and the IP Policy of the university, the copyright of this thesis has been reassigned by the author to the legal entity of the university,

Institute of Technology PETRONAS Sdn Bhd.

Due acknowledgement shall always be made of the use of any material contained in, or derived from, this thesis.

© Mebrahitom Asmelash Gebremariam, 2013

Institute of Technology PETRONAS Sdn Bhd

All rights reserved.

TABLE OF CONTENT

ABSTRACT.....	vii
ABSTRAK.....	ix
LIST OF FIGURES.....	xvi
LIST OF TABLES.....	xix
LIST OF ABRIVATIONS.....	XX
CHAPTER 1 INTRODUCTION.....	1
1.1 Over view.....	1
1.2 Background.....	1
1.3 Problem statement.....	6
1.4 Objective of the research.....	8
1.5 Scope of the research.....	8
1.6 Organization of the thesis.....	9
CHAPTER 2 LITRATURE REVIEW.....	11
2.1 Overview.....	11
2.2 Alumina, silica and zirconia.....	11
2.2.1 Alumina.....	11
2.2.2 Silica.....	12
2.2.3 Zirconia.....	13
2.2.4 Mullite.....	14
2.3 Particle characterization and selection.....	15
2.4 Fundamental of sintering.....	17
2.4.1 Sintering mechanisms.....	20
2.4.2 Theoretical analysis of sintering.....	22
2.5 Pressureless sintering of ASZ systems.....	26
2.5.1 Alumina - Zirconia (AZ) composites.....	27
2.5.2 Alumina–Silica (AS).....	27
2.5.3 Zirconia-Silica (ZS).....	28
2.5.4 Mullite-Zirconia (MZ).....	28
2.5.5 Alumina-Silica-Zirconia (ASZ) composites.....	29
2.6 Toughening of ceramics.....	31

2.6.1 Toughening mechanisms in ceramic composite.....	33
2.6.1.1 Toughening by crack propagation	37
2.6.1.2 Crack shielding mechanism	38
2.6.2 Crack bridging.....	43
2.7 High temperature properties of ceramic composites	43
Summary.....	45
CHAPTER 3 METHODOLOGY	47
3.1 Overview.....	47
3.2 Methodology.....	47
3.3 Sample preparation and material characterization.....	50
3.3.1 Sample preparation.....	50
3.3.2 Characterization and Testing.....	56
3.3.2.1 Density measurement.....	56
3.3.2.2 Hardness Measurement.....	57
3.3.2.3 Fracture Toughness Measurement.....	58
3.3.2.4 Flexural Strength Measurement.....	59
3.3.2.5 X-Ray Floresence analysis (XRF)	61
3.3.2.6 FESEM Characterization	61
3.3.2.7 Atomic Force Microscope (AFM)	62
3.3.2.8 XRD Characterization of the Sintered sample.....	63
3.3.2.9 Dilatometry Study	64
3.3.2.10 Thermal Shock Resistance.....	65
Summary.....	68
CHAPTER 4 RESULTS AND DISCUSSION	69
4.1 Overview.....	69
4.2 Pressureless Sintering and Characterization of Al ₂ O ₃ -SiO ₂ -ZrO ₂ composite system.....	70
4.2.1 Powder characterization	71
4.2.1.1 Particle Size Analysis	71
4.2.1.2 Particle shape	74
4.2.1.3 Effect of Compaction Pressure on the Green density	77
4.2.1.4 Effect of Zirconia on the Densification of ASZ composite	78

4.2.1.5 Effect of SiO ₂ on the Densification of ASZ Composite.....	79
4.2.2 Microstructure and Phase Composition of Sintered Samples	80
4.2.2.1 Microstructure ASZ composite.....	81
4.2.2.2 X-Ray Diffraction of the ASZ Composite	82
4.2.2.3 Effect of Sintering Temperature on the microstructural development of the ASZ Composite.....	83
4.2.2.4 Effect of ZrO ₂ on the Mechanical Properties of the sintered Samples	86
Summary.....	88
4.3 Dilatometry Study of the ASZ Composite system	90
4.3.1 Overview	90
4.3.2 Shrinkage and the Phase change Study	90
Summary	96
4.4 Mechanical Properties Comparison of monolithic Alumina, AZ and ASZ Composites	98
4.4.1 Overview	98
4.4.2 Hardness, Fracture Toughness and Flexural Strength of the Sintered ASZ Composites	98
4.4.2.1 Fracture Behavior and Toughening Mechanisms of the ASZ Composite	106
4.4.2.2 Cracking behavior of the Monolithic and ASZ composites...	108
4.4.2.3 Toughening Mechanism in the ASZ Composite.....	111
Summary	116
4.5 The Thermal Shock Resistance of the Al ₂ O ₃ -SiO ₂ -ZrO ₂ (ASZ) Composite.	117
4.5.1 Overview	117
4.5.2 Effect of thermal Shock on the Mechanical properties of Al ₂ O ₃ - SiO ₂ -ZrO ₂ Composite	117
4.5.3 Microstructure change during the Thermal shock Test.....	122
Summary	124
CHAPTER 5 CONCLUSION AND RECOMMENDATIONS	125
5.1 Conclusions	125
5.2 Recommendations.....	127

REFERENCES	128
PUBLICATIONS DURINNG THE RESEARCH WORK	142

LIST OF FIGURES

Figure 1.1: Binary vs ternary component systems	7
Figure 2.1: Schematic diagram to show the three forms of silica.....	13
Figure 2.2: Structure of (a) Tetragonal and (b) cubic zirconia	14
Figure 2.3: Alumina–silica phase diagram showing the phase stability	15
Figure 2.4: SEM micrograph of alumina powder	17
Figure 2.5: Linear shrinkage versus sintering temperature	18
Figure 2.6: Schematic representation of neck formation during solid sintering due to (a). Powder compaction (b). Neck growth (c). Neck growth accompanied by densification	19
Figure 2.7: The possible mechanism contributing to sintering process: VD-Volume diffusion, GB- grain boundary diffusion, SD- surface diffusion, PF- plastic flow diffusion, E-C- Evaporation condensation flow	22
Figure 2.8: Schematic plot of three stage of liquid phase sintering	25
Figure 2.9: Fundamental mode of crack propagation	35
Figure 2.10: Schematic illustration of mutual competition between intrinsic mechanisms of damage/crack advance and extrinsic mechanisms of crack-tip shielding involved in crack growth	36
Figure 2.11: Toughening mechanisms.....	37
Figure 2.12: Transformation toughening through the addition of a second phase. Region (a) indicates the process zone around the crack tip in which second phase particle undergo dilation transformation and region (b) the resultant zone of transformed particles left in the crack wake.....	40
Figure 2.13: Mechanism for forming particle in bridging particles in the wake of a crack	43
Figure 3.1: Research methodology adapted in this research.....	49
Figure 3.2: Weighing precision balance	53
Figure 3.3: Ball Mill (US STONEWARE, 764 AVM).....	53
Figure 3.4: Hydraulic Autopallet Press Machine.....	54
Figure 3.5: Carbolite sintering alumina tube furnace setup used for the study	55

Figure 3.6: Sintering schedule for the composite preparation	55
Figure 3.7: Schematic crack generated by Vicker's Indenter.	58
Figure 3.8: Experimental set up for the flexural strength of the sintered samples	60
Figure 3.9: FESEM used for the research.....	62
Figure 3.10: AFM (SII Nano Technology Unit, Nano Navi (e-sweep)) used for the research.....	63
Figure 3.11: XRD-Bruker AXS D8 Advance	64
Figure 3.12: Dilatometer in horizontal configuration used in the study (SIRIM Berhad Malaysia).....	65
Figure 3.13: Water quenching set up for thermal shock resistance test.....	67
Figure 4.1: Particle size distribution of (a) silica sand (b) alumina (c) zirconia (d) as- milled $\text{Al}_2\text{O}_3\text{-SiO}_2\text{-ZrO}_2$ composition.....	73
Figure 4.2: FESEM micrograph of the initial powders (a) alumina (b) Silica (c) zirconia.....	75
Figure 4.3: FESEM micrograph of particles morphology appearance of $\text{Al}_2\text{O}_3\text{-SiO}_2\text{-ZrO}_2$ (a) non milled powder mixture (heterogeneous) (b) milled powder (homogenous) particles morphology.....	76
Figure 4.4: Green density of the powder plotted against compaction pressure	77
Figure 4.5: Failures in compacted samples when the pressure is more than 500 MPa.	78
Figure 4.6: Densification trend with respect to the zirconia composition	79
Figure 4.7: Densification trend with respect to the silica composition.....	80
Figure 4.8: FESEM microstructure examination of the sintered sample at different magnification.....	81
Figure 4.9: AFM micrograph of the ASZ composite and grain size measurement	82
Figure 4.10: X-Ray diffraction pattern of the sintered A-10S-20Z sample	83
Figure 4.11: FESEM micrograph of the grind and polished ASZ specimen sintered at (a). 1450°C (b). 1300°C (c). 1200°C (d). 1000°C	85
Figure 4.12: X- ray Diffraction pattern of the ASZ sample sintered at different sintering temperature	86
Figure 4.13: Flexural strength and fracture toughness with respect the ZrO_2 composition.....	87

Figure 4.14: Effect of ZrO ₂ weight percentage on the micro hardness of the ASZ sample	88
Figure 4.15: Dilatometric plot of monolithic Al ₂ O ₃	92
Figure 4.16: Dilatometric plot of sample 2 (10% wt. SiO ₂)	93
Figure 4.17: Dilatometric plot of sample 3 (10% wt SiO ₂ + 10%wt. ZrO ₂).	94
Figure 4.18: Phase diagram for the Alumina- Zirconia system.	95
Figure 4.19: SEM + EDS images of the sintered Al ₂ O ₃ -10SiO ₂ -10ZrO ₂ composite ..	96
Figure 4.20: Indent to determine the vicker's hardness of the samples.....	99
Figure 4.21: Micrograph showing the indentation cracks of the ASZ samples.....	100
Figure 4.22: FESEM micrographs and EDS spot scan of (a) A-20Z and (b) A-10S-20Z composites	105
Figure 4.23: FESEM micrograph of the polished surface for the sintered ceramic corresponding EDX line-scan across the adjacent grains:	107
Figure 4.24: Load-displacement curve for (a). monolithic Al ₂ O ₃ and.....	109
Figure 4.25: FESEM micrographs of the fractured surfaces of (a) monolithic alumina (b) Al ₂ O ₃ - ZrO ₂ and (c) Al ₂ O ₃ -SiO ₂ -ZrO ₂	110
Figure 4.26: FESEM micrograph of the fractured surfaces of ASZ composite.....	112
Figure 4.27: FESEM micrographs showing crack deflection and bridging by ZrO ₂ and mullite particles in ASZ composite: (a) deflection and bridging by ZrO ₂ (b) deflection and bridging by mullite (c) EDS line scan at point along A	113
Figure 4.28: Flexural strength versus temperature difference (ΔT) for	119
Figure 4.29: Micro indentation of the Al ₂ O ₃ -10SiO ₂ - 20ZrO ₂ after series of thermal shock cycles (a) 4 th cycle (b) 5 th cycle (c) 6 th cycle (d). 7 th cycle.....	121
Figure 4.30: FESEM micrographs of thermal shock-induced crack propagation on fractured surfaces at the 6th cycle: (a ₁) Al ₂ O ₃ (a ₂) Al ₂ O ₃ (b) A-20Z (c). A-10S-20Z	123

LIST OF TABLES

Table 2.1: Alumina, Silica, zirconia and mullite room temperature engineering properties	12
Table 2.2: Powder characteristics that have significant influence on ceramics	16
Table 2.3: Sintering mechanisms in polycrystalline and amorphous materials	21
Table 2.4: Exponents of scaling laws	23
Table 2.5: molecular electronegativities of various compounds and partial charges on the ions	30
Table 3.1: composition of alumina, silica and zirconia used in the study	51
Table 3.2: Composition of the powder mix of the composite samples used in the study	52
Table 3.3: The composition of samples showing the varying concentration of ZrO ₂ to study the effect of zirconia concentration.....	52
Table 4.1: Properties of monolithic Al ₂ O ₃ and Al ₂ O ₃ -10SiO ₂ -20ZrO ₂ composite ...	101

LIST OF ABRIVATIONS

ASZ	$\text{Al}_2\text{O}_3\text{-SiO}_2\text{-ZrO}_2$
AZ	$\text{Al}_2\text{O}_3\text{-ZrO}_2$
AFM	Atomic Force Microscope
ΔTC	Critical temperature difference
EDS	energy dispersive spectroscopy
FESEM	Field emission scanning electron microscopy
IF	Indentation Fracture
MZ	Mullite-Zirconia
PVA	Polyvinyl alcohol
PDF.	Powder Diffraction File
PSZ	Partially stabilized zirconia
MTS	Universal testing machine
Hv	Vickers hardness
XRD	X-ray diffraction
XRF	X-Ray Florescence
ZDC	Zirconia dispersed ceramics
ZTA	Zirconia toughened alumina

CHAPTER 1

INTRODUCTION

1.1 Over view

Various processing procedures and techniques as well as material combinations have been studied over the years to potentially improve the mechanical properties, toughness and mechanisms of ceramic composite materials. In this introduction part of the research, the background and state of the art in the ceramic composite research that motivated the study was briefly discussed. Problem statement and objectives were developed based on the issues and the need from the technological advancements to fill the gap. At the end of the chapter, organization and content of each chapter is explained to help the readers to go through the dissertation more easily.

1.2 Background

Since the 20th century, the researches in the development of materials have now produced almost every possible combination of metal alloys and the capabilities of those alloys are fairly well known and exploited. The demand of industries for tailor made, more efficient, less costly material system continues today. For example, the operating temperature ceramic materials can withstand is 1400°C which is far exceeding to those of conventional metallic alloys; the bulk material temperature of a heat exchanger made of carbon steel should not exceed 425°C [1]. Similarly, the maximum working temperature for a heat exchanger manufactured from stainless steel is 650°C. The other example is that the need for greater efficiency in gas turbine and automobile engines has required an increase in their working temperatures. It is now generally agreed that metals used for some of the critical parts of those parts are reaching the limit of thermal shock resistance, oxidation and hot corrosion. Such

components include turbine blades, inlet nozzles, seals, bearings and turbochargers with typical working temperatures starting from around 650°C for industrial and marine engines and rising to approximately 1300°C for high performance aeroengines [2-7]. The use of ceramics composites in turbines should enable the operating temperature to be raised to 1350°C - 1370°C, and give better specific power [8, 9]. The components should also be more corrosion, thermal shock and creep resistant. Other advantages might include lower costs compared with nickel and cobalt alloys and the ability to use cheaper lower grade fuel oil than used with these alloys. The main reasons for the limited number of applications of ceramics in turbines to date are their brittleness, low thermal shock resistance and difficulty in fabrication.

These days, as the technological advancements are ever increasing, the use of metal based systems is surpassing the limit. The trend is demanding for new materials capable of operating under higher temperature, high speed, longer life and lower maintenance and operating costs which make industries competitive. Metals have been the most available for material development due their unique properties like ductility, tensile strength, abundance, simple chemistry, relatively low cost of production and very easy for the forming and joining processes. By contrast ceramics due to their brittleness, having more complex internal structure and requiring advanced processing technology and equipment to produce, they are performing best when combined with other ceramics, metals and polymers in structural areas. This combination make possible for the production of large and complex structures used to replace the advanced materials in area for example, in space shuttle, car engines and turbines [10, 11]. But the application of ceramics in many structural and functional applications is limited by their relatively low fracture toughness and difficulty in machining complex structures from these high strength materials.

Oxide ceramics such as Al_2O_3 , SiO_2 , ZrO_2 , TiO_2 , Cr_2O_2 , and T_2O_3 are commonly used materials owing to ease of fabrication and their stability at high temperature compared with those of nitrides, sulphides and borides. They also have advanced technological applications due to their high hardness, resistance to corrosion and high dynamic modulus [5, 6]. The system of ceramic composite materials consisting of Al_2O_3 , SiO_2 and ZrO_2 is the topic of this research owing to the high hardness,

oxidation resistance and structural application in the industry. Therefore, motivation exists to involve in this ceramic composite development and improvement of its mechanical properties and toughening mechanisms in the alumina matrix which ultimately affecting the material's performance.

Recently, alumina based ceramic tool material is one of the most widely used in structural applications [4, 12-15]. The focus of researches during the past years on the alumina based ceramic structural materials was on the addition of one or several of the reinforcement phases, such as TiC, TiN, TiB₂, (W,Ti)C, Ti(C,N), ZrO₂, SiCP, SiCW, etc. into Al₂O₃ matrix [5, 7, 10, 11, 16, 17]. The development of Al₂O₃-ZrO₂ is the most researched and it has been applied to a variety of areas like cutting tool, engine parts, bone replacements and others. Toughening alumina ceramics by dispersing zirconia particles in the matrix has been actively researched for the last more than three decades. There are reports that the addition of a small amount (1000 to 2000 ppm) of zirconia into alumina as a sintering aid allowed the formation of a solid solution which promoted the densification processes by the introduction of lattice defects [12, 18, 19]. In contrast, the microstructural studies of zirconia toughened alumina (ZTA) showed the presence of the two distinct phases, which do not react with each other to form a solid solution. The toughening of alumina by dispersing zirconia particles was first encouraged by the development of the partially stabilized zirconia (PSZ). The presence of zirconia grains in the alumina matrix as a discrete second phase enable the former to behave in an intrinsic manner, that is, to undergo the tetragonal to monoclinic transformation or to be retained as the metastable tetragonal form during cooling of the composites from the fabrication temperatures. It was the volume expansion and shear strain associated with the tetragonal to monoclinic (t→m) transformation that results in toughening mechanisms in these composites, including stress induced transformation toughening, microcrack toughening, compressive surface stresses and crack deflection. One way or another, improvement of the mechanical properties such as flexural strength and fracture toughness is the main theme of all research to be applied in the structural application.

A variety of approaches have been used to enhance the fracture toughness and resistance to fracture of monolithic ceramics. The essential idea behind all toughening

mechanisms is to increase the energy needed for crack propagation, that is G_{IC} , in Equation 1 as the basic approaches are crack deflection, crack bridging and transformation toughening [20-22].

$$G_{IC} = \frac{(1-\nu)^2 K_{IC}^2}{E} \quad (1)$$

Where ν is poisson ratio, E is Young's Modulus and K_{IC} is Fracture toughness

Although there has been considerable interest for the past three decades on research of mechanisms of ZrO_2 in the toughening of ceramics e.g zirconia toughened alumina, a technically clear and explanatory finding has started to emerge after 1995. Grain refinement, microcracking and dynamic t-m transformation were the main toughening factors in the $Al_2O_3 + ZrO_2$ and other alumina based composites. Recently, several studies on the systems mullite – ZrO_2 and cordierite – ZrO_2 have shown that fine ZrO_2 dispersions in a ceramic matrix can also affect the sinterability and considerably improve the mechanical properties of the composite [7, 12, 23, 24].

Most available studies in literature are mainly concentrated on the toughening behavior of the composites containing only one toughening reinforcement [4, 8, 12, 23, 25]. Unfortunately many of the binary ceramic composite systems have shown limitations in terms of wide applicability and reliability of the materials produced. The improved mechanical properties have shown significant degradation. For this reason, three component ceramic composite systems are receiving great research interest.

Regarding the processing method, pressure assisted sintering, reaction sintering, reaction bonding, liquid phase sintering spark plasma reaction sintering and chemical processes were the common routes to produce a dense zirconia toughened ceramics with alumina matrix [6]. Based on the simplicity and the potential technical applications, focus is placed on pressureless reaction sintering as an alternative process in the fabrication of the tri-component composite. This is because it is a more affordable ceramic processing technology than the other alternative powder processing techniques like Hot Isostatic pressing (HIP) and requires less preparation of the components (e.g., no protective container and set ups for pressureless sintering)

In addition to that, no expensive equipment is necessary, and only a few items are required for fabrication. The only material necessities are material powders that form the basis of the composite material system. These materials are mixed together in various concentrations to develop the desired composites. Recently there are a number of high density ceramic composites produced using pressureless sintering. Tuan et al. [15] developed a $\text{Al}_2\text{O}_3\text{-ZrO}_2\text{-Ni}$ composite using pressureless sintering and improved the strength by 40 % of the monolithic alumina. They used a temperature of 1700°C for sintering. In this research, the pressureless sintering is considered as an inexpensive route for producing $\text{Al}_2\text{O}_3\text{-SiO}_2\text{-ZrO}_2$ ceramics containing dispersed zirconia and mullite grains after reaction with enhanced mechanical properties. Two concepts are considered in this sintering process, namely, (i) The components are homogeneously mixed and subsequently heated at a suitable temperature where sintering and reaction take place; and (ii) During heating of a transitory liquid phase is evolved which enhances sintering and/or reaction at lower temperature.

On the other hand, use of additives as a sintering aid is often reported to increase the densification kinetics and to limit the grain growth. It also could depress the temperature of the composite system via by reducing the corresponding activation energy [4]. However, no in depth study has been reported so far in literature on the mechanism through which the silica sand effectively aids the sintering and toughening effect in the $\text{Al}_2\text{O}_3\text{-SiO}_2\text{-ZrO}_2$ composite. According to the phase diagram of the $\text{Al}_2\text{O}_3\text{-SiO}_2$, the secondary intergranular phase created is mainly composed of mullite when the percentage of silica exceeds certain value due to the reaction between alumina and silica. The formation of intergranular phases could play a positive role by inhibiting the grain growth process and improve the toughness and mechanical properties of the composite system.

The continued improvements in efficiency of high temperature mechanical components depend on the improved materials and on design that may fit for the specific working conditions. Ceramic composite materials are mainly designed for the application of high temperature working conditions. The demand of ceramic materials for high temperature structural application is increasing due to the high temperature

resistance and good mechanical strength at high temperatures. However, when they are subjected to sudden change of temperature (thermal shock) or repetitive cycling of temperatures (thermal fatigue), the applicability is limited. In areas where the thermal system is varying, the change in temperature exceeds the critical temperature difference (ΔTC) of the material; thermal tensile stress will be generated in the material due to temperature gradient that exceeds its actual tensile strength resulting in failure of the material. In this work, the effect of the tri-component composite system on the thermal shock resistance will be studied by comparing the monolithic alumina, $Al_2O_3-ZrO_2$ (AZ) and $Al_2O_3-SiO_2-ZrO_2$ (ASZ) composites fabricated.

The work presented here is based on the properties of the $Al_2O_3-SiO_2-ZrO_2$ system when using silicon oxide (silica sand) as sintering aid with x level $0 < x < 30$ and ZrO_2 with y level 5-25 wt.% (weight (wt) percentage), to compare the properties of both low and high x and y material with each other. The advantages of the silica sand in the $Al_2O_3-ZrO_2$ system include the possibility of (a), easy sintering due to the low ternary oxide eutectic temperature giving low viscosities of the liquid phase between $1200-1650^\circ C$ and (b) crystallizing the interpenetrating glass to more refractory crystalline phases e. g. mullite which is hard and has a high decomposition temperature and was once regarded as a structural ceramic in its own right.

1.3 Problem statement

Ceramic materials are very attractive and known to have very important properties. When compared to metals and polymers, they generally have high melting point high strength, hardness, wear resistance and chemical stability. Unfortunately the application of ceramics in many structural and functional applications is limited because of their low toughness and difficulty in machining complex structures from the high strength materials. Al_2O_3 based ceramic composites are an improved materials compared to the monolithic ceramics in many aspects of the mechanical properties. Significant advancement have been made to improve the mechanical properties of the $Al_2O_3-ZrO_2$ composite through a number of methods such as using pressure assisted sintering (HIPing), particle refinement (use of nano particles) and

chemical processes which are very expensive in the set up of the process. There were also toughness improvements thorough the development of ternary composite $\text{Al}_2\text{O}_3\text{-ZrO}_2$ by the addition of metallic additives such as Ti, and cobalt. Unfortunately, many of the composites developed have shown early significant degradation in the strength and toughness when operated on room temperature and thermal shock environments due to the metallic inclusions [26, 27]. This has led interest in developing a tri-component oxide ceramic composite to improve the mechanical properties. The research investigates the improvement of the mechanical properties of the composites by developing three component oxide ceramic system using a pressureless sintering route. Selection of material which helps in lowering the sintering temperature of the composite is as equal important as improving the mechanical properties. The materials selected for this research are representatives of ionic and covalently bonded compounds both of which have a high potential use as high temperature structural component. The interest of this research is to develop $\text{Al}_2\text{O}_3\text{-SiO}_2\text{-ZrO}_2$ composite using a pressureless sintering powder processing route and study the mechanical properties and toughening mechanism. The influence of zirconia and silica on the microstructure and mechanical properties of alumina matrix ceramics material was analyzed to fill the research gap.

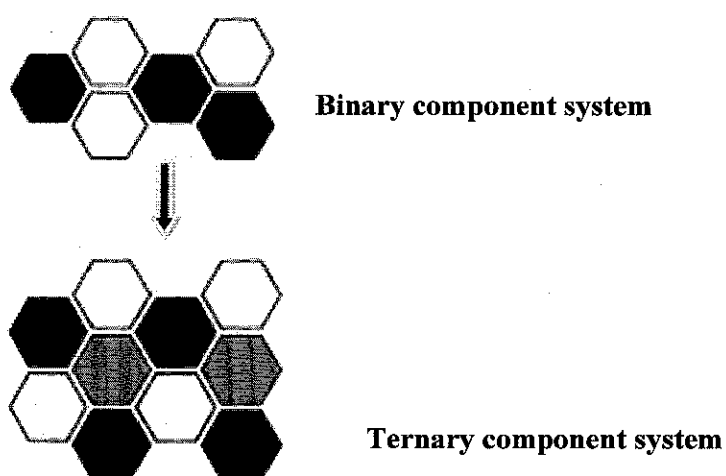


Figure 1.1: Binary vs ternary component systems

Therefore, with an increase in the amount of the second and third components, the cracking rate becomes more stable, indicating that the tri-component microstructure

(Figure 1.1) helps to limit grain growth. This research investigates the possibility of using Al_2O_3 matrix dispersed with SiO_2 (silica sand) and ZrO_2 to develop tougher ASZ composite.

1.4 Objective of the research

The main objective of the research has been to develop a three-component Al_2O_3 - SiO_2 - ZrO_2 (ASZ) composite using pressureless sintering and characterize mechanical properties.

Along with the main objective, the following specific tasks were to be accomplished:

- i. Determine the compositional mix of the composite which resulted in maximum physical and mechanical properties.
- ii. Study the effect of silica and zirconia on the physical and mechanical properties of the composite.
- iii. Investigate the pressureless sintering mechanism of the composite
- iv. Investigate the effect of SiO_2 (silica sand) in the densification of the ASZ composite
- v. Characterize the physical, mechanical and thermal properties of the developed composite materials.

1.5 Scope of the research

The research work developed the three component particulate ceramic composite using a pressureless sintering powder processing route. The starting powders were Al_2O_3 , SiO_2 , and ZrO_2 ceramics which both of have a high potential use as high temperature structural component. The SiO_2 powder was produced in the laboratory by a dry ball milling process from a locally silica sand found around Tronoh, Perak Malaysia where as the other two components were commercially available in the laboratory. Even though there were fractions of impurities in the component particles

the effect due to the impurities on the property of the composite was out of the scope of this research.

The effect of reinforcing the alumina matrix with silica and zirconia particles was investigated and the resulting mechanical properties were measured. The effect of silica on the behavior of phase formation during $\text{Al}_2\text{O}_3\text{-SiO}_2\text{-ZrO}_2$ sintering was also studied using dilatometer. It is one of the most powerful techniques used in this research to study the shrinkage behavior in the sintering process, because it permits the real time monitoring of the evolution of transformations in terms of dimensional changes occurring in the sample by application of a thermal cycle [28-30].

Mechanical reliability and long time use in extreme environments is a key issue in ceramic based composites for the ultimate use in specific applications. In order to investigate the behavior of the composite, several experiments, characterization and analytical works have been done. Room temperature mechanical tests such as flexural strength, fracture toughness and hardness tests have been carried out. Microstructural study like FESEM, EDX, and XRD results were the main parameters to investigate internal behavior of the material produced. High temperature applicability and the reliability tests were also done by studying the thermal shock resistant behaviour of the tri-component composite. Water quenching method according to the ASTM (C525-04 (2009) standard procedures were used to study the thermal shock behavior of the composite.

1.6 Organization of the thesis

The thesis is organized according to the following scheme.

Chapter 1 (the current chapter) is the introduction part discussing with the background to the research topic and shows the main issues in the development of three component ceramic composite. The problem statement has been elaborated followed by the objective of the research.

Chapter 2 reviews the theoretical framework of the research area through literature survey on the development of the oxide ceramic composites and the

processing. It starts with the study of the properties of the component oxide ceramics which build up the composite. The ceramic processing was also dealt in depth and it has been discussed the research works related topics regarding the findings that has been achieved. The fundamental concept of pressureless sintering and the factors which affects the process has been discussed. It has been reviewed the factors which affect the densification of the resulting composite and practices to improve the performance of the sintered part. Toughening mechanisms of binary and some other ternary systems previously developed composite were also surveyed in depth.

Chapter 3 is the sample preparation and material characterization part where the different parameters which the researcher is going to analyze. The equipments needed and the procedures to be followed have been discussed. The powder preparation, microstructural characterization techniques and methods (equations) to determine the mechanical properties of the resulted composites were discussed briefly.

Chapter 4 analyse the results achieved in chapter three. The results for each experiment were discussed. The chapter is divided in to three sections where the first section is reporting the findings that have been achieved in the optimization of the appropriate composition of the composite system and comparing the different physical and mechanical properties. The second section deals with role of silica in the composite system where it was determined the exact quantity needed for the good densification and better mechanical property of the product. The third section is studying the toughening mechanisms of the ternary system compared to the binary one.

Chapter 5 draws the conclusion and recommendation from the results achieved and forwarding future works which should be done parallel to this work. Finally, the list of references used in supporting the findings of the research was compiled.

CHAPTER 2

LITERATURE REVIEW

2.1 Overview

This chapter contains a review on the theory and previous works that are relevant with this research. The first section deals with the materials used in the development of the composite. The second section presented the basic understanding of the thermodynamic and kinetic phenomena of the diffusion process in pressureless sintering. Within this section it was also discussed previous works of pressureless sintered composite of related materials. In the third section, the mechanical properties and toughening methods in relation with the microstructural design, has been reviewed. In the last section, the need for thermal shock resistance of the material produced was discussed related to the objectives of the research. Generally, the chapter attempted to examine the previous works and identify the issues which are relevant to this work.

2.2 Alumina, silica and zirconia

2.2.1 Alumina

Alumina (Al_2O_3) is the most cost effective and widely used material in the family of engineering ceramics. It possesses strong ionic interatomic bonding giving rise to its desirable material characteristics. It can exist in several crystalline phases which all revert to the most stable hexagonal α - phase at elevated temperatures [31]. The properties of alumina compared to the reinforced components are shown in Table 2.1. It has excellent properties in hardness, corrosion resistance, high electrical resistance,

high thermal conductivity and heat resistance; it has been used in a variety of structural and electrical applications [31, 32] . Alumina is very stable and highly resistant to chemical attack under both oxidizing and reducing conditions. Alumina also possesses the advantage of being fairly inexpensive to manufacture. However, alumina suffers from lower thermal shock resistance as compared to mullite. It needs a reinforcement of mullite in the application of high thermal shock.

Table 2.1: Alumina, Silica, zirconia and mullite room temperature engineering properties [32, 33].

Properties	Alumina	Silica	Zirconia	Mullite
Density, g/cm ³	3.8	2.22-2.65	5.5	3.30
Modulus of elasticity, GPa	370-380	69-74	138-200	145-229
Poisson's Ratio	0.22	0.71	-	-
Compressive strength, MPa	2500	2070	1800-4820	
Tensile strength, MPa	300	110-273	-	-
Coefficient of thermal expansion (10 ⁶ /°C)	8.1	8.2	5-10	4.5-5.6
Melting point, °C	2054	1750	2560	1725

2.2.2 Silica

Silica (SiO₂) is one of the most common and abundant chemical compound. The three forms of silica are quartz, tridymite and cristoblite as shown in Figure 2.1. For each form, at low temperatures (the α phase) we find structure that is a distortion of high temperature form (the β phase). In each case, changing from the α to β structure involves a displacive phase transformation; the atoms need to move only slightly relative to one another [32]. However, to change form one form to another form requires breaking bonds. The properties of SiO₂ are shown in Table 2.1. The glass forming ability, along with the widespread occurrence of quartz sands, has resulted in the use of SiO₂ as the basic material for the glass industry.

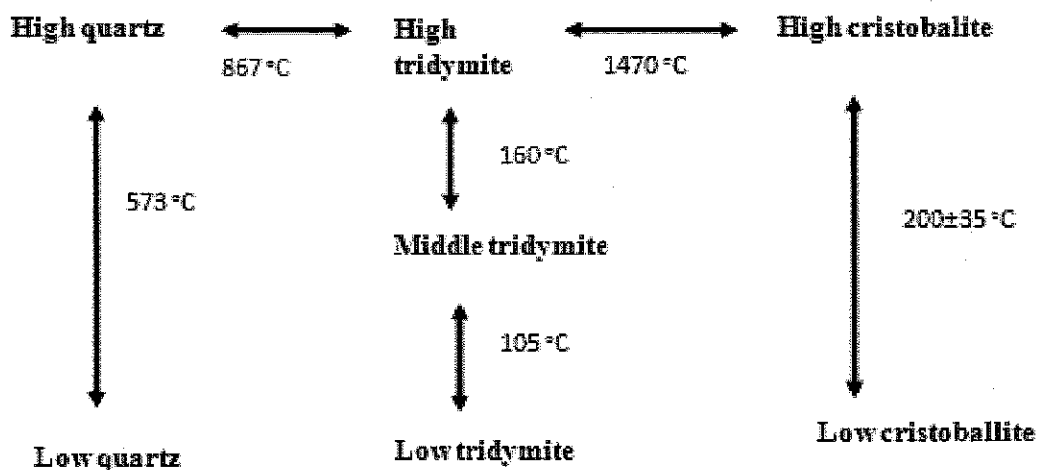


Figure 2.1: Schematic diagram to show the three forms of silica converted in to one another [34].

2.2.3 Zirconia

Zirconia (ZrO_2) ceramics have a martensite-type transformation mechanism of stress induction, giving the ability to absorb great amounts of stress relative to other ceramic materials. It exhibits the highest mechanical strength and toughness at room temperature. Zirconia has excellent wear, chemical and corrosion resistance and low thermal conductivity [32]. Pure zirconia exists in three crystal phases at different temperatures. At very high temperatures (>2370 °C) the material has a cubic structure. At intermediate temperatures (1170 to 2370 °C) it has a tetragonal structure. At low temperatures (below 1170 °C) the material transforms to the monoclinic structure as shown at the end of this paragraph. The transformation from tetragonal to monoclinic is rapid and is accompanied by a 3 to 5 percent volume increase that causes extensive cracking in the material. This behavior destroys the mechanical properties of fabricated components during cooling and makes pure zirconia useless for any structural or mechanical application [7, 15, 21, 23, 35]. The properties of Zirconia are shown in Table 2.1 on page 12.



Several oxides which dissolve in the zirconia crystal structure can slow down or eliminate these crystal structural changes. Commonly used effective additives are MgO, CaO, and Y₂O₃ [36]. With sufficient amounts added, the high temperature cubic structure can be maintained to room temperature. Cubic stabilized zirconia is a useful refractory and technical ceramic material because it does not go through destructive phase transitions during heating and cooling. The structure of tetragonal and cubic are shown in Figure 2.2.

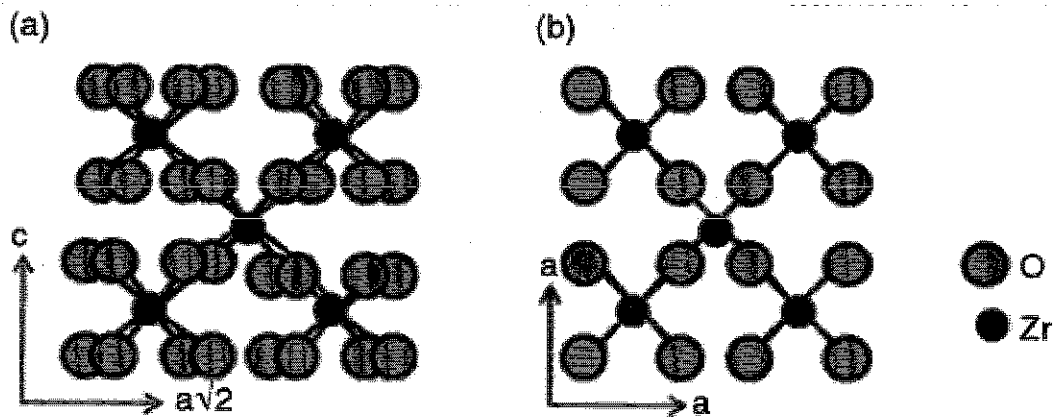


Figure 2.2: Structure of (a) Tetragonal and (b) cubic zirconia [37].

2.2.4 Mullite

Mullite has excellent high temperature properties with good thermal shock and low thermal stress owing to the low thermal expansion, good strength and interlocking grain structure [4, 38, 39]. The typical physical and mechanical properties are shown in Table 2.1 on page.12.

Mullite is an intermediate compound of Al₂O₃ and SiO₂ with ideal stoichiometry of 3Al₂O₃.2SiO₂. It is the only stable unhydrated compound in the alumina- silica phase diagram system as shown in Figure 2.3. It has an orthorhombic silicate structure

made up of chains of AlO_6 octahedral running parallel to the z axis and cross linked by tetrahedra containing Si and Al.

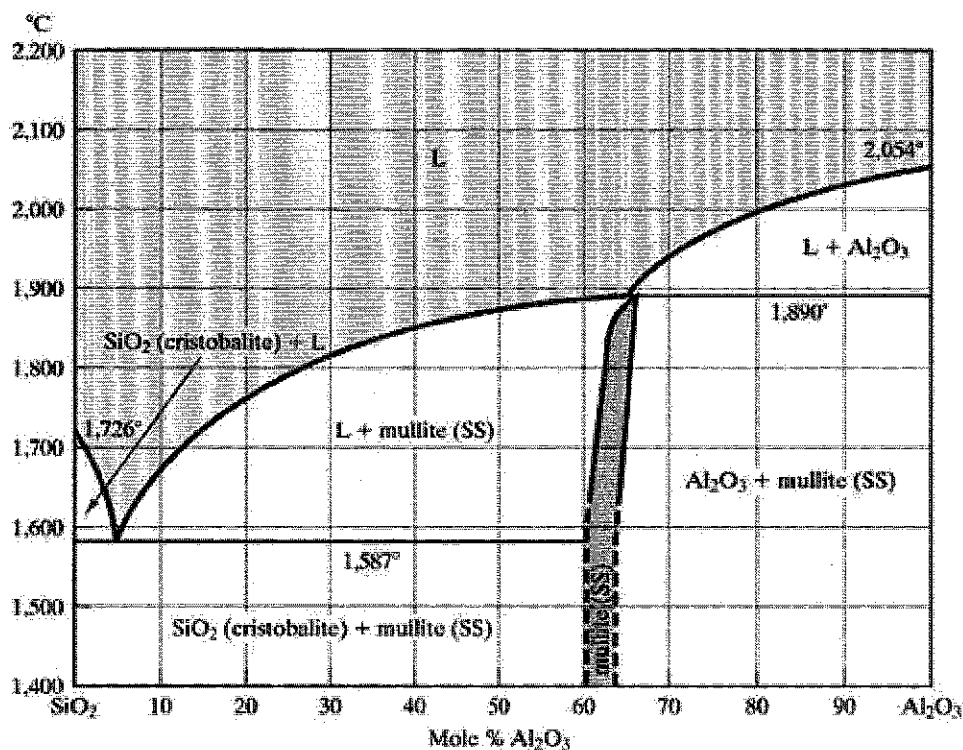


Figure 2.3: Alumina-silica phase diagram showing the phase stability [40].

2.3 Particle characterization and selection

The final properties of ceramic composites are dependent upon the behavior and characteristics of the raw materials. The characteristics of raw powder materials have a major effect on the outcome of the composite. The important characteristics of the powders can be categorized as show on Table 2.2, as physical properties, chemical compositions, phase compositions and surface characteristics [41]. For example, purity, particle size distribution, reactivity, polymorphic form, availability and cost must be considered and carefully controlled.

Table 2.2: Powder characteristics that have significant influence on ceramics [41, 42].

Physical characteristics	Chemical composition	Phases	Surface characteristics
Particle size and distribution	Major elements	Structural(crystalline or amorphous)	Surface structure
Particle shape	Minor elements	Crystal structure	Surface composition
Degree of agglomeration	Trace elements	Phase composition	-
Surface area	-	-	-
Density and porosity	-	-	-

The high temperature properties such as strength, stress rupture life and oxidation resistance is strongly affected by the purity of the powder. The chemistry of both the matrix material and the impurity, the distribution of the impurity, and the service conditions of the component (time, temperature, stress, and environment) are the factors which determine the effect of the impurity [42].

Hyung Bond et al. [43] prepared a glass-infiltrate alumina composite by mixing coarse and fine alumina powder and achieved a highest bending strength of 510 MPa. Cemal Aksel et al. [44] investigated the influence of varying the amounts of spinel with a similar median particle size, but with different distribution, on the mechanical properties and thermal shock performance of MgO-spinel composites. Narrow distributed spinel particles resulted in shorter initial crack propagation distances from the spinel particles, while a significantly broader distribution were the origins of longer interlinked cracks. This shows particle size and size distribution have a significant effect on the mechanical strength, density, electrical and thermal properties of the finished object. The particle size distribution and the morphology can be studied using SEM as shown in Figure 2.4. It is important depending on which consolidation technique is to be used. In most cases the objective of the consolidation technique is to achieve the maximum particle packing and uniformity, so that minimum shrinkage and retained porosity will result during densification. A single particle does not produce good packing, optimum packing of particles of the same

size results in over 30% void space. However, mixing particles of the size equivalent to the largest voids may reduce the void content to 26%. Adding a third to the binary particle, still smaller particle size can reduce the pore volume to 23%. Therefore, to achieve the maximum particle packing, a range of particle size is required. Particle shape also influences the flow properties and packing of powders as well as their interaction with fluids (e.g., viscosity of a suspension).

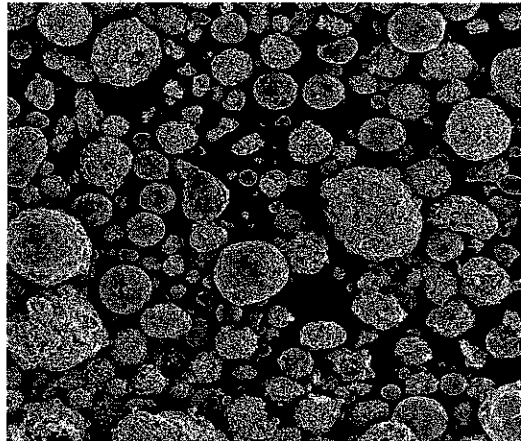


Figure 2.4: SEM micrograph of alumina powder [40]

Another important aspect of starting powder is reactivity. The primary driving force for densification of a compacted powder at high temperature is the change in surface free energy. Very small particles with high surface area have high surface free energy and thus have a strong thermodynamic drive to decrease their surface area by bonding together [22].

2.4 Fundamental of sintering

Sintering is the most important step in powder processing because it is at this stage that the material is subjected to very high temperatures, causing the particles to form bonds that are needed to hold the mass together.

The type and classification of sintering is based on the mechanisms that are mainly responsible for shrinkage or densification. Solid state sintering is the mechanism occurred during solid state diffusion of particles. Polycrystalline materials usually sintered by this process [45]. The second classification is when amorphous

materials sinter by viscous flow and are thus considered to undergo viscous sintering. Another type of sintering that makes use of a transient second phase that exists as a liquid at the sintering temperature is known as liquid phase sintering. The liquid phase under the right conditions can provide a path for rapid transport and, therefore, rapid sintering.

A number of researchers [45-47] have been studying the entire sintering process and it was considered to occur in three stages (I, II and III) as shown in the dilatometry graph in Figure 2.5. There is no clear-cut distinction between the stages since the processes that are associated with each stage tend to overlap each other. However, some generalizations can be made to distinguish one stage from another.

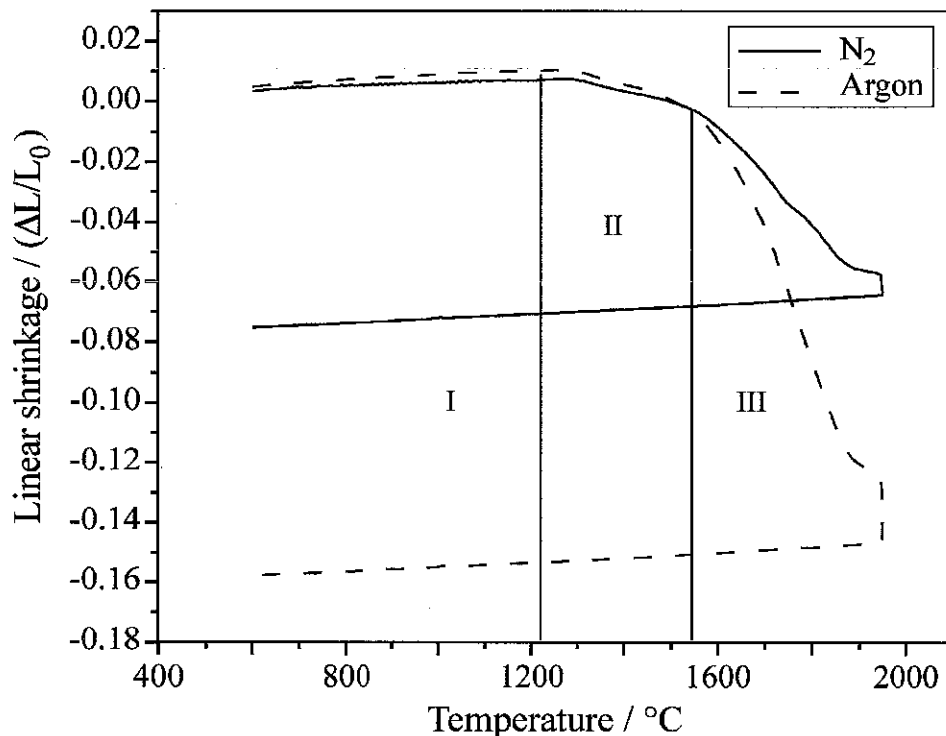


Figure 2.5: Linear shrinkage versus sintering temperature [48].

In the initial stage of sintering as shown in Figure 2.6. (a), where L_0 is the overall optimum length of the particles in the initial sintering, we can see that the sintering force move the particles into a more stable position by rotating and sliding. This contributes to shrinkage and an overall increase in density. The increase in the interparticle contact during the rearrangement process facilitates the formation of necks between particles. The mechanisms responsible for the neck formation and

growth to take place are diffusion, vapour transport, plastic flow, or viscous flow. The initial stage is assumed to last until a neck radius of around 0.4 to 0.5 of the particle radius is attained. The intermediate stage (Figure 2.6. (b)) is considered to begin when the pores have attained their equilibrium shapes as dictated by surface and interfacial energies. Because the density remains low at this point, the pores are still continuous or interconnected. Densification is assumed to take place by the reduction in cross section of the pores. Eventually, pores become unstable and are pinched off from each other, leading to the final stage of sintering. Of the three stages, the intermediate stage covers the majority of the sintering process. The final stage (Figure 2.6.c) covers the elimination of the isolated pores until the theoretical density is reached. This stage is also characterized by grain growth in which the larger grains tend to increase in size at the expense of the smaller grains. The extent of grain growth is dependent on both the material and the sintering condition [33].

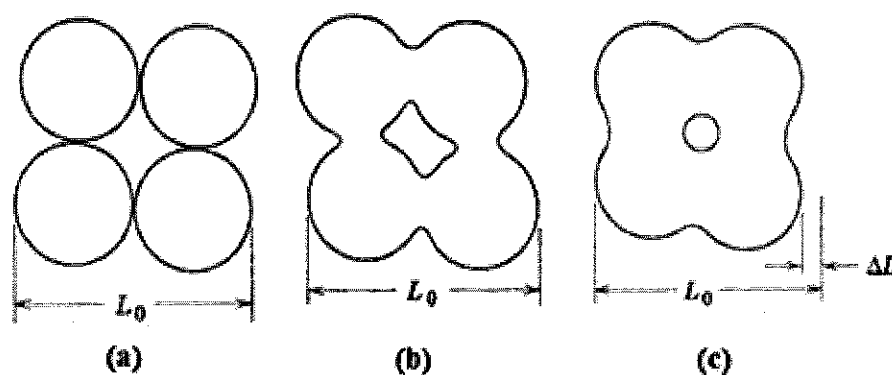


Figure 2.6: Schematic representation of neck formation during solid sintering due to
 (a). Powder compaction (b). Neck growth (c). Neck growth accompanied by
 densification [33]

In liquid-phase sintering, the liquid phase can be initiated via two common techniques [33, 45, 46]. In the first method, powders of different chemistries are mixed so that the interaction of the powders results in the formation of a liquid during sintering. The liquid formation in this method can be a result of the melting of one component of the formation of a eutectic phase. In the second method, the liquid can be formed by heating a powder to a temperature between the liquidus and solidus temperatures, resulting in co-existing liquid and solid phases.

Liquid phase sintering can also be described by three phases that are driven by surface energy reduction [28, 29, 45]. In the first stage, capillary action pulls the liquid into pores so that the liquid wets the solids. This will result in rearrangement of grains into the most favorable packing arrangement. In the second stage, the liquid has solubility for the solid and this will result in densification. When smaller particles in the solids go into solution, they will preferentially precipitate on larger particles, leading to densification. In the final stage, a solid skeletal network forms and the liquid moves into pores so that the wetting liquid reduces the porosity and interfacial energy of the solid phase, leading to additional densification .

In the final stages of both solid and liquid phase sintering, the sizes of larger grains increase at the expense of smaller ones. Because the sintering process is so dependent on diffusion and grain growth, particle size distributions must be carefully controlled. A broad particle size distribution will result in hinder diffusion, abnormal boundary growth and isolation/entrapment of pores. Studies show that powders with a narrower initial particle size distribution will result in a lower initial rate of densification before grain growth but a higher rate after [42].

2.4.1 Sintering mechanisms

In the sintering of ceramic materials, diffusional process for polycrystalline and viscous flow for amorphous materials are the main transportation methods which are responsible for the densification of the material. These transportation methods are derived by the chemical potential or energies created along the surfaces, intersurfaces and grain boundaries which are associated with the size of the surface or boundary curvature. The stable or minimized overall energy is achieved by reducing or minimizing the surfaces or curvature radius of the boundaries [14, 49, 50]. The different mechanisms of sintering for both polycrystalline and amorphous materials are summarized in Table 2.3 and Figure 2.7. The only mechanism which can produce densification is the volume diffusion from grain boundaries or from dislocations in the neck region. The effect of the other mechanisms is to reduce the neck curvatures formation and reduces the driving force; hence contribute for the densification rate.

Table 2.3: Sintering mechanisms in polycrystalline and amorphous materials [49].

Type of solid	Mechanism	Source of matter	Densification effect
polycrystalline	Surface diffusion	Surface	No
	Volume(Lattice) diffusion	Surface	No
	Vapour transport	Surface	No
	Grain boundary diffusion	Grain boundary	Yes
	Volume(Lattice) diffusion	Grain boundary	Yes
Amorphous	Viscous flow	Unspecified	Yes

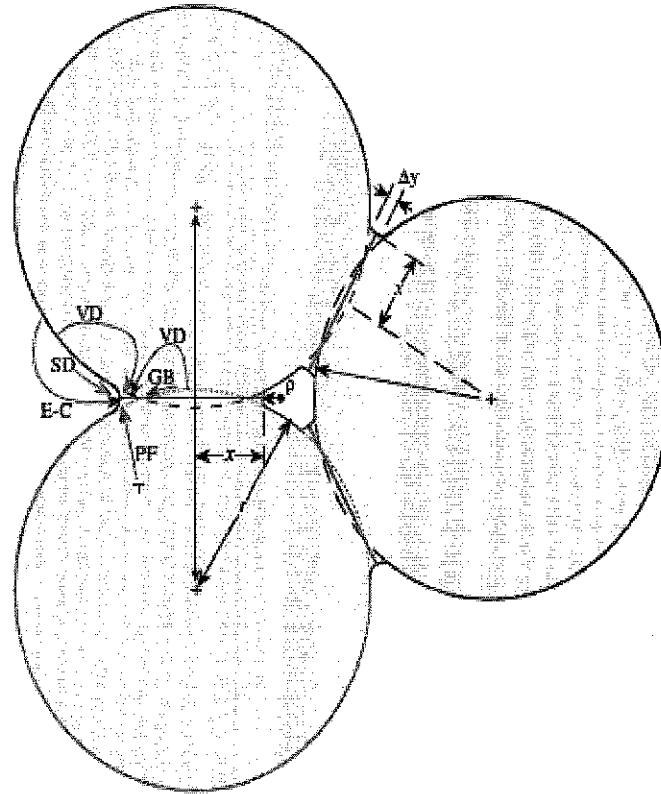


Figure 2.7: The possible mechanism contributing to sintering process: VD-Volume diffusion, GB- grain boundary diffusion, SD- surface diffusion, PF- plastic flow diffusion, E-C- Evaporation condensation flow [51].

2.4.2 Theoretical analysis of sintering

In the study of sintering behavior different theoretical approaches were practiced. Among the most known approaches are the scaling laws [49, 52], analytical models [53], empirical or phenomenological equations, and statistical and numerical techniques. When we study the sintering behavior we used simplified, idealized models to represent of the particles in a sintering body. Because of the complexity of the real mechanisms in the sintering process, the structure of the powder system needs to be idealized. Hence, it would be difficult to fully deploy the analytical models because real systems are far from being ideal.

Among the models, scaling laws, and analytical models are most popular. The scaling law simply assumes that the particle size of any given system remains the same and the shape of the particles remains similar during sintering. Though this model is oversimplified, it is useful for the understanding of particle size dependence of the sintering mechanism [49], and is also useful for determine how the relative rates of the different mechanisms are influenced by the particle size. One of the most important equations of the scaling laws is:

$$\frac{\Delta t_2}{\Delta t_1} = \left(\frac{R_2}{R_1}\right)^m = \lambda^m \quad (2.2)$$

Where Δt_1 and Δt_2 are respectively the time to produce similar microstructural change for particles of radius R_1 and particles of radius R_2 , λ is the ratio between R_2 and R_1 , m is the exponent of various mechanisms are given in Table 2.4.

Table 2.4: Exponents of scaling laws [49].

Sintering mechanism	Exponent (m) value
Surface diffusion	4
Lattice diffusion	3
Vapour transport	2
Grain boundary diffusion	4
Plastic flow	1
Viscous flow	1

To determine the relative rates of the different mechanisms, the above equation can be written as:

$$\frac{\text{Rate}_1}{\text{Rate}_2} = \lambda^{-m} \quad (2.3)$$

The scaling laws do not consider the shape of particles. To derive a more accurate equation, the geometrical details must be adopted. The analytical model assumes a relatively simple, idealized geometry, and, for each mechanism, the mass transport

equations are solved analytically to derive the sintering kinetics. In the analytical model, sintering can be divided into three [11, 49, 51]:

1. The initial stage: rapid interparticle neck growth by diffusion, vapour transport, plastic flow, or viscous flow.
2. The intermediate stage: pores begin to reach their equilibrium shape which is dictated by the surface and interfacial tension. Pores are continuous, and densification is caused by pore shrinkage.
3. The final stage: channels between pores are closed. Pores become isolated at the grain boundaries. Abnormal grain growth during this step could lead to pore entrapment inside the grains, and removal of these pores becomes impossible.

The densification of a polycrystalline powder compact is normally accomplished by coarsening of the microstructure: the average size of the grains and the average size of the pores become larger. The achievement of high density and controlled grain size is dependent on reducing the grain growth rate, and increasing the densification rate. Controlling grain growth is extremely important because the grain size affects the ceramics properties as well as the final relative density of the product. Theoretical approaches have not given fruitful results up to now. In practice, the way to avoid abnormal grain growth includes:

- a. Use of dopants to segregate the grain boundaries
- b. Use of second phase powder that does not react with the grains
- c. Homogeneous packing of powder with a narrow size distribution
- d. Sinter with an applied pressure
- e. Use of a second phase that forms a liquid at the firing temperature

The use of liquid phase sintering is to enhance densification rate and to decrease the fabrication temperature of a system requiring too high temperature in a conventional solid-state sintering. The microstructures of ceramics produced by liquid-phase sintering consist of two phases:

- (1) The crystalline grains and

(2) The grain boundary phase resulting from the solidified liquid.

Compare to solid state sintering, the additional phase makes liquid phase sintering more difficult to analyze.

The only systematic study of pressureless sintering kinetics applies the Kingery liquid-phase sintering model in which three stages are identified, as summarized by the log shrinkage/log-time plot of Figure 2.8.

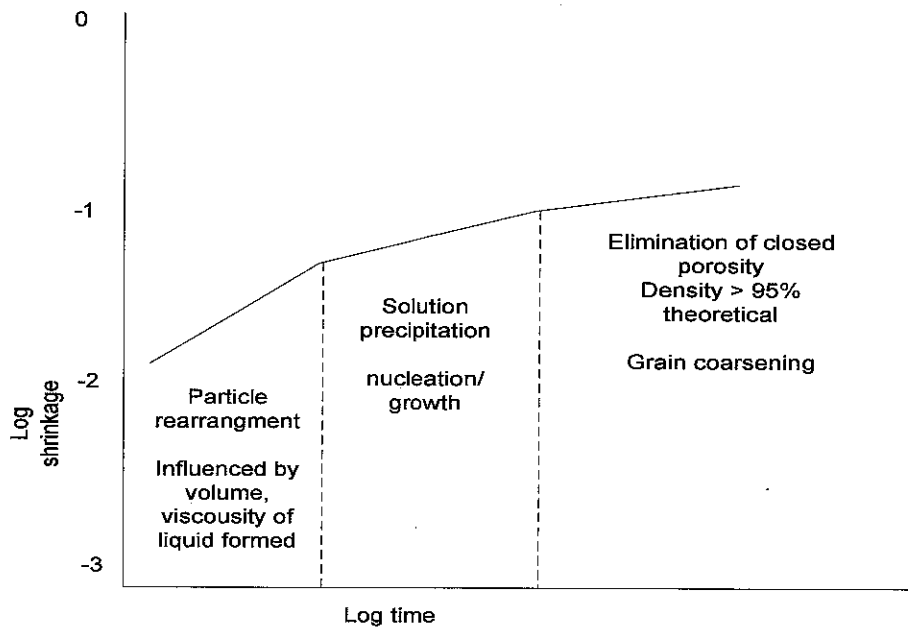


Figure 2.8: Schematic plot of three stage of liquid phase sintering [54].

The stages are [14, 45, 55]:

1. Particle rearrangement within the initial liquid, where the rate and the extent of shrinkage depend on the volume and viscosity of the liquid; this is the incubation period for the $\alpha \rightarrow \beta$ transformation;
2. Solution-diffusion reprecipitation, where shrinkage can be expressed as

$$\frac{\Delta V}{V_0} = \alpha t^{1/n} \quad (2.4)$$

Where t is time, $n = 3$ when the solution into or precipitation from the liquid is rate controlling and this was found to be the case for MgO additive. $n = 5$ when diffusion through the liquid is rate controlling as is the case for the Y_2O_3 additive, where

diffusion through a more viscous oxynitride liquid is much slower; the $\alpha \rightarrow \beta$ transformation begins during this stage and is more rapid for Y_2O_3 ;

3. Final elimination of closed porosity during which the liquid acts to form a more rounded grain morphology; final density is greater than 95% of the theoretical value.

The type and amount of additive used for sintering, not only aids densification but also determines the nature and quantity of the resulting grain boundary phase as indicated in Equation 2.4. The concept of "grain boundary engineering" sought to control the structure of, and reactions occurring at, the grain boundaries in silicon nitride based materials and significant advances in materials properties were realized as a result of this approach.

2.5 Pressureless sintering of ASZ systems

For alumina based ceramics, composites have been produced using zircon ($ZrSiO_4$) rather than zirconia (ZrO_2) as the initial precursor [6, 18, 19, 56]. A dissociative reaction of the zircon provides zirconia and silica. This free silica reacts with alumina, producing mullite in a process known as reaction sintering. Depending on the amount of reactants (alumina and zircon), a mullite-zirconia composite (mullitic matrix with zirconia inclusions) or an alumina-mullite-zirconia one (alumina matrix with mullite and zirconia inclusions) was obtained. In the latter, it was possible to associate toughening mechanisms provided by the zirconia inclusions, as well as those related to the presence of the needle-like mullite. Furthermore, the addition of mullite in an alumina matrix offers additional benefits due to its high refractoriness and lower thermal expansion coefficient.

In order to produce the ASZ composite, there are many ways of introducing zirconia into an alumina matrix to produce these composites, e.g. conventional or chemical processing of alumina and zirconia powders [57] as well as sol-gel [58, 59] can be used. The same holds true in pressureless sintering, in which alumina and zircon ($ZrSiO_4$) [59, 60] are used as the initial powders. The disadvantage is that the

dissociation reaction of zircon causes porosity that may lead to degradation of the mechanical properties. In an attempt to control this porosity, this research used a dissociated zirconia and silica powders as reinforcement for the production of alumina-zirconia-mullite composite. It is also cheaper compared to the starting raw materials zircon to use zirconia and silica as raw materials to easily be implemented industrially (in view of conventional equipment and processing techniques and energy consumption).

2.5.1 Alumina - Zirconia (AZ) composites

AZ ceramic composites are the most researched and represented a class of high strength and high toughness structural materials. The improved toughness is achieved through a phenomenon known as “Transformation toughening”. Many researches have been done so that marked increase in the bending strength and fracture toughness was observed when the alumina matrix was reinforced through metastable, tetragonal zirconia particles of an average size of 0.7 μm [7, 57, 61, 62]. Mechanisms of toughening and strengthening in each of zone of composition (AZ) was analyzed and it was found that stress induced transformation ZrO_2 and dispersion strengthening of Al_2O_3 were the two main factors [62]. W.H.Tuan et.al [7] developed a composite of $\text{Al}_2\text{O}_3/\text{t-ZrO}_2/\text{m-ZrO}_2$ and the result showed the toughness is two times and the strength three times of the pure alumina ceramic using pressureless sintering process. Now days, an increase in toughness and strength ($K_{\text{IC}} \approx 1.5\text{-}8 \text{ MPa}\sqrt{\text{m}}$; $\sigma_b \approx 200\text{-}1300 \text{ MPa}$) due to the zirconia inclusions in combination with hardness (16-19 GPa), Young's modulus (320-370 GPa) as well as low specific weight (4-2 g/cm^3) has resulted in several technical applications of zirconia toughened alumina (ZTA), like cutting tools, grinding media, wear resistant parts.

2.5.2 Alumina–Silica (AS)

Limited research has been taken place in this composite type because, alumina and silica do have wide difference in the thermal coefficient of expansion. But there are reports [63, 64] that an alumina–silica composite that a critical limit exists on the

second phase (silica powder) reinforcement volume that can be accepted by the alumina matrix in order to achieve a densification of >90%. The exact value of this limit remains to be verified, but it can be stated that if large size second phase particles are present, they hinder the die cold pressing process and finally reduce the sintered density. There are observations that an addition of 30% SiO₂ particles drastically reduced the sintered density of the composite to 70% of its theoretical density [30].

There is also a work [65] that has been done in producing alumina –silica ceramic with mullite whisker structure as armor material for protecting high velocity projectiles. The mixing composition as a starting powder was alumina, quartz, kaoline, feldspare and talc, sintered from 1200 to 1450°C for 5 to 3 hrs .

2.5.3 Zirconia-Silica (ZS)

From the phase diagram of Zirconia and Silica oxides, it can be observed that there is no solid solution formed but at high temperature (1300°C–1400°C) there is a reaction between them to form zircon - ZrSiO₄ [66]. But T. Ahmad and O. Mamat [67] claimed that, a more dense and harder composite was produced by adding 20% wt. nano silica sand. They observed a decreasing trend of green density but an improvement in the sintered density. Also the addition of silica sand nanoparticles with 20 wt.% increased the hardness up to 12.45 GPa and microstructures indicated the diffusion mechanism of silica sand nanoparticles into pore sites of the composites

2.5.4 Mullite-Zirconia (MZ)

Mullite (3Al₂O₃.2SiO₂) ceramics has been available as a structural material with excellent thermal shock resistance, hot load-bearing characteristics, and high refractoriness. Due to the poor toughness, however, the applications of the mullite ceramics have been restricted. In order to improve such toughness, some researchers examined the fabrication of mullite-zirconia composite ceramics, using the starting

powders prepared by mechanical mixing [68, 69], coprecipitation [70], sol-gel [58], and alkoxide [58] techniques.

T. Ebadzadeh et al. [71] has analysed the influence of starting materials on the reaction sintering of mullite–zirconia composites. They use $ZrSiO_4$ as an additive to alumina ceramics for the following reaction:



The microstructure observed of samples sintered after 2 hr at 1600°C revealed complex microstructures which contain different intergranular ZrO_2 particle morphologies surrounded by the mullite matrix.

2.5.5 Alumina-Silica-Zirconia (ASZ) composites

From the works of Nagarajan et al. [58], in situ preparation of Al_2O_3 - SiO_2 - ZrO_2 composite system, it was noted that, of the three oxides involved in the system, SiO_2 is acidic, Al_2O_3 is amphoteric, and ZrO_2 is basic in their chemical nature. The expected products are therefore cristoballite, Al_2O_3 , ZrO_2 , mullite, and zircon. There is no reported compound formation between ZrO_2 and Al_2O_3 they form a perfect mix to each other. An important driving force for the direct ZrO_2 - SiO_2 reaction in the ternary system could be the difference in the molecular electronegativities (χ_{av}) of ZrO_2 and SiO_2 . As it can be observed from Table 2.5, SiO_2 and ZrO_2 have the highest electronegativity difference which is the chemical driving force for the reaction between ZrO_2 and SiO_2 .

Table 2.5: Molecular electronegativities of various compounds and partial charges on the ions [58].

Ceramic compound	χ_{av}	Partial charge			
		O	Si	Al	Zr
SiO ₂	2.820	-0.2143	+0.4278	-	-
Al ₂ O ₃	2.537	-0.3121	-	+0.4683	-
ZrO ₂	2.500	-0.3249	-	-	+0.6503
ZrSiO ₄ (Zircon)	2.654	-0.2718	+0.3504	-	+0.7356
Al ₆ Si ₂ O ₁₃ (mullite)	2.615	-0.2853	+0.3323	+0.5075	-

It is interesting to note here from Table 2.5 that, Al₂O₃ and ZrO₂ have almost equal molecular electronegativities and have no chemical driving force for reactions. This is substantiated by the fact that there is no reported compound formation between ZrO₂ and Al₂O₃. Indeed recently it is observed that they form solid-solutions over a wide range of compositions.

It is well known that ZrO₂ imparts very desirable mechanical properties such as high toughness and strength when it is present in composite ceramics. Al₂O₃ and SiO₂ are traditional ceramic materials of great utility. It is therefore necessary to examine the effect of ZrO₂ on ceramics containing both Al₂O₃ and SiO₂ as well as SiO₂ effect on the same system. As we can see from the phase diagrams, of the three oxides chosen for the study, Al₂O₃ and ZrO₂ react independently with SiO₂ giving rise to well defined compounds at high temperatures. The compound formation influences the properties of the resulting ceramics.

The result of different proportion of the component elements (alumina and zircon) shows that an increase in the zircon content in the reaction (given by the chemical reaction above) increases porosity and lowers density. Observation of the micrographs also enables to describe the composites' microstructure. The matrix shows a homogeneous distribution of mullite and zirconia inclusions (resulting from the good homogeneity achieved in the mixing process and from the use of zircon with a small

average particle size). Of all the composites produced from the different sample proportion, the most effective one appeared to be the one with 15% of zircon. This sample showed the best mechanical properties and R-curve behavior. With regard to the thermomechanical properties evaluated, composite of 15% zircon also showed the best ΔT_c (variation of critical temperature for initiation of crack propagation) and a value of R (thermal shock damage resistance) 1.6 times higher than the value obtained for pure alumina.

2.6 Toughening of ceramics

Toughening is one of the important key parameter in improving the mechanical properties of ceramics. Thus, the understanding of the fracture mechanisms brittle materials is very important to study the behaviour of ceramic and composites. In these materials plastic deformation by dislocation motion does not occur, or occurs to such a limited extent that cracks are sharp to the atomic level of the solid. Resistance to fracture is provided by the lattice itself, and not by the movement of dislocations. Ceramics can be made tougher by modifying the microstructure of the solid in such a way as to reduce stresses near crack tips. Our ability to make tougher ceramics has increased gradually with our deepening understanding of brittle fracture. The purpose of this review is to outline the evolution of this understanding and to show how the knowledge gained is currently being applied to the development and manufacture of tougher ceramics.

The low fracture toughness or lack of ductility in ceramics is associated with the fact that ceramics typically possess less than the five independent slip systems necessary for arbitrary shape changes in that this material possesses strong ionic and covalent bonds [3, 5, 11, 20, 21, 40, 72]. Planar slip for ceramics involves, first, the breaking of strong bonds which do not reform, and second, the coming in contact of ions of different charges which may generate strong attractive and repulsive forces. In addition ceramics do have low symmetry crystal structures; possess long range order, and are extremely flaw sensitive. In order to increase the end uses of ceramics, extensive research has been and is being conducted in developing tougher ceramics.

For structural materials, toughness usually means fracture toughness, or the resistance of a material to the propagation of a crack. For a perfectly brittle and elastic material with an initial crack size of a ,

$$\sigma = \sqrt{\frac{2 E \gamma_s}{\pi a (1-\nu^2)}} \quad (2.6)$$

The above Equation 2.6 is for a tri Axial stress state and for biaxial state stress is written as:

$$\sigma = \sqrt{\frac{2 E \gamma_s}{\pi a}} \quad (2.7)$$

where

σ is the fracture stress,

γ_s is the specific surface energy

E is Young's modulus

a is the existing, or initial, crack length

ν is Poisson ratio.

It has been found that for ionically bonded solids this equation provides a good predication for the one set fracture, however, for covalently bonded ceramics this formula underestimate the energy necessary to cause failure.

The inherent brittleness of ceramics provides a severe mechanical disadvantage which largely limits a broader use of these materials in advanced structural components. Furthermore, often the poor reliability due to the scatter in fracture stresses does not facilitate applications. About two decades ago, it was first observed that certain technical ceramics are able to develop a kind of flaw tolerance by an increase of toughness with crack extension. Since then this favorable crack resistance (R-curve) behavior has gained considerable interest in the ceramic community. In the following section a brief outline of the mechanisms of toughening and the application of it will be discussed.

2.6.1 Toughening mechanisms in ceramic composite

The toughness of materials is very important in engineering design process because it is related to the fracture toughness of materials. It is the one used to describe a material's resistance to fracture when a crack is present. It is defined by "the irreversible work (per unit area of fracture surface) accompanying crack propagation". In other words, it measures the ability of a material to absorb energy up to the fracture point [11, 23, 38, 40, 61, 73-75]. In the past several decades, much effort has been concentrated on improving the fracture toughness of ceramics.

The toughening techniques of ceramics are classified into three groups:

- (A) Particle dispersion toughening [20, 76, 77],
- (B) Multilayer toughening [78, 79], and
- (C) Phase transformation toughening [80]. In this research paper, toughening techniques of A and C will be the focused mechanisms to discuss.

Particle dispersion toughening of ceramics was studied analytically and experimentally mainly in the 1960s. In the analytical field, Weyl et al. [20] and Selsing et al. [20] derived an analytical solution of residual stress around a spherical particle dispersed in an infinite body. In the experimental field, Davidge and Green [76] and Swearingen et al. [81] fabricated composites of spherical ceramic particles within glassy matrices with different thermal expansion coefficients, examined the relationship between the residual stresses and the crack path behavior, and revealed that the residual stresses due to thermal expansion mismatch have no notable effects on improvement of toughness of the materials.

Ceramic composites developed by Niihara et al [82] and his coworkers [83] are one of the particle-dispersed materials, but the strengthening and toughening mechanisms are quite different, where the strength of the composites was improved significantly and also moderate enhancement in toughness was found. The microstructure of the composites is constructed by dispersing second phase nanosize particles within the matrix grains and on the grain boundaries. Thermal expansion mismatch between the matrix and second-phase particles produces a marked

improvement in fracture properties, such as strength, hardness, creep resistance, and wear resistance. The mechanism is believed to be chiefly due to generation of dislocations around the second-phase particles. The dislocations form networks or sub-grain boundaries in the matrix and disperse into the matrix to serve as origins for nanocrack nuclei because dislocations in ceramics are difficult to move. The concept of ceramic composites is, therefore, considered to be quite reasonable as a means to enhance the fracture toughness of brittle ceramics. The enhancement mechanisms behind the mechanical properties of ceramic based composites are still unclear, although several models for the toughening and strengthening mechanisms of composites have been proposed, such as a steep R-curve behavior model [77, 84], a residual stresses model [85, 86] and a reduction model in processing defect size [87, 88]. The following review discusses the fracture of ceramic composites and the type of toughening mechanisms available.

For any fracture to take place in a material, two steps must be involved: (1) crack formation and (2) crack propagation. As it shows in Figure 2.9, there are three fundamental modes of crack propagation. Mode I is the “tensile opening mode”, within this mode the applied tensile stress is normal to the crack surface and tends to open the crack. In Mode II, the “in-plane sliding mode” the direction of crack propagation is parallel to the applied shear stress. Mode III is the “out-of-plane sliding mode”. In this mode the crack propagates in the direction normal to the shear stress, which produces a “tearing” type of fracture [3, 5, 11, 21, 72, 89]. To prevent crack propagation in order to avoid fracture, the fracture toughness of materials can be increased. Due to the difference in toughening mechanisms, the material classes including metals, ceramics, composites and polymers, are toughened in different ways.

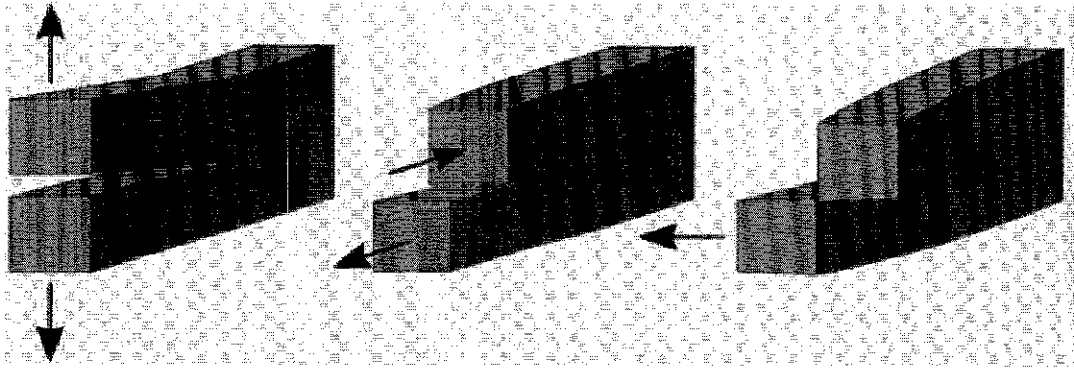


Figure 2.9: Fundamental mode of crack propagation [89].

Considerable effort has been expended to produce structural ceramics with enhanced toughness with some success, although toughening mechanisms which remain effective at high working temperatures remain elusive. Recently it has been observed that enhancements in the toughness may be achieved if a number of different energy dissipative mechanisms are present in the ceramics [5, 11, 20, 21, 37, 40, 86, 89]. These mechanisms can be classified as either as intrinsic or extrinsic in the nature as shown in Figure 2.10. Intrinsic mechanisms are associated with material chemistry in terms of the ductility and or flow of constituents within the ceramic. Extrinsic mechanisms are associated with energy dissipating events which happen in two different regions of an advancing crack, namely the wake of the crack and frontal zone ahead of the advancing crack tip [90, 91]. These mechanisms consume energy that would otherwise go towards crack propagation and will be examined in detail in this section.

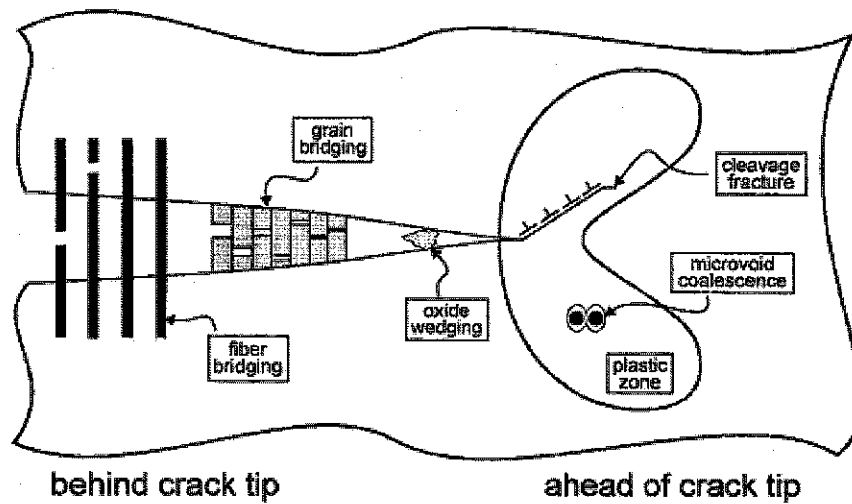


Figure 2.10: Schematic illustration of mutual competition between intrinsic mechanisms of damage/crack advance and extrinsic mechanisms of crack-tip shielding involved in crack growth [91].

Figure 2.11 shows example of these various energy dissipative mechanisms. These mechanisms can be seen to take place in either in the frontal zone ahead of the crack tip or in the wake of the crack. These mechanisms include: Crack deflection and Crack shielding mechanisms (Transformation toughening, Microcracking induced toughening, toughening by the generation of compressive surface Stress, Toughening in Zirconia Toughened Al_2O_3 system) as shown Figure 2.11.

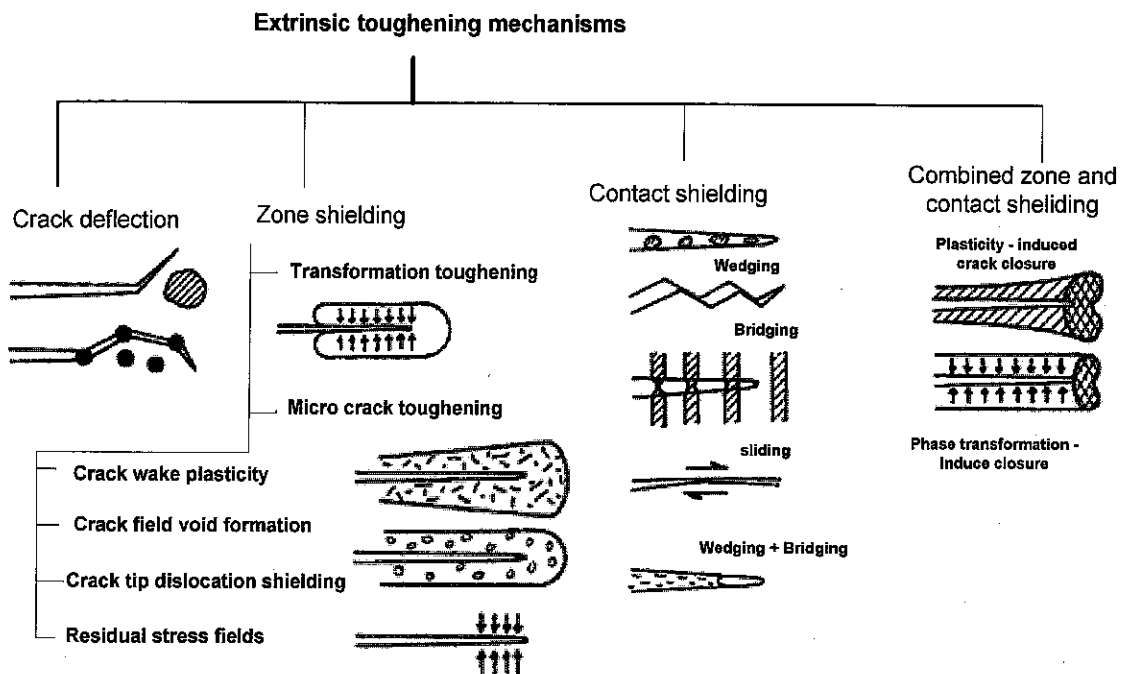


Figure 2.11: Toughening mechanisms [20, 33, 62, 92]

2.6.1.1 Toughening by crack propagation

Localized residual stress fields are generated during any type of phase transformation involving volume change or due to thermal expansion mismatch between the two phases or arising from the fracture of a second phase. This residual stress field can deflect the main propagating crack thereby causing toughening of the composite. This deflection toughens by increasing the net resistance $G_c=R$ where G_c is the experimental mechanical energy release rate with theoretical surface energy of $2\gamma_B$ and R is the net crack resistance [21]. The extent of toughening depends on the reduction in the force on the deflected portion of the propagating crack. However, for crack deflection involving second phase particulates, the extent of deflection and thereby the toughness increment is dependent on the volume fraction of second phase particles, its morphology and aspect ratio.

Crack deflection has been shown to improve toughness by increasing the overall energy needed for crack advance to two ways [20-22, 74, 90]. First, energy is consumed in creating extra fracture surfaces upon crack deflection. Second, the effective stress at the crack or notch tip is decreased for a deflected crack compared to a straight crack under the same far field loading conditions.

Crack interaction occurs when there are obstacles in the crack path which act to change the stress distribution at the crack tip and thus change the direction of crack propagation. Crack deflection is the major cause for a propagating crack to bypass particles and is frequently assisted by the local areas in a ceramic that have a lower resistance to crack propagation, such as grain boundaries. Thus a crack advancing in a particulate reinforced composite will tend to follow the grain boundaries and result in tilted fracture surface.

When the crack is tilted, its stress intensity factor is reduced and speed is decreased. Faber and Evans [93, 94] were among the first who developed expressions for the contribution of crack deflection to the toughening of ceramic materials. Their analysis can be calculated from the expression (Equation 2. 8).

$$\frac{\langle G \rangle}{G_e} = \frac{1}{\phi_{max}} \int_0^{\phi_{max}} \frac{\sin \phi}{\sin \phi + \cot \phi} [(K_1')^2 + (K_2')^2] d\phi + \frac{1}{\phi_{max}} \int_0^{\phi_{max}} \frac{\cot \phi \cos \phi}{\sin^2 \phi + \cot \phi} \left[\left(\frac{1}{\phi} \int_0^{\phi} K_1' d\phi \right) + \left(\frac{1}{\phi} \int_0^{\phi} K_3' d\phi \right) \right] d\phi \quad (2.8)$$

Where $\langle G \rangle$ and G_e are strain energy release rate of tilted and flat crack respectively. In addition to lowering the stress intensity factor, there is an increase in toughness due to an increase in surface area of the crack.

2.6.1.2 Crack shielding mechanism

There are two kinds of crack shielding mechanism. One is based on the process zone formed in the wake of crack propagation and the other is based on martensitic phase

transformation in ZrO_2 . These mechanisms are governed by a critical stress for the onset of nonlinearity in elements near the crack and by the associated stress-free [95].

In some microstructures, it is possible for a large number of small secondary cracks to be formed near the primary crack as the result of the high local stress around the crack tip. Microcracks occur within the regions of local residual tension, caused by thermal expansion mismatch and /or by transformation. The crack shielding can be separated into dilation contribution due to a permanent strain caused by microcracks and modulus contribution due to a decrease in elastic modulus. The dilation contribution depends on process zone size and shape and a steady-state toughening can be estimated by [95]:

$$\Delta K_c = 0.4E\varepsilon_\gamma \sqrt{\omega_a} \quad (2.9)$$

Where E is the young's modulus, ε_γ is the misfit strain by microcracks, and ω_a is the process zone size.

The modulus contribution depends only on process zone shape and can be estimated by [95],

$$(1 - \nu) \frac{\Delta K_c}{K_c} = \left(K_1 - \frac{5}{8} \right) \left(\frac{G}{\bar{G}} - 1 \right) + \left(K_2 - \frac{3}{4} \right) + \left(\bar{\nu} \frac{G}{\bar{G}} - \nu \right) \quad (2.10)$$

$G, \bar{G}, \nu, \bar{\nu}$ are shear moduli and poisson's ratio of cracked and microcracked bodies, respectively. The parameters K_1, K_2 depend on the material properties.

Equation 2.9 predicts that increase in toughness is directly related to level of strain by thermal contraction or phase transformation of particles distributed in the matrix, and the size of the process zone. In turn, the size of the process zone is controlled by the stresses developed at the tip of the propagating crack and is a characteristic of the material.

2.6.1.2.1 Transformation toughening

Transformation toughening has been investigated in ceramics containing zirconia as a second phase. It relies on the transformation of zirconia from the tetragonal to the monoclinic phase and applied stress [5-7, 11, 20-22, 40, 89, 90]. This transformation occurs in the stress field around the crack tip in Figure 2.12 (a), and the resultant strain involved in the transformation locally relieves the stress field and absorbs fracture energy. Figure 2.12 (b) shows the resultant zone of transformed particles left in crack wake. This toughening mechanism is directly affected by the stability of tetragonal phase of the zirconia. The phase can be made stable through the addition of small amounts of dopants such as yttria and is also dependent on the grain size of zirconia phase and the testing temperature. This metastability of the tetragonal phase is key because one wants to create the largest transformation zone possible to expand the most fracture energy.

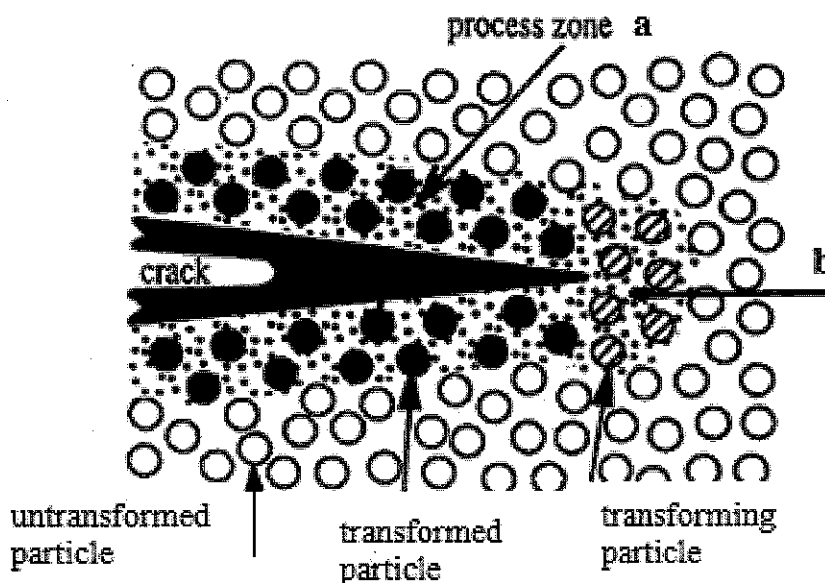


Figure 2.12: Transformation toughening through the addition of a second phase. Region (a) indicates the process zone around the crack tip in which second phase particles undergo dilatation transformation and region (b) the resultant zone of transformed particles left in the crack wake [90].

The basic idea behind the development of any transformation toughened ceramics is the retention of $t\text{-ZrO}_2$ in a metastable state and to ensure that this $t\text{-ZrO}_2$ undergo

stress induced $t \rightarrow m$ ZrO_2 transformation in the stress field of an advancing crack tip at stress level not exceeding the material fracture strength. Thus this transformation acts as a crack shielding mechanism. These prerequisites are met through composition control, use of stabilizer for ZrO_2 (which shifts the critical particle size for t - ZrO_2 retention to higher value) as well as by controlling mertsensite (M_S) temperature closer to room temperature (this helps to prevent spontaneous $t \rightarrow m$ ZrO_2 transformation during cooling from the sintering temperature. For a single or a multiphase brittle ceramic material/composite, [7, 12, 14, 15, 20, 21, 23, 33, 41, 62, 88, 90, 96, 97] the fracture toughness is given by:

$$K_{IC} = K_0 + \Delta K_C \quad (2.11)$$

Where, K_0 is the matrix toughness and ΔK_C is the contribution to the toughness from various crack shielding mechanism .

In the case of zirconia dispersed ceramics (ZDC), the stress induced $t \rightarrow m$ ZrO_2 transformation may increase the toughness through a change in the transformation zone shape. The volume change (4-6%) and the strain energy associated with the above transformation generate a compressive strain field around the crack tip which acts to stop or retard the crack tip propagation. Further increase in toughness can be realized from the microcracking associated with the $t \rightarrow m$ ZrO_2 transformation, the associated strain energy and the crack deflection by microcracks [98, 99].

In most of the transformation toughed ceramics, strength is inversely related to toughness. Swain et al. [92, 100] observed that for achieving toughness $> 8 \text{ MPam}^{1/2}$, the strength need to be sacrificed. It was noted that for $K_{IC} < 8 \text{ MPa}\sqrt{\text{m}}$, the strength value is flaw controlled while for $K_{IC} > 8 \text{ MPam}^{1/2}$, it is controlled by the extent of transformation toughening.

2.6.1.2.2 Microcracking induced toughening

Microcrack accounts for improved toughness in two ways. The first and major contribution comes in the form of a dilatational effect in the crack wakes. The opening of microcracks results in volumetric expansion in the crack wake which tends to deter crack opening. The crack is pinned or closed due to the volumetric expansion caused by dilatational strains open microcrack in the crack wake. The second effect arises from microcrack ahead of crack tip. These cracks effectively reduce modulus of the material locally at the crack tip. Cracks act as pseudo process zone, giving the region the near the crack tip a certain degree of plasticity thereby making the material more compliant locally and less likely to fail in the brittle fashion. It has also been noted that the effect of the latter contribution must be balanced with the possible degradation caused by the cracks. Typically microcrack form at grain boundary junctions or triple points and occur within the regions of residual tension caused by thermal expansion mismatches or by phase transformation around an advancing crack and they will be found in a frontal zone ahead of the crack as well as in the wake of the cracks once the crack propagates through the initial frontal zone. Microcracks are usually on the size scale of the microstructural grain size [101].

2.6.1.2.3 Toughening by the generation of compressive surface stress

The compressive strains are generated during the volume expansion and shear strain developed during controlled t→m ZrO₂ transformation [62]. The presence of these surface compressive stress (500 to 1000 MPa and concentrated in a depth of about 20 μm) acts to toughen and strengthen the ZTA ceramics because the crack has to overcome these compressive stresses before it can propagate. The compressive stress can be generated through various processes like grinding [102], impact [103] and low temperature quenching [104].

2.6.2 Crack bridging

In this mechanism, the toughening is from bridging of the crack surfaces behind the crack tip by a strong reinforcement phase. By providing some partial support of the applied support of the applied load, the bridging constituent reduces the crack tip stress intensity. Several mechanisms involving bridging of micro-crack tip have been identified as playing an important role in toughening. It has been shown that uncracked grains have been bridging in large grain such as single phase alumina [21, 22, 25, 62, 73, 84, 86, 101]. The bridging grains were observed to survive far back as one hundred grain diameters beside the tip. It was hypothesized that local stresses are the protecting mechanisms as the stress intensity at the tip of the crack is very severe to survive. Although bridging mechanism is most of the time applied to fiber reinforced ceramic composites, bridging particles is also observed in the wake of crack tips in monolithic ceramics. Figure 2.13 shows the mechanism for forming bridging in the wake of a crack.

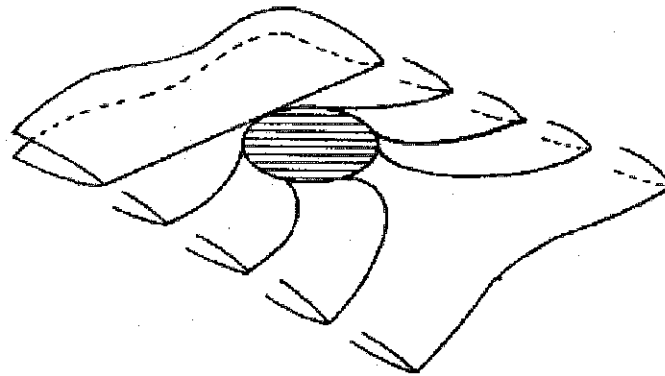


Figure 2.13: Mechanism for forming particle in bridging particles in the wake of a crack [101].

2.7 High temperature properties of ceramic composites

Ceramic composite materials are mainly designed for the application of high temperature working conditions. There is a growing demand of ceramic materials for high temperature structural applications mainly due to their high melting point and good mechanical strength at high temperature. However, their application is limited due to catastrophic failure of these materials when subjected to sudden change of

temperature (thermal shock) or repetitive cycling of temperatures (thermal fatigue). In a thermal shock experiment, when the change in temperature exceeds critical temperature difference (ΔT_C) of the material, the tensile stress generated in the material due to temperature gradient exceeds its actual tensile strength resulting in failure of the material [68, 88, 105, 106].

Thermal shock resistance is one of the important parameters of ceramic composites since it determines their performance in many applications, from ceramic manufacturing to oil refractory, thermal insulation, nuclear power, chemical and petrochemical Industries.

Thermal shock is the thermal stresses that occur in a component as a result of exposure to a temperature difference between the surface and interior or between various regions of the component. The classic theory on the thermal shock resistance of brittle ceramics is established by Hasselman [107] including critical stress fracture theory and thermal shock damage theory. In the theories, some parameters of the thermal shock resistance are introduced to evaluate resistance of crack initiation and propagation or strength degradation after a severe thermal shock. It is well known that the fracture strength is one of the most important factors to improve the thermal shock resistance of ceramics [58, 88, 107, 108]. On the other way, to further improve the thermal application of ceramic composite materials, a number of researches have been done by inclusion of a covalent bonding Si-based ceramics such as silicon carbide and silicon nitride as they have low thermal expansion coefficient and high thermal conductivity [58, 107].

The thermal stress induced typically occurs at the surface during cooling as per Equation. 2.11 and this is applicable for most shapes such as long cylinder (solid or hollow), a sphere (solid or hollow) and flat slabs.

$$\sigma_{th} = \frac{E \alpha \Delta T}{1-\nu} \quad (2.12)$$

Where σ_{th} is the thermal stress, E the elastic modulus, α the coefficient of thermal expansion, ν poisson's ratio, and ΔT the temperature difference.

The equation 2.11 also indicates that the thermal stress resistance increases as the elastic modulus and thermal expansion coefficient of the material increases and at the imposed ΔT in the material can be decreased by configuration modification and possibly by modification of the heat transfer conditions.

Summary

As the most important oxide ceramic materials for structural application, an extensive review of the microstructural and mechanical properties of alumina, silica and zirconia and the combination of them have been well reviewed. In powder processing, purity, particle size distribution, reactivity, polymorphic form, and availability of the powder components has to be considered. Besides that, the densification process and the further sintering process have to be well understood in terms of analytical models, empirical or phenomenological equations, and statistical and numerical techniques so that we will have a controlled output of the composite.

The review comprehensively discussed the possible combinations of the oxide ceramics (alumina, silica, zirconia and mullite) that mechanical properties were improved in the binary system. There were also ternary systems some researchers worked on to understand the interaction of the ASZ composite. However, we can deduce from the discussion that the effect of three component system on the improvement in the mechanical properties was over looked. More importantly, toughening mechanisms such as particle dispersion toughening, crack deflection and crack shielding mechanisms (Transformation toughening, micro cracking induced toughening and toughening by the generation of compressive Surface Stress) were well discussed.

It was stated that the fracture behavior of ceramic materials is essentially different from that of metals. Fracture of ceramic materials is controlled by the direct effect of microstructure on the crack tip. Crack tips in ceramic materials are atomically sharp and crack motion occurs only when the atomic bonds at the crack tip have been stretched to the breaking point. Because of this, fracture toughness is achieved by modifying the microstructure of the solid to reduce stresses near the crack tip. This

stress reduction is achieved by processes such as crack tip deflection or crack tip shielding, which dominate the fracture behavior of ceramic materials. Control of these processes offers the only real possibility of improving the toughness of ceramic materials.

In addition to that, in the last two decade significant advancements have been made in the understanding and development of toughening mechanisms in binary ceramic composites. Unfortunately, many of the system have been affected by the early degradation in the thermal properties. Therefore, the review directs to the development of three (ternary) components systems which are high temperature resistant, thermal shock and high toughening as well.

Finally, the heat resistant properties and the factors which affect the ceramic composites were discussed. Thermal shock resistance refers to a material's ability to withstand rapid changes in temperature. Mullite is heat tolerant material, which displays superior resistance to thermal shock, is expected to improve the thermal shock resistance of the ternary ASZ composite.

CHAPTER 3

METHODOLOGY

3.1 Overview

This chapter explains the methodologies and specific procedures used to investigate the objectives set by the research. Several experiments, characterization and analytical works have been carried out in a systematic way. The chapter is divided into two main sections. The general steps followed are discussed in the methodology section where the steps would be outlined in detail. In the second section, the detail of the sample preparation and characterization is presented. In this discussion the material used, techniques and equipments utilized are explained. Procedure and settings as well as the considerations in executing the experiments are also presented.

3.2 Methodology

The research work investigated a systematic development of ASZ composite and its microstructure, phase evolution, room temperature mechanical properties, thermal shock behaviour in high temperature application and the toughening mechanisms. Several ceramic composites of different composition of alumina, silica and zirconia have been prepared and investigated. All the sample materials were prepared in the similar method, i.e. ball milling, drying, pressing followed by sintering at the appropriate temperature. The overall methodology, typical procedures, materials used and the equipments used are explained in this chapter.

Figure 3.1 shows the research methodology mapping in which the flow and the activities listed in a systematic way. On the start of the process, the particle size and shape analysis of the starting powders has been done to justify and predict the

property of the mix and compacted samples. An iterative optimization process was done to determine the appropriate pressure needed for the cold uniaxial compaction of the mix powders. An arbitrary mix was taken 80% wt Al_2O_3 , 10% wt SiO_2 and 10% wt ZrO_2 for an equal amount of the reinforcement to determine the appropriate pressure. Five samples were prepared for each compaction pressure and then the average green density was taken as a result. The consecutive compaction pressure range applied was 150, 180, 200, 250, 300, 350, 400, 450, 500, 550, and 600 MPa.

To determine the optimum mix, twelve samples shown in Table 3.2 with different proportion of each component. At a sintering temperature of 1650°C , each sample was sintered and measured for density. This process was repeated for five times and the result with highest density from each component composition was taken as the optimum mix for further study.

In order to identify the optimum sintering temperature used in the experiment, a successive temperature ranges (950, 1000, 1050, 1100, 1150, 1200, 1250, 1350, 1400, 1450, 1500, 1550 1600 and 1650°C) were used and the produced samples were characterized for density, crystallinity and hardness. The temperature at which optimum results in terms of the parameters mentioned above is used as the sintering temperature for further experiments. After setting the appropriate compaction pressure, component mix and sintering temperatures, samples of standard size were produced and different analytical and characterization parameters were measured to understand the behaviour of the composites produced.

In order to achieve a cohesive and structurally integrated shape, a loose ceramic powder must be compacted before sintering. Although a number of other processing techniques are also being developed, die compaction will continue to be a widely used means of material manufacture simply because of its economy in large-scale production. In this research, uniaxial compaction methods have been used. The standard sample size has been prepared according the die manufactured in the laboratory.

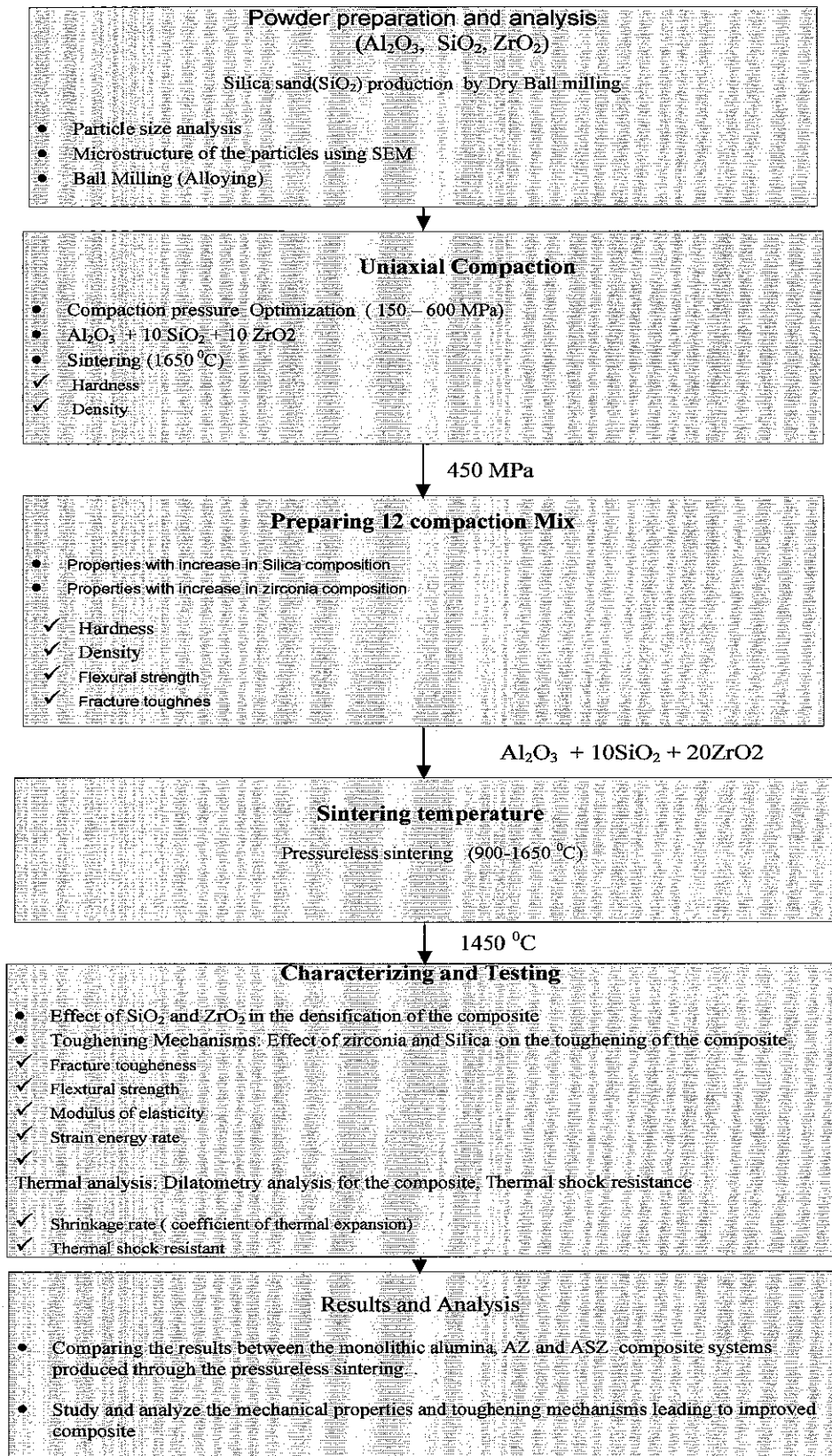


Figure 3.1: Research methodology adapted in this research

After sintering, the composites were investigated for different mechanical and physical properties. Effects of SiO₂ and ZrO₂ in the densification of the composites system were investigated. Mechanical properties (fracture toughness, flexural strength, modulus of elasticity and strain energy rate) were measured and compared among the monolithic, binary and ternary composites produced. Finally the application of the composites produced in high temperature was evaluated by exposing the samples in a high temperature gradient so that the resistance to thermal shock was studied.

3.3 Sample preparation and material characterization

The selection of materials and processing routes are key decisions which must be made wisely in order to achieve dense structurally sound ceramics or ceramic compounds. Unwise material preparation may lead to excessive porosity, material inhomogeneity, and cracking. An optimal relationship for the distribution of fine particles in the selected alumina–zirconia–silica compositions and an established pressureless sintering route were used.

3.3.1 Sample preparation

Powder preparation

In this research, the commercially available micro size Al₂O₃ (90 μm) and zirconia (ZrO₂) (17 μm) both from Merck KGaA Germany starting powders, as well as SiO₂ (6.6 μm) were used. The SiO₂ ceramic was produced in the laboratory by the dry milling process from locally found silica sand around Tronoh, Perak, Malaysia. Mullite has a composition of 3Al₂O₃.2SiO₂ and formed from the reaction between alumina and silica during sintering. X-ray fluorescence was used to analyze the purity of each component powder as shown in Table 3.1.

Table 3.1: composition of alumina, silica and zirconia used in the study

	Purity (wt.%)	Impurities (wt.%)			
		CaO	P ₂ O ₅	Fe ₂ O ₃	Ga ₂ O ₃
Al ₂ O ₃	98.79	0.156	1.04	-	0.008
SiO ₂	94.75	2.01	2.35	0.90	-
ZrO ₂	98.74	0.558	0.688	0.0289	-

Powder particle size analysis was done in a Malvern™ Mastersizer equipment operated between the size range of 0.02 - 3000 μm. The apparatus has a stirring mechanism so that possible agglomeration can be avoided. Multiple recursive trials were made with each batch to account for the statistical size discrepancies of irregularly shaped particles and the last trial was accepted as the final data.

The ceramic oxides used and the composition to prepare the samples are given in Table 3.2 and Table 3.3. The range of weight percentages (wt.%) of the constituent oxides was benchmarked based on previous works when each element used for reinforcing purposes of other ceramic oxide composites [67, 109-111]. Ceramic composite samples ranging from zero to 25 weight percentage of SiO₂ and from zero to 30 weight percentage of ZrO₂ was used as reinforcements. In order to prepare the composite mixtures, the constituent powders were weighed in a precision balance (Mettler Teldo, Switzerland) as shown in Figure 3.2 in various proportions and mixed thoroughly. Wet ball Milling (US stoneware, 764AVU) equipment was used for the mixing as well as alloying and further crushing the mixture as shown in Figure 3.3. In preparing the mix, it was ensured that the powder mix was evenly distributed. This was achieved through the use of a dispersant (alcohol) which helped in avoiding agglomeration. Polyvinyl alcohol (PVA) was used as a binding agent and Polyethylene glycol as a plasticizer in the preparation.

Table 3.2: Composition of the powder mix of the composite samples used in the study

Sample	Composition (wt %)		
	Al ₂ O ₃	SiO ₂	ZrO ₂
S ₁	90	10	0
S ₂	85	10	5
S ₃	80	10	10
S ₄	75	10	15
S ₅	70	10	20
S ₆	65	10	25
S ₇	90	0	10
S ₈	85	5	10
S ₉	80	10	10
S ₁₀	75	15	10
S ₁₁	70	20	10
S ₁₂	65	25	10

Table 3.3: The composition of samples showing the varying concentration of ZrO₂ to study the effect of zirconia concentration

Sample	composition wt.% ZrO ₂ , wt 10% SiO ₂	No. Of sample	composition wt.% ZrO ₂ , wt 10% SiO ₂
1	2.5	7	17.5
2	5	8	20
3	7.5	9	22.5
4	10	10	25
5	12.5	11	30
6	15		

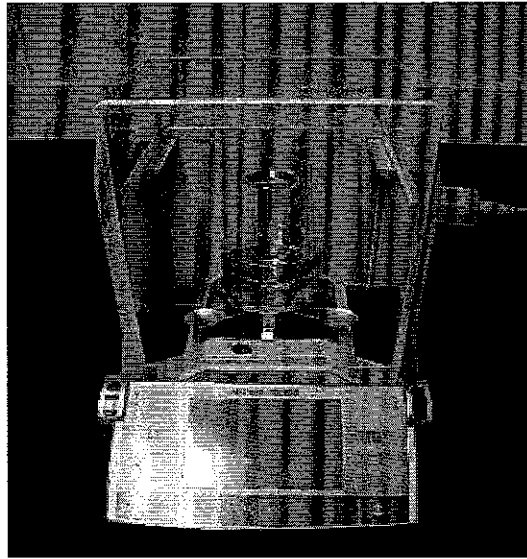


Figure 3.2: weighing precision balance

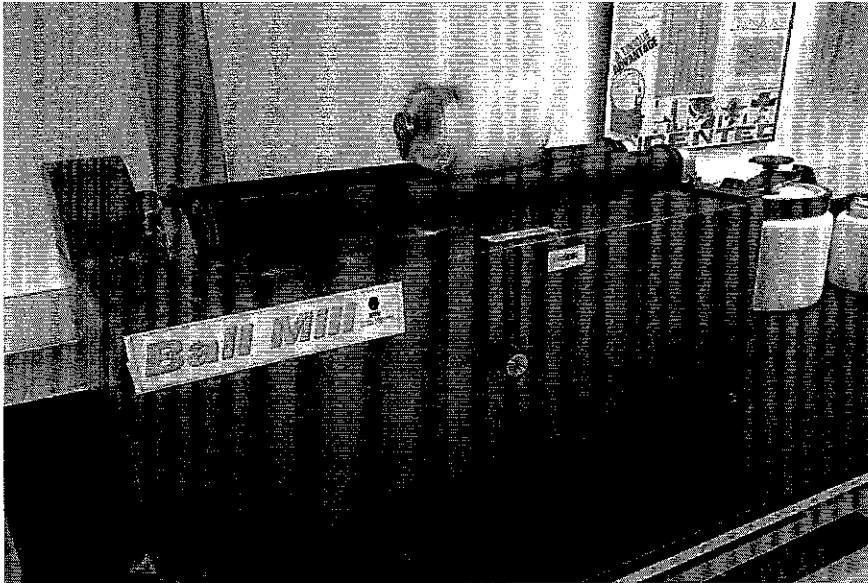


Figure 3.3: Ball Mill (US STONEWARE, 764 AVM)

Powder compaction

The ball milled powders were then dried and sieved to a particle size $< 63 \mu\text{m}$. The prepared powder mix were then filled in a standard rectangular (4x6x35 mm) and circular die cavities (with 13.4 mm internal diameter) and were cold pressed using a hydraulic press (Carver, PW190-60, US) show in Figure 3.4 up to a maximum

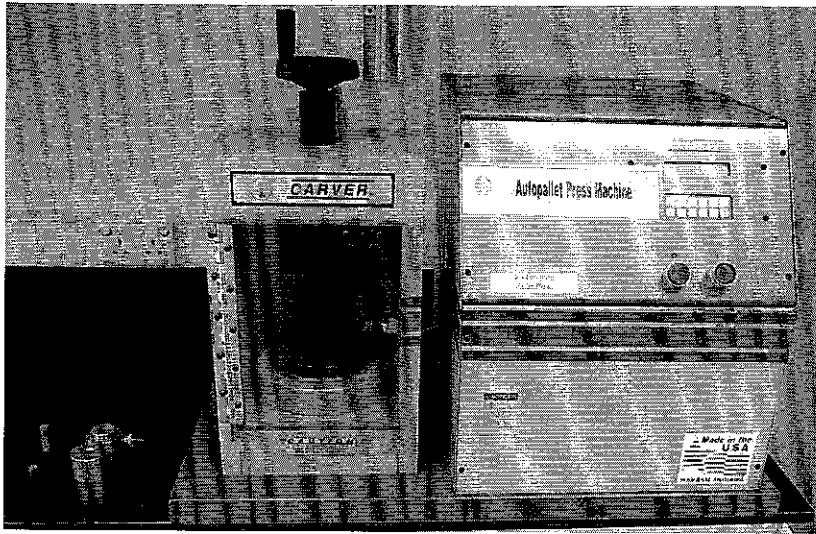


Figure 3.4: Hydraulic Autopallet Press Machine

applied pressure of 600 MPa. The green compacted samples were prepared and measured for density.

Sintering

The pallets or cold compacted samples were reaction sintered in an electrical temperature – controlled tube furnace (heated by graphite elements shown in Figure 3.5 with a heating rate of 10°C/min to 600°C, held it at this temperature for 15 minutes to remove the binder constituent. It was then heated at the same rate to 900 °C, held again for 25 min for chemical homogenizing. At same rate the temperature was increased up to 1650°C and then soaking it isothermally for 4 hours. Finally, with a cooling rate of 20°C/min, the temperature dropped to room temperature. Figure 3.6 shows the sintering schedule of the process.

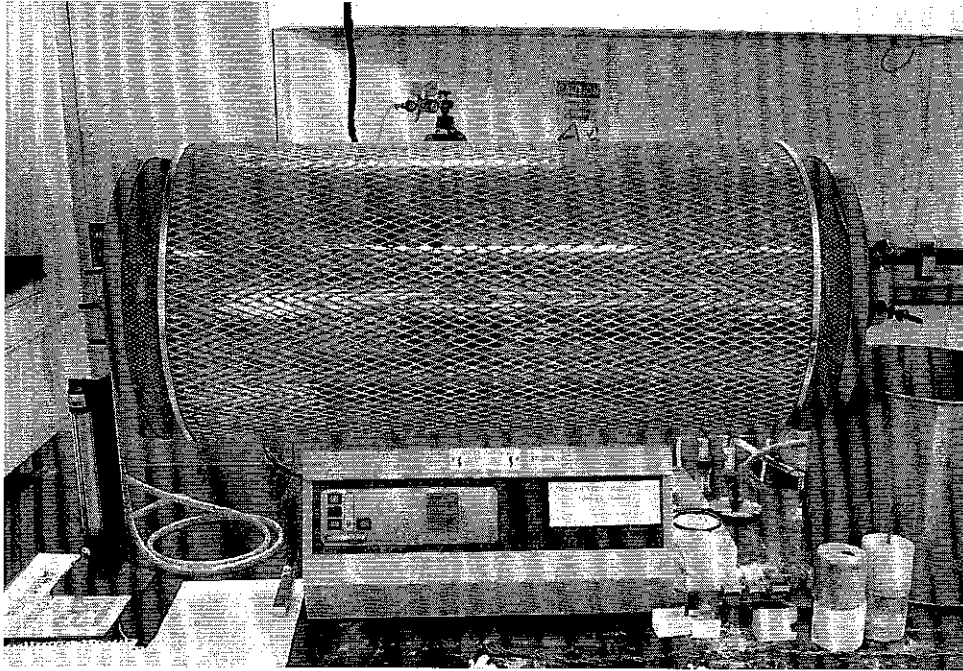


Figure 3.5: Carbolite sintering alumina tube furnace setup used for the study

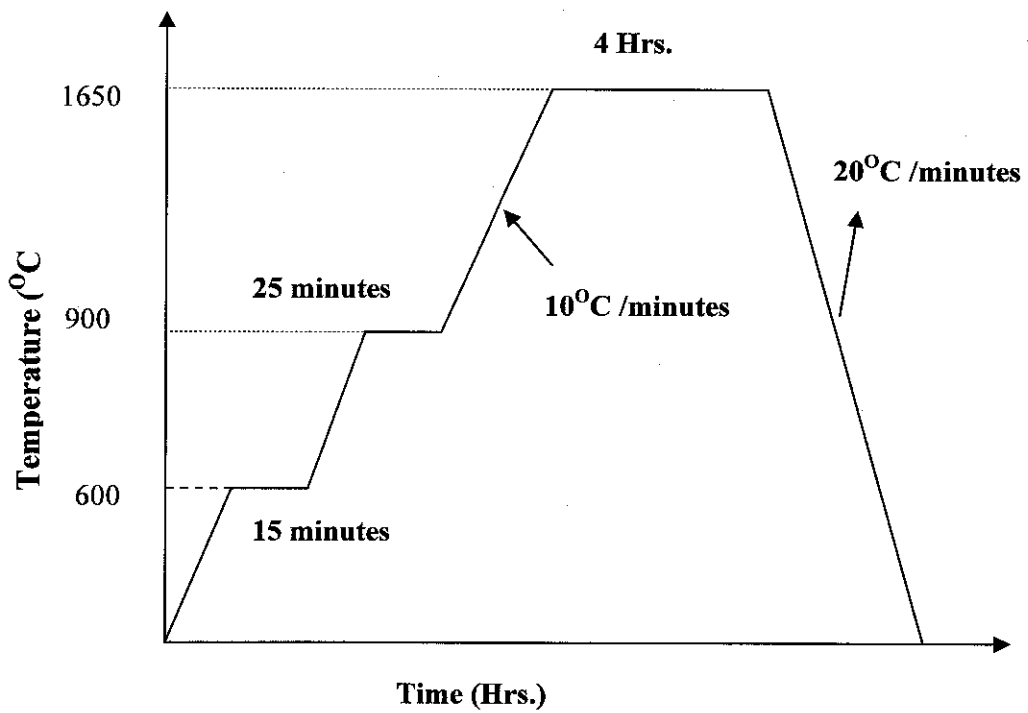


Figure 3.6: Sintering schedule for the composite preparation

3.3.2 Characterization and Testing

The samples were smoothly ground and polished using a SiC paste and cleaned. The phase composition and crystalline properties of the samples were studied by XRD (Bruker AXS D8 diffractometer) using Ni-filtered Cu K α radiation and the microstructure features and fragmented surfaces of the composite were observed by Field emission scanning electron microscopy (FESEM) (Zeiss Supra 55 VP) with simultaneous chemical analysis by energy dispersive spectroscopy (EDS).

The densities of the bulk sintered samples were measured by Archimedes water immersion method, while their hardness was obtained under a 1000 g load for 15 seconds by using micro Vicker's Indentation. Vickers hardness (Hv) was determined from a minimum of 10 indents.

The flexural strength was measured using three point bending method on a universal testing machine, while Indentation Fracture (IF) method was used to determine the fracture toughness of the composite. For the flexural strength, a rectangular bar of 4 x 6 x 45 mm was produced for the material system. It was placed on support 25 mm apart and the test was conducted at a crosshead speed of 0.5 mm/min by means of a universal testing machine (Instron Model 1185, Instron, USA). The load applied to the test specimen and the corresponding deflections were measured at the point of fracture.

In the following subsections the details of the characterizing equipments and procedures used will be elaborated in detail.

3.3.2.1 Density measurement

The densities of sintered samples were measured by Archimedes density principle in distilled water. Before testing, the sample was completely dried and then weighed in air (A). Then the sample was soaked in water to weigh its wet weight (B). Little oil was added to the water to remove the attached air bubbles from the surface of the sample. After the sample was soaked in the distilled water, it took minutes until the

weight becomes stable, and then the wet weight was recorded. The density of the sample (ρ_{sample}) was calculated using the Equation 3.1

$$\rho_{\text{sample}} = \frac{A}{A-B} [P_o - P_l] + P_l \quad (3.1)$$

Where ρ_{sample} is the density of the solid

A-Weight of the sample in air

B-Weight of the sample in auxiliary liquid

Po-Density of the auxiliary liquid (water)

Pl-Air density (0.0012 g/cm³)

The densification of the sample is calculated using the equation 3.2.

$$\text{Densification} = \rho_{\text{sample}} / \rho_{\text{theory}} \quad (3.2)$$

Where ρ_{theory} is the theoretical density which can be calculated using the rule of mixtures in Equation 3.3

$$\rho_{\text{theory}} = \rho_1 \cdot V_1\% + \rho_2 \cdot V_2\% + \rho_3 \cdot V_3\% \quad (3.3)$$

Where ρ_I is density of the I phase and V_I is the volume percent of the I phase.

3.3.2.2 Hardness Measurement

In this current work, to measure the hardness and fracture toughness of the sintered ceramic composite, a micro hardness test was used for indentation. The load to be tested was well polished and finished with 1200 grit paper until there is no scratch on the surface when observed under optical microscopy.

The hardness measurement was obtained under a 1000g load for 15 seconds by using Vicker's Indentation. Vickers hardness (Hv) was determined from a minimum of 10 indents and then it was calculated using Equation 3.4 [35]. The diagonal of the indentation and crack length was measured using the optical microscopy as shown in Figure 3.7.

$$H_v = 1.85 \frac{P}{D^2} \quad (3.4)$$

Where p = Load in kgf

D = Arithmetic mean of the two diagonals, d_1 and d_2 in mm

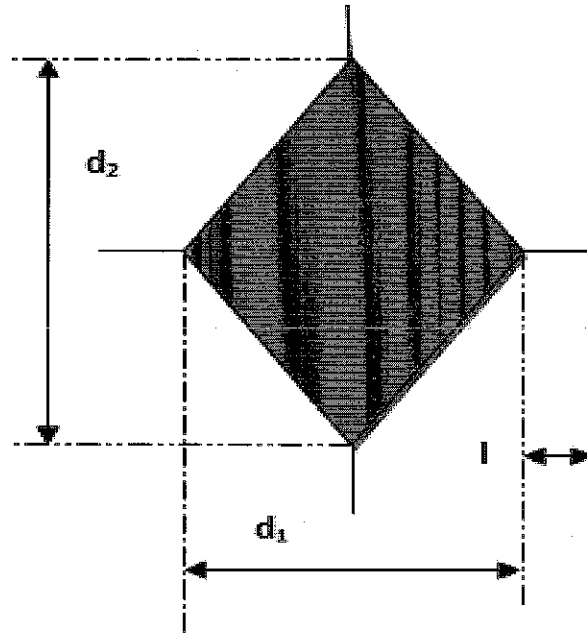


Figure 3.7: Schematic crack generated by Vicker's Indenter.

3.3.2.3 Fracture Toughness Measurement

Fracture toughness measurement was performed by first making an indentation on the samples and then using the Indentation Fracture (IF) method [4], involving calculation of K_{IC} from measured crack lengths emanating from corners of indent diagonals. K_{IC} calculations are based on relations proposed by various models [112, 113]. In this work however, fracture toughness for the samples was calculated using an equation derived by Anstis et al [114] from a two-dimensional fracture mechanics analysis, as follows:

$$K_{IC} = 0.016 \frac{P}{C_0^{3/2}} \left[\frac{E}{H} \right]^{1/2} \quad (3.5)$$

where P is the load in Newtons, $C_0 = \left(\frac{d}{2} + 1 \right)$ (from Figure 3.7) is the crack length from the center of the indent to the crack tip in meters, E is the Young's modulus in GPa and H is the Vicker's hardness in GPa.

3.3.2.4 Flexural Strength Measurement

The flexural strength was measured using three point bending method on a universal testing machine, while Indentation Fracture (IF) method was used to determine the fracture toughness of the composite. For the flexural strength, a rectangular bar of 4 x 6 x 45 mm was produced for the material system. It was placed on support 25 mm apart and the test was conducted at a crosshead speed of 0.5 mm/min by means of a universal testing machine (Instron Model 1185, Instron, USA) shown in Figure 3.8. The load applied to the test specimen and the corresponding deflections were measured at the point of fracture. The three point bend stress was calculated by the following Equation [7].

$$Stress(\sigma) = \frac{3Lp}{2WT^2} \quad (2)$$

Where: Stress in (MPa)
 L= distance between supports (mm);
 p= load (N);
 W= width of specimen bar (mm);
 T= thickness of specimen bar (mm)

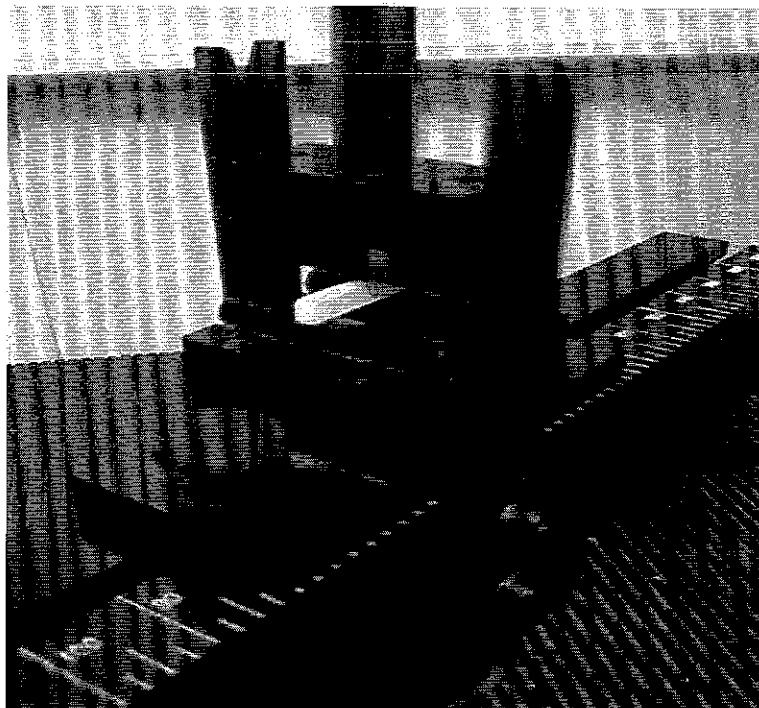
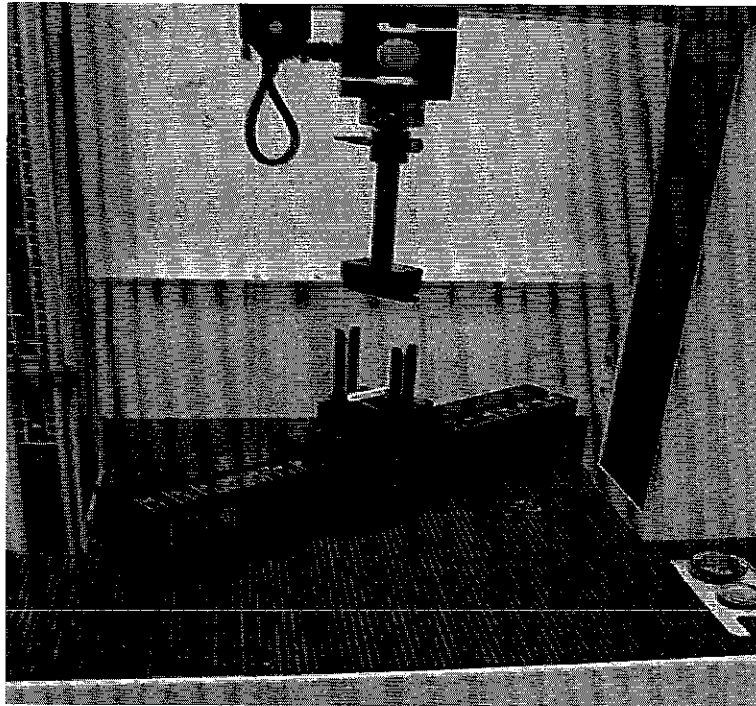


Figure 3.8: Experimental set up for the flexural strength of the sintered samples

3.3.2.5 X-Ray Floresence analysis (XRF)

To determine the major and trace elements of each powder, the XRF analysis was used. By this analysis, it was possible to know the detail information on chemical composition of the alumina, silica sand and zirconia powders. The principle and analysis of the major elements is dependent by the behavior of the atoms when they interact with the radiation.

3.3.2.6 FESEM Characterization

FESEM was used primarily to identify the phases present and determine the mean grain size. Specimens for analysis were ground flat and polished using 1 um diamond paste. It was also used to analyze the elements (aluminum, zirconia and silica) level at a point using the EDS system which detects X-rays emitted from the sample as a result of the high-energy electron beam penetrating into the sample. X-ray spectra can be collected and analyzed, yielding quantitative elemental information about the sample produced. A "standardless" routine is utilized, which yields an accuracy of 1-2% and sensitivities for some elements down to 0.1 weight percent. Lines cans and x-ray maps can also be generated. The FESEM (Ziess Supra 55 VP) used for this research is as follows shown in Figure 3.9.

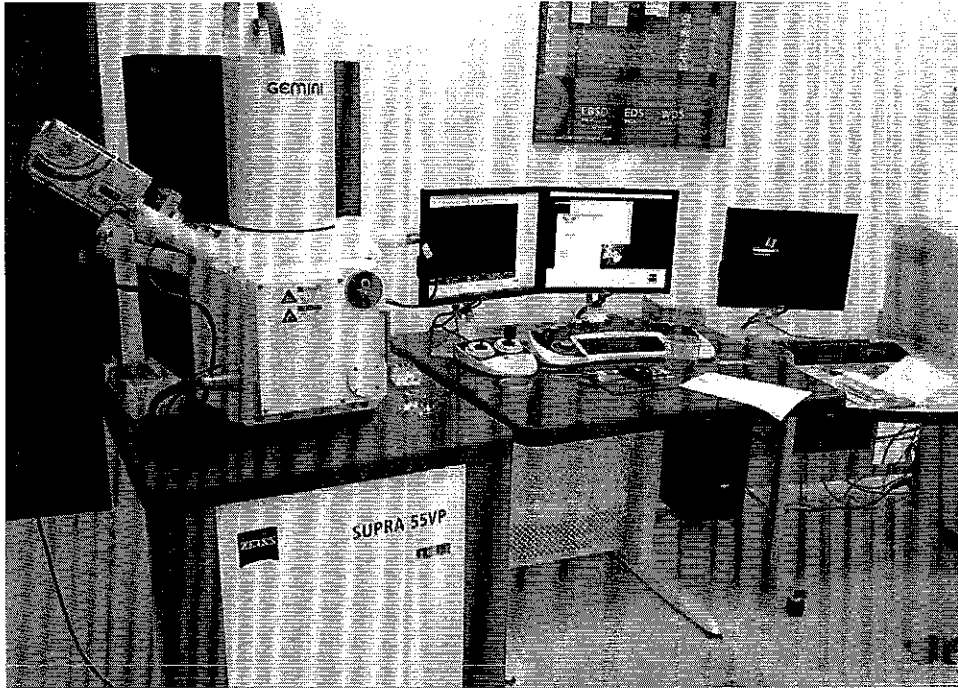


Figure 3.9: FESEM used for the research

3.3.2.7 Atomic Force Microscope (AFM)

The grain sizes of the sintered samples were measured using the Atomic Force Microscope (AFM) shown in Figure 3.10. It was developed to image almost any type of surface, including polymers, ceramics, composites and glass samples. It can image conducting or semiconducting surfaces. AFM or scanning force microscopy (SFM) is a very high-resolution type of scanning probe microscopy, with demonstrated resolution on the order of fractions of a nanometre, more than 1000 times better than the optical diffraction limit. We used a laser beam deflection system, introduced by Meyer and Amer, where a laser is reflected from the back of the reflective AFM lever and onto a position-sensitive detector. AFM tips and cantilevers are microfabricated from Si or Si_3N_4 .

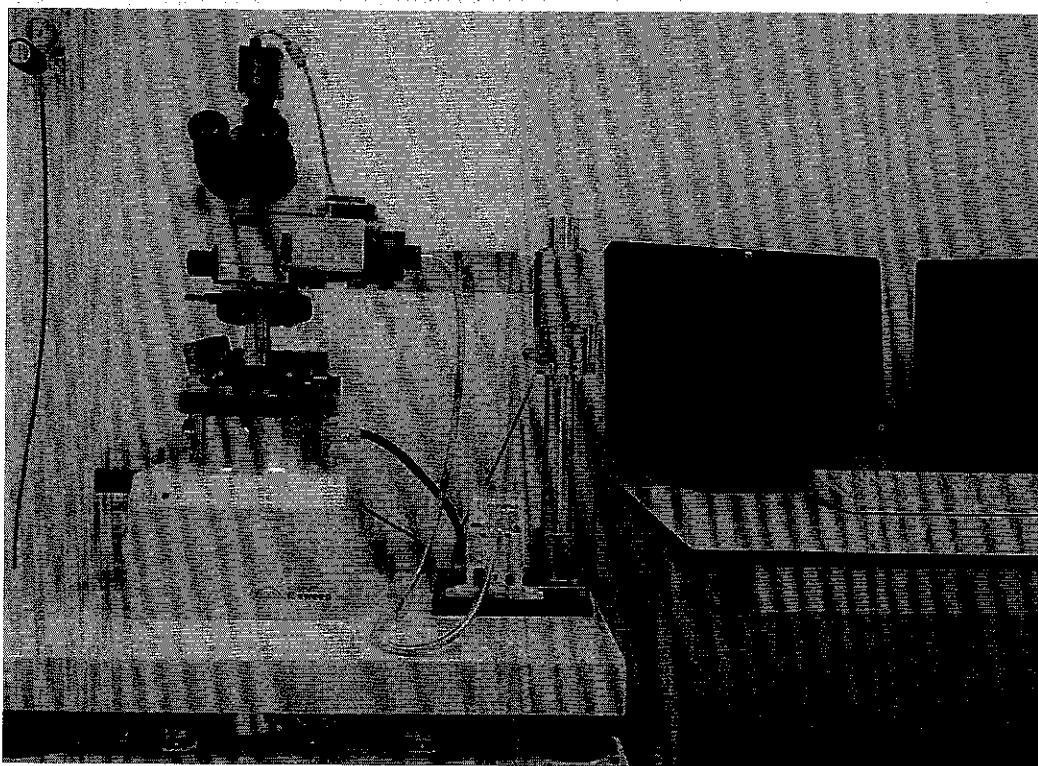


Figure 3.10: AFM (SII Nano Technology Unit, Nano Navi (e-sweep)) used for the research

3.3.2.8 XRD Characterization of the Sintered sample

As a means of identifying sintering reactions X-ray diffraction (XRD) as shown in Figure 3.11 was used to identify crystalline phases that formed during and at the end of the sintering process. Samples were analyzed with grains in random orientations to insure that all crystallographic directions are "sampled" by the beam. When the Bragg conditions for constructive interference are obtained, a "reflection" is produced, and the relative peak height is generally proportional to the number of grains in a preferred orientation. The analysis is performed by comparing the diffraction pattern collected from an unknown sample with the diffraction patterns of known compounds. The experimental patterns were compared with the diffraction scans of pure compounds maintained in the ICDD Powder Diffraction File (PDF). Data reduction and S/M analysis was performed using the ANOVA software package. All scans were

smoothed, theta corrected, and the background was removed. The results of Search/Match analyses are shown below each plot as a set of stick lines from the PDF.

Analyses were carried out on a standard Philips diffractometer operating at 30 mA at 40 kV using CuK α radiation. The scanning speed was 0.5 degree per minute. Samples were cut and surface ground and mounted using 'Blutac' adhesive.

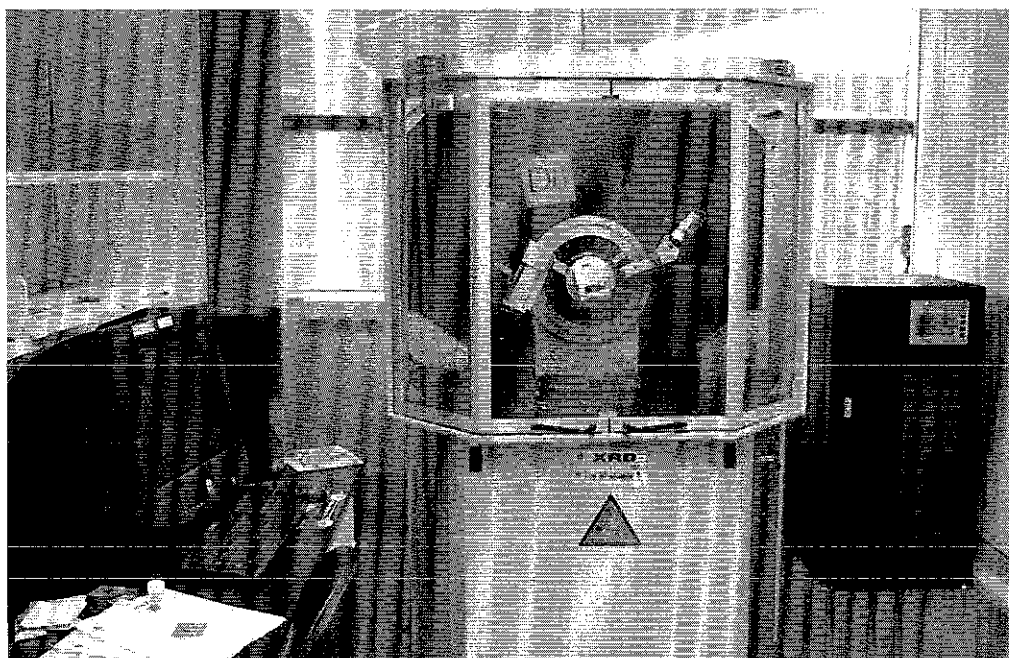


Figure 3.11: XRD-Bruker AXS D8 Advance

3.3.2.9 Dilatometry Study

The alumina rode delatometer (Netzsch DIL 402) as shown in Figure 3.12 was used to measure the changes in volume or length of the samples as a function of temperature while the sample is subjected to a controlled sintering cycle. Dilatometer is a very sensitive experimental tool to analyse the kinetics of solid state transformations according to its dilation. The amount of expansion depends on the characteristics of the material. The curve generated is a function of dimension against temperature [48, 115].

The dilatometric study allowed us to study the following properties:

- Thermal expansion and coefficient of thermal expansion was determined to understand the rate at which a material expands as a function of temperature.
- Sintering temperature and shrinkage behavior:

The test sample was heated in a furnace and displacements of the ends of the specimen were transmitted to a sensor by means of push rods to determine the linear displacement as a function of temperature.

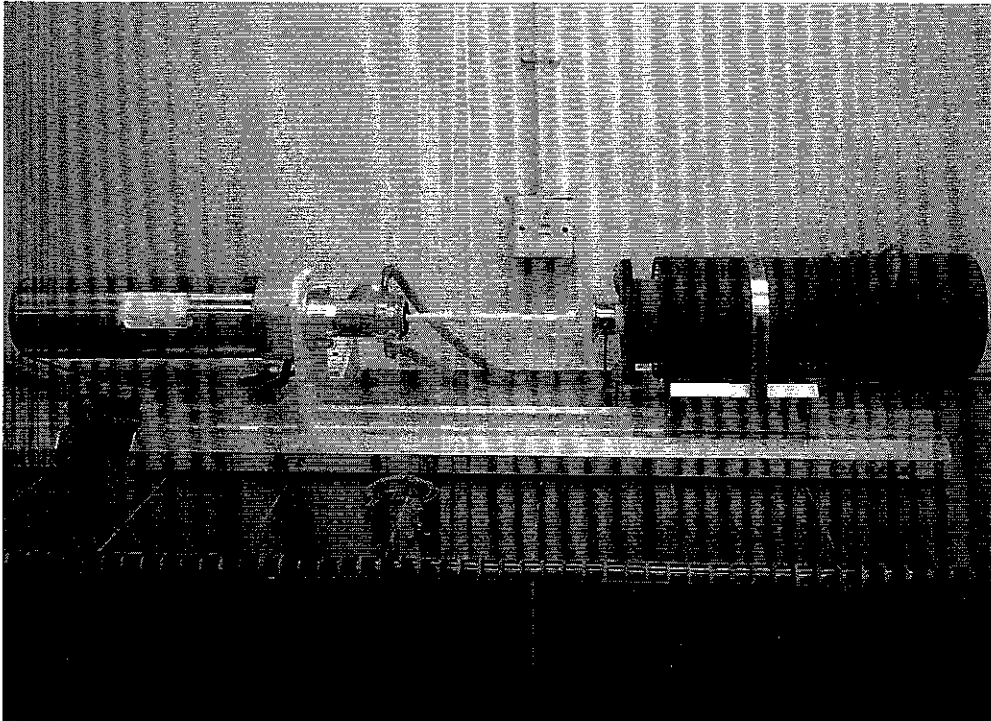


Figure 3.12: Dilatometer in horizontal configuration used in the study (SIRIM Berhad Malaysia)

3.3.2.10 Thermal Shock Resistance

The thermal shock resistance of the sintered test sample is the resistance to crack initiation or propagation under thermal stress when subjected to a rapidly cooling down from high temperature to low temperature. Standard test (ASTM C1171) [116] method for quantitative measurement of the effect of thermal shock on refractories was applied.

- The strength was measured by the difference in the modulus of rupture (MOR) between uncycled specimens and the specimen subjected to thermal cycling.
- The reduction in structural continuity was measured by the difference in the mechanical property before and after thermal cycling.
- Recommended furnace temperature for thermal cycling : 95 °C
- Dryer of 105°C, for 30 min.
- Soaking quenching temperature: 25°C for 30 seconds.

The thermal shock resistance of composites was evaluated by water quenching technique as shown in Figure 3.13. Therefore, to study the effect of number of cycles for failure, the experiment was done by heating the samples at 5°C /min up to a temperature of 950°C with a soaking time of 30 min at the temperature and followed by rapid cooling in quenching water till the samples attained room temperature. To investigate the effect of thermal shock on the cracking behaviour of the sample, thermal shock resistance tests were performed on the samples. A microstructural study was done to investigate the effect of thermal cycling on the monolithic alumina, A20Z and A10S20Z composites.

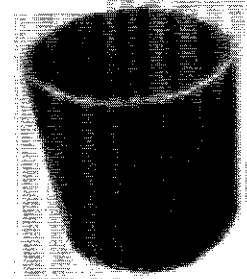
A programmable control thermal shock Furnace

(1)



Heating rate: 5°C /min
Cyclic temperature: 950 °C
Soaking time: 30 min

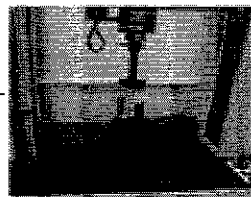
(2)



Temp.: 25±2 °C
Soaking time: 10 min

Water bath

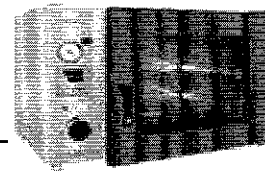
(4)



Three point bending test



Indentation Test



Dryer of 105°C

(3)

Figure 3.13: Thermal shock resistance test using water quenching method

In order to study the critical temperature change of the composite sample, a thermal shock experiments were performed in a box furnace (in air). Specimens were inserted into the preheated furnace and were held there for 30 min before quenching by dropping into a bath of water (25°C). Tests were carried out at temperature differences, T , between 250 and 650°C. The flexural strength at room temperature was measured by a universal testing machine (MTS tester) at each soaking temperature using a three point bending method. The span length and cross-head speed were 25 mm and 0.1 mm/min respectively. The hardness and the fracture

toughness were measured on a H_V hardness tester by vickers indentation technique with a load of 1kgf. The reported values were the mean of 5 samples.

Summary

In this chapter the methodology used to implement the experiments in the research was discussed. Experimental investigations and observations were undertaken at each stage, starting from powder processing to the process of developing the ASZ composites. The procedures used in executing the experiment have been clearly discussed and the equipments used were described. From the starting, the material preparation and study of the particle was carried out to predict the property of compaction and sintering process. Density, hardness and mechanical properties such as flexural strength and fracture toughness measurement tests were undertaken for the composite developed. Microstructure and phase change analysis using FESEM, XRD and dilatometry was carried out during the composite development. Finally, ASTM standard water quenching experiment was carried out to investigate the thermal shock resistance of the composites developed.

CHAPTER 4

RESULTS AND DISCUSSION

4.1 Overview

This chapter discussed the overall results of the experimental works. The formation of ASZ ceramic composite by pressureless sintering route is discussed. Reactions that may occur during sintering are suggested and parameters that affect the resulting density are discussed including the mechanical properties.

In the first section of the chapter, the results on the particle shape and size analysis was discussed. Based on the results from the FESEM and XRD, a prediction of the resulting material was discussed. Similarly, an optimization process for the compaction pressure and composition of the tri-component composite was done. In the same section, microstructure, compositional and mechanical properties were studied.

In the second section of the chapter, a dilatometry study was done to measure the shrinkage behaviour and thermo physical changes during the process of pressureless sintering. This would help to understand the process parameters such as sintering temperature used.

In the third section of the chapter, comparisons of the mechanical properties of the monolithic alumina, alumina-zirconia and alumina-silica-zirconia composites is proceeded to understand the improvements and some trends in the properties. The Fracture behaviour and toughening mechanisms were also studied for each of the composite.

In the final section of chapter, the materials were investigated for the resistance to thermal shock resistance working for high temperature application. The study was

also focusing on the effect of cyclic temperature and critical temperatures in the mechanical properties like fractural toughness and flexural strength. Finally a conclusion and remarks were done for the outcome of the results.

4.2 Pressureless Sintering and Characterization of $\text{Al}_2\text{O}_3\text{-SiO}_2\text{-ZrO}_2$ composite system

It is not only the number of components in a system that affect the properties of the composite, processing method also does. As it was explained about the different ceramic powder processing, there are many processing route methods to produce a ternary oxide ceramic such as reaction sintering, hot press sintering technique, hot isostatic press technique, sol-jel technique, colloidal processing technique and laser zone remelting [3, 4, 18, 117]. However, owing to raw material availability and production related costs, the most common routes are reaction sintering and solid-state reaction between oxides and hence, controlling the final microstructure would be a determinant factor in limiting the severity of critical defects for it has to adjust the phase transformations and microcracking.

The application of oxide systems of ASZ have been mainly used as a refractory material. This study aimed to investigate the role of SiO_2 and ZrO_2 in the densification, hardness and microstructure for further study in its application as a structural material. A conventional powder processing route with a pressureless sintering is used to investigate the sintering behavior of the ternary oxides. Different composition of the component elements were taken to obtain some of the needed experimental data and provide further insight into the powder processing, densification and characteristics of the developed composite. Specifically, this section investigates how the starting component composition affect the phase and chemical composition of the sintered product and hence the density, hardness and microstructure. Material characterization techniques such as SEM observation and XRD analysis were performed to identify the morphology and crystal structure.

4.2.1 Powder characterization

Particle size and distribution of fine ceramic powders are the primary physical parameters that have considerable impact on the properties of unsintered (green compact) and fully dense ceramic components. The particle size distribution (PSD) affects powder consolidation and densification steps during powder processing through the packing density. Most often, the objective of these steps is to achieve a maximum particle and uniformity of packing, so that a minimum shrinkage and porosity are retained in the dense ceramic. One of the principal requirements in ceramic powders processing is the knowledge of the agglomerates and the size distribution of primary particles. Therefore, the measurement of PSD is needed for the starting powders as well as during processing so that the desired properties and microstructures can be achieved.

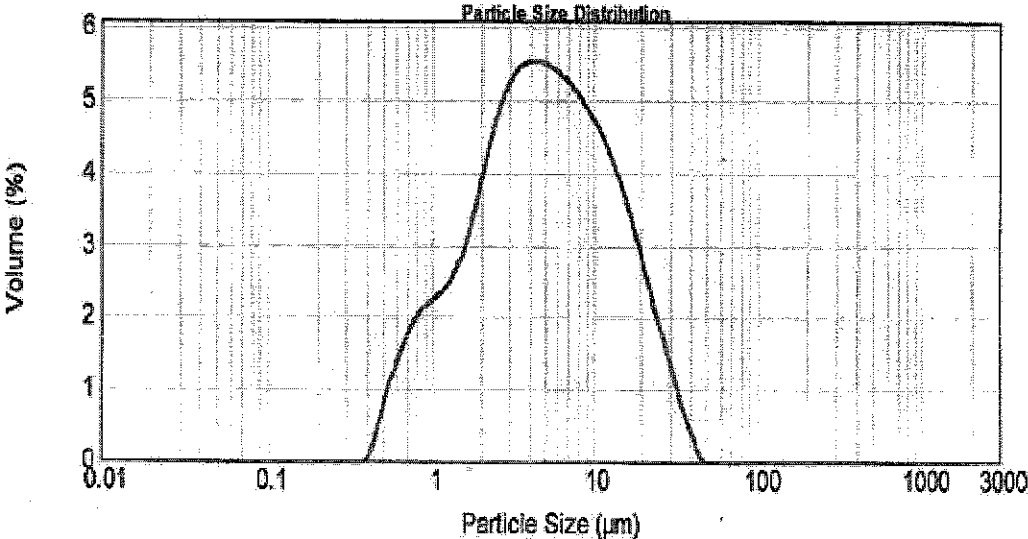
4.2.1.1 Particle Size Analysis

In order to analyze and tailor the composite microstructure, discrete particle reinforcement is desired. By controlling the particle sizes and size ratio between the matrix and inclusion phases, it is possible to obtain adequate sinter bonding in the alumina-rich compositions and acceptable mechanical properties. In this study, a bigger particle was used for the dominant matrix phase and smaller particle for the reinforcing inclusion phase.

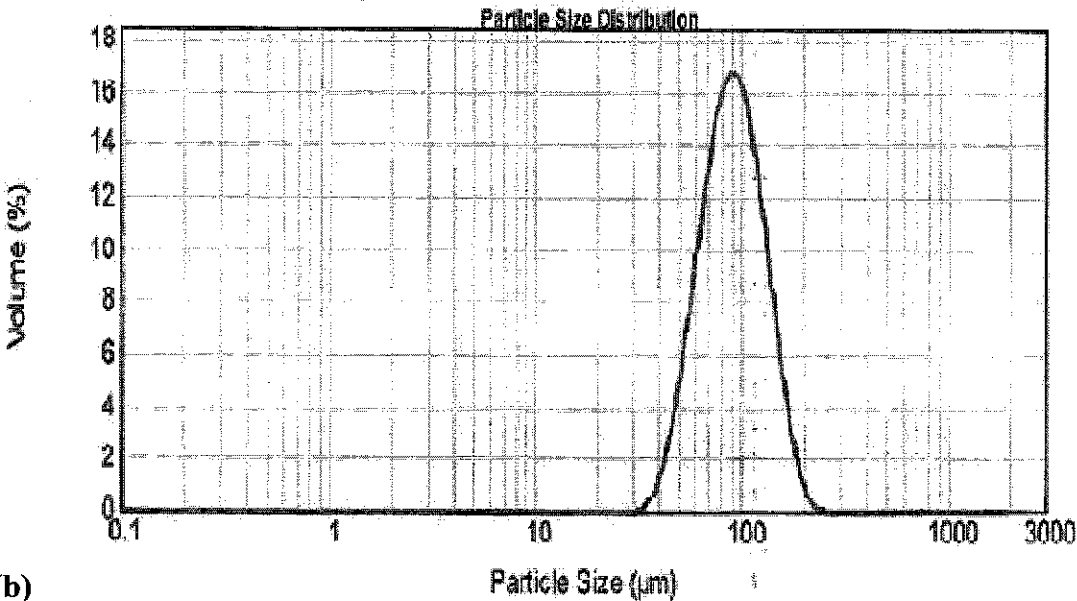
The starting materials used are listed in Table 3.1. They were mixed in appropriate amounts to produce a range of ceramics of known composition on sintering. For each of the particle powder an XRF test was made to study the purity of the powder as well as to predict the final properties.

To achieve submicron particle size the mixture was ball milled in isopropyl alcohol using high purity zirconia balls (i. e. wet ball milling) for six hours. This had previously been found to be sufficient to produce a thoroughly mixed submicron grain size powder [49]. Particle sizes were determined by particle size analyzer.

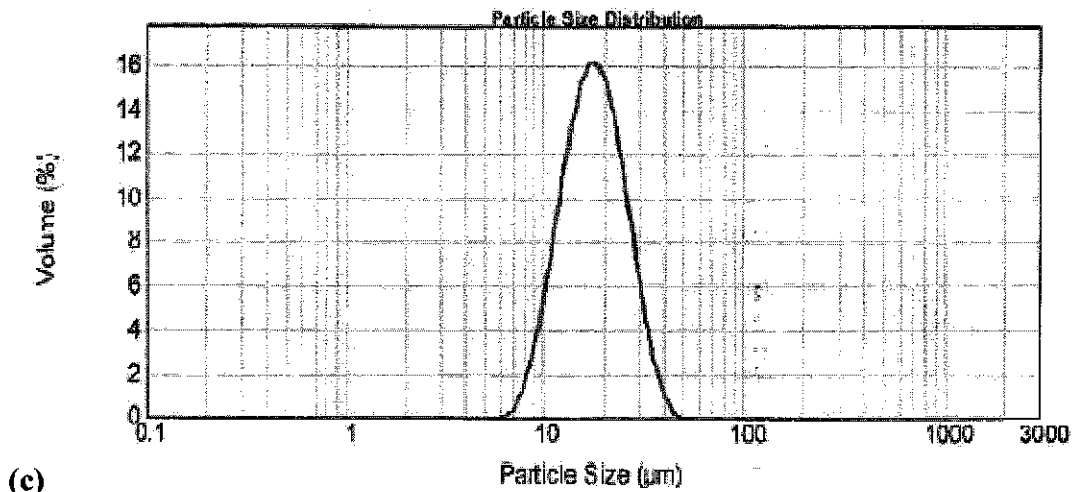
As can be shown in Figures 4.1(a), 4.1(b) and 4.1(c), the ceramic powders used have a Gaussian particle size distribution and they have an average particle size of 90, 6.6 and 17 μm with an estimated specific surface area of 0.07, 2.1 and .36 m^2/g respectively. Figure 3d shows that the average median particle size of the ball milled mix of the three ceramic powder system is 6.5 μm and the specific surface area is a 2.2 m^2/g .



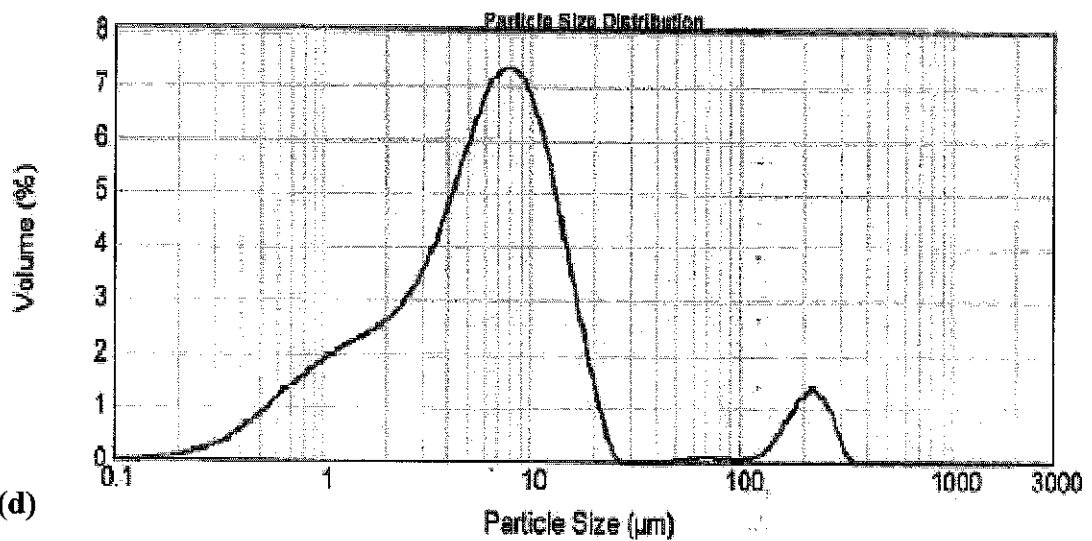
(a)



(b)



(c)



(d)

Figure 4.1: Particle size distribution of (a) silica sand (b) alumina (c) zirconia (d) as-milled $\text{Al}_2\text{O}_3\text{-SiO}_2\text{-ZrO}_2$ composition

A broader particle size distribution also results in an enhanced degree of variations in local particle packing, hence local differential densification, in the compact. Beyond a certain particle size distribution, this could result in a coarser pore structure in the sintering compact, which, in turn, would offset the beneficial effect on sintering brought about by particle size distribution. The alumina and zirconia particles distribution showed a narrow particle distribution which was important for the composite development. However, the silica size particle distribution was wide,

which may be because of the agglomerates inside the particles. To reduce the non uniform size distribution a ball milling process was used for further homogenization. Therefore, based on the distribution graphs shown in Figure 4.1, a less wide particle distribution has been designed by mixing the three components to get a better distributed mix as shown in Figure 4.3b.

4.2.1.2 Particle shape

Particle shape was also carried out by FESEM as shown in Figures 4.2(a), (b), (c) for alumina, silica, and zirconia powders respectively.

From the FESEM micrographs shown in Figures 4.2 and 4.3, the powders were investigated for the particle shape in order to predict the behavior of the packing property. Particle shape influences sintering primarily through its effect on the packing of the green body. Deviation from the spherical or equiaxial shape leads to a reduction in the packing density and packing homogeneity, resulting in reduction of densification. In Figures 4.2(a) and (c), it was observed that fine subrounded particles with narrow particle-size distribution and limited aggregation were detected for the powders alumina and zirconia respectively. In Figure 4.2 (b), the shape of the particles is not uniform. There was an indication of aggregate or agglomerate, which could cause difficulty in the packing of particles during compaction stage and consequently in the densification during sintering. In order to avoid the non uniformity of the shape and size distribution, mechanical alloying was implemented using the ball milling process.

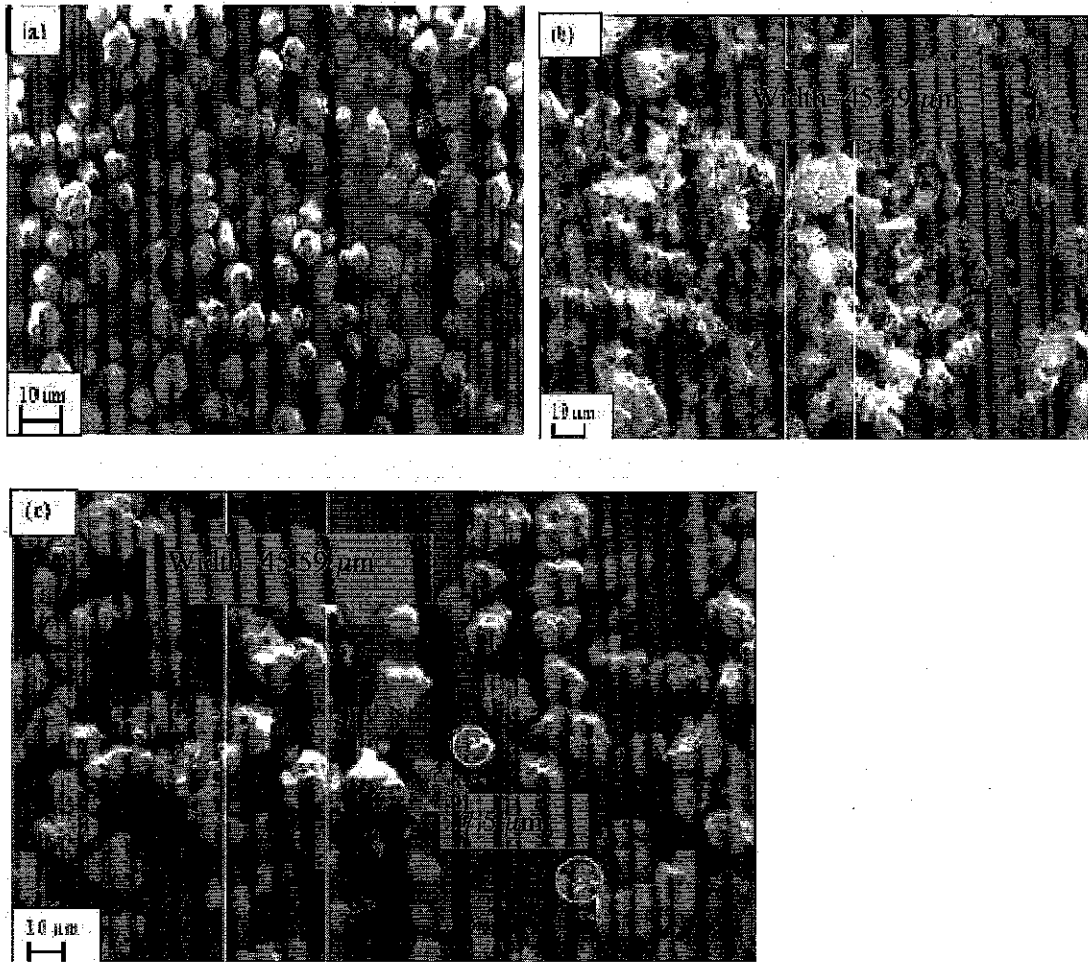
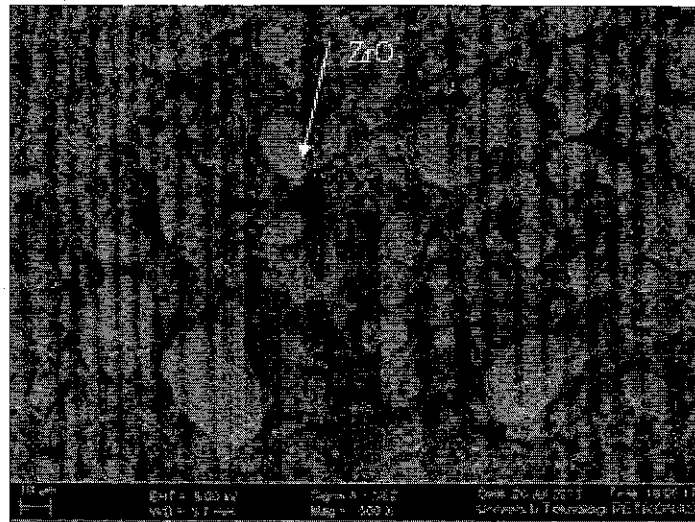
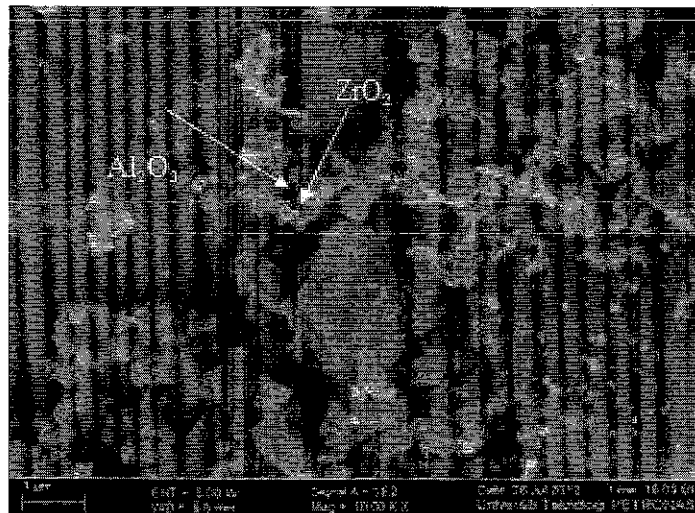


Figure 4.2: FESEM micrograph of the initial powders (a) alumina (b) Silica (c) zirconia

Figure 4.3 is FESEM micrograph of mixture of Al_2O_3 , SiO_2 , and ZrO_2 particle morphology. Figure 4.3(a) shows the micrograph of the non milled powder mixture (heterogeneous) with the amount of ZrO_2 and SiO_2 particles that attached on the surface of the alumina is very limited. In Figure 4.3(b), we can observe the ball milled powder mixture (homogenous) particles morphology with high amount of ZrO_2 and SiO_2 particles attached on the surface of the alumina powders. It was also shown in the non-milled powders the shape of the SiO_2 was irregular and the ZrO_2 was agglomerate. The ball milling process and mechanical alloying, produced homogeneous particle morphology with the surface of finer Al_2O_3 powders and Al_2O_3



(a)



(b)

Figure 4.3: FESEM micrograph of particles morphology appearance of $\text{Al}_2\text{O}_3\text{-SiO}_2\text{-ZrO}_2$ (a) non milled powder mixture (heterogeneous) (b) milled powder (homogenous) particles morphology

particles were fully covered with ZrO_2 and SiO_2 . This microstructure was due to the result of the wide particle size distribution which result in increased packing density or finer particles fitted within the larger particles [49].

4.2.1.3 Effect of Compaction Pressure on the Green density

A powder having good compaction behavior gives a high density green compact and, more importantly, a fine and homogenous porosity. This results in a high density sintered body as already shown in many studies [55, 59, 118].

In this work, a room temperature compaction was conducted to investigate the density trend of the compact with respect to pressure applied as shown in Figure 4.4. An arbitrary composition 80, 10 and 10 %wt. of alumina, silica and zirconia respectively was used for the study.

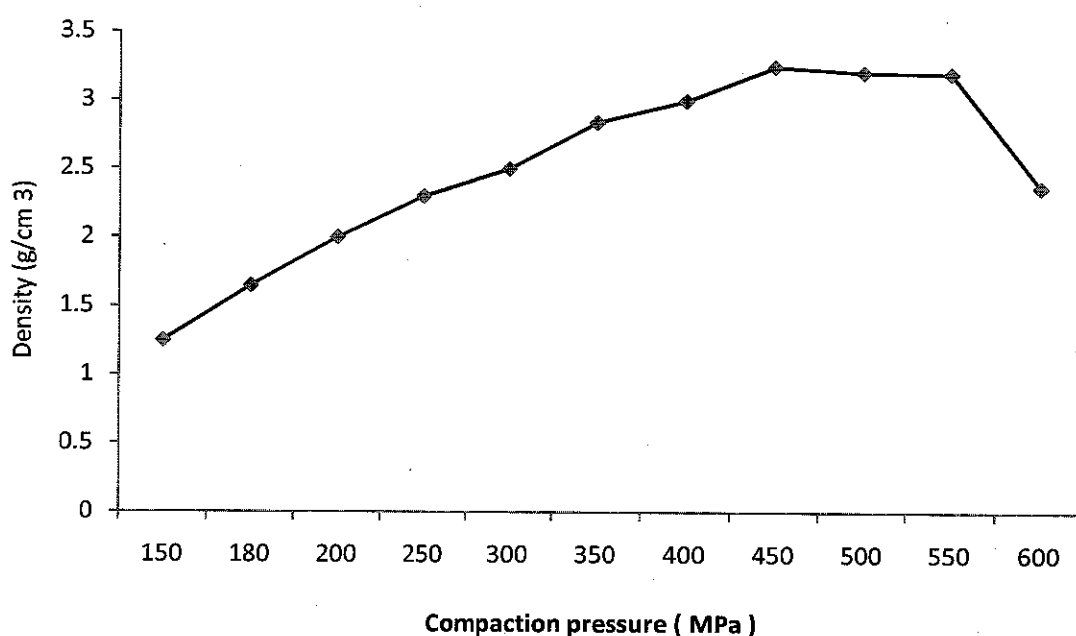


Figure 4.4: Green density of the powder plotted against compaction pressure

The general compaction trend showed a rapid increase in green density during the initial stages of compaction pressure until 450 MPa. But a decrease in the green density was observed with further increase in the applied pressure from 450 to 600 MPa. As it is shown in Fig. 4.4, the rapid increase in densification of the green compact from 150 to 300 MPa was considered due to the granule (agglomerate) rearrangement, deformation and fracture. The low densification rate in the pressure ranges between 300-500 MPa was due to the particles and hard agglomerate fracture which needs very high amount of pressure. The samples shown in Figure 4.5 were observed to be fractured and cracked at the surface due to the high pressure which

leads to decrease in density after the 500 MPa compaction pressure. This implies that using more than the optimum compaction pressure to disintegrate the agglomerate resulted in crushing a part of the agglomerates and stronger agglomerates were unaffected.

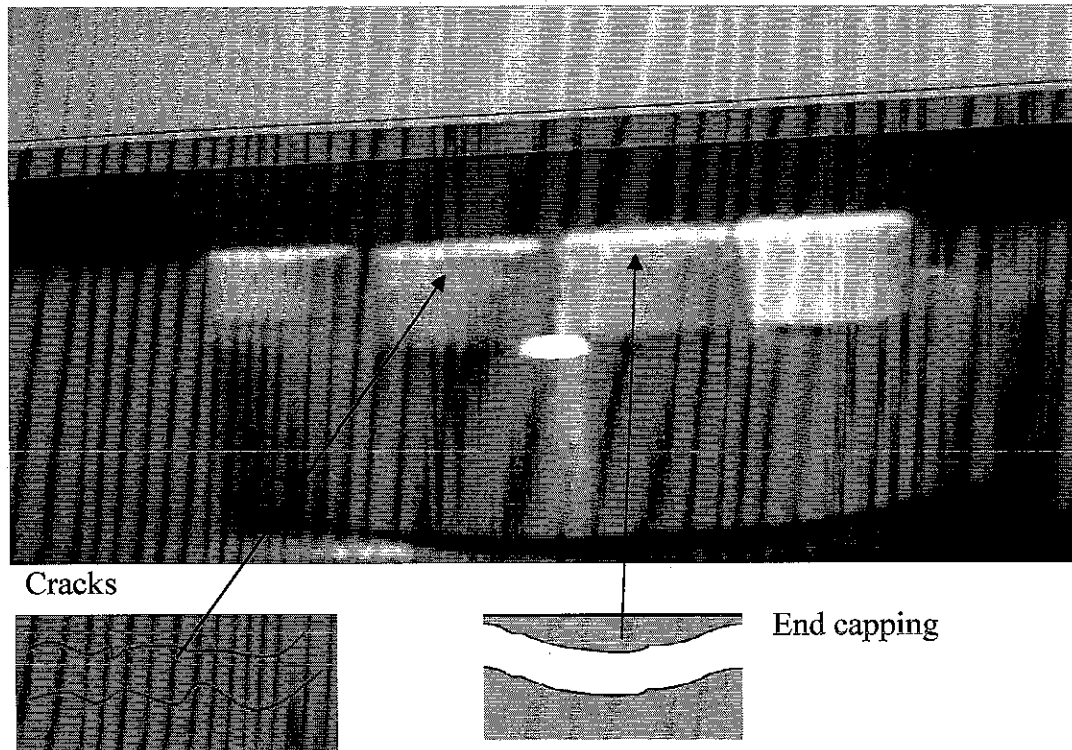


Figure 4.5: Failures in compacted samples when the pressure is more than 500 MPa.

4.2.1.4 Effect of Zirconia on the Densification of ASZ composite

Pressureless sintering experiment with different proportion of the elemental composition (Table 3.2) was carried out at 1650°C in tube furnace and the densification result as of the composition of each is shown in Figures 4.6 and 4.7.

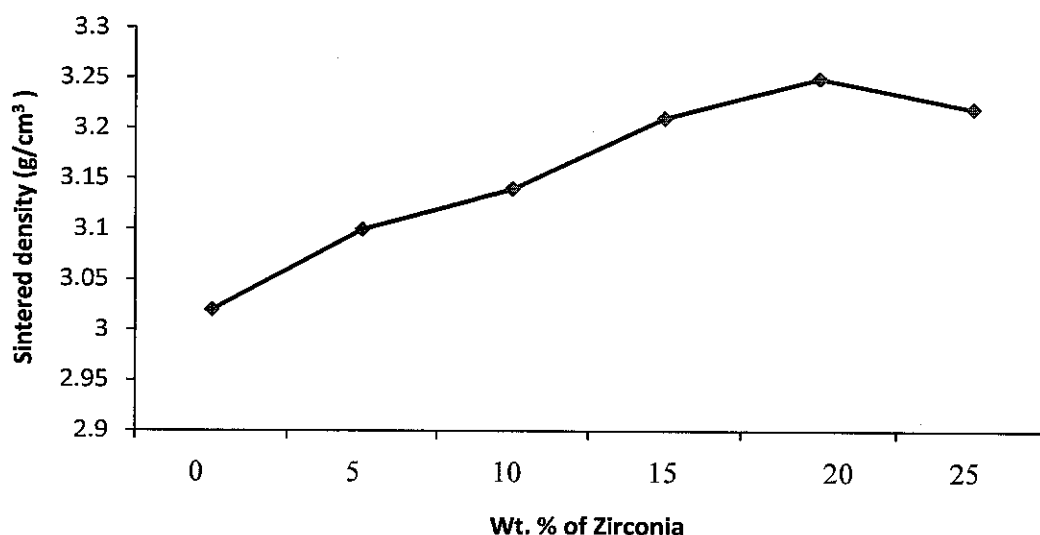


Figure 4.6: Densification trend with respect to the zirconia composition

From Figure 4.6, it can be depicted that the densification trend of the composites increasing up to sample 5, however, it started decreasing with the further increase of zirconia content above 20 wt.%, indicating that the presence of high amount of zirconia particles prohibits the densification of alumina matrix. It can be observed that samples for more than 20 wt. % of zirconia tend to exhibit a comparatively lower densification. The XRD plots and EDS for the corresponding composites revealed the presence of considerable amount of monoclinic ZrO_2 . This can be explained from the fact that excessive transformation from tetragonal to monoclinic ZrO_2 during cooling from sintering temperature might have resulted in microcracking due to the constituent volume expansion, thus leading to lower densification. Microcracking behaviour of the sintered samples will be explained in section 4.4.2.

4.2.1.5 Effect of SiO_2 on the Densification of ASZ Composite

Figure 4.7 showed an increase in the densification of the ASZ composite until a maximum amount of 10% by weight of silica. A drop in bulk density as the concentration of silica was increased after 10% by weight was also observed from the graph. The densification results showed that the amount of silica sand (SiO_2) addition

is very critical. It is expected that the silica addition attributes an increase in grain boundary coefficient due to the occurrence of secondary phase. This effect due to the secondary silica phase could also result in a solid solution formation by substitution of Al^{3+} by Si^{4+} in tetrahedral sites of the crystallographic structure [34] which may be the reason for the high densification of the stated concentrations of silica particle. On the other hand, the decrease in density as the concentrations of silica increased more than 10% by weight of the composite can be explained by two factors: first, as a consequence of increased porosity due to the excess amount of silica, and second, as a result of the increased amount of mullite phase, which is less dense than alumina.

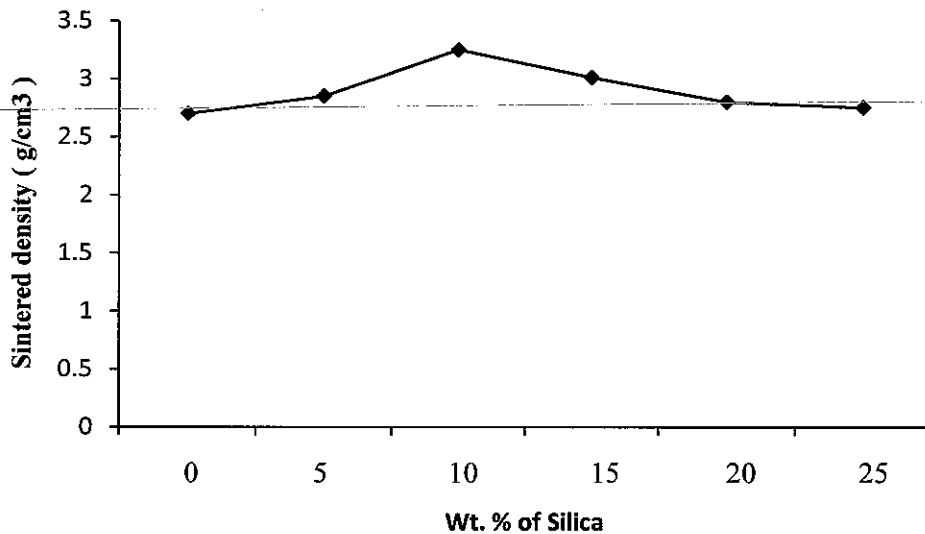


Figure 4.7: Densification trend with respect to the silica composition

4.2.2 Microstructure and Phase Composition of Sintered Samples

In this subsection, the microstructure, grain size and composition of the sintered samples have been investigated at room temperature by scanning electron microscopy, AFM and X-ray diffraction method. The effect of ZrO_2 reinforcement on the mechanical properties of the composites was also calculated to determine the optimum composition of the ZrO_2 particles.

4.2.2.1 Microstructure ASZ composite

Figure 4.8 shows the FESEM images with EDS for the sintered A-10S-20Z at 1650°C. Microstructure of the composite was characterized by the presence of finer, equiaxed Al₂O₃ matrix grains and elongated ZrO₂ reinforcements. The darker phase was Al₂O₃ and the lighter was ZrO₂, as would be expected based on the atomic weights, and as simplified by the EDS spectra of marked regions. It was also noted that there was a mullite compound with a high concentration of alumina and silica in the grain boundaries of the alumina matrix. The secondary phases appeared to be well distributed in all samples, indicating good mixture homogeneity. The Figures 4.8 (a) and (b) also show that all sintered composites have heterogeneous microstructure having large dark regions which were porosities.

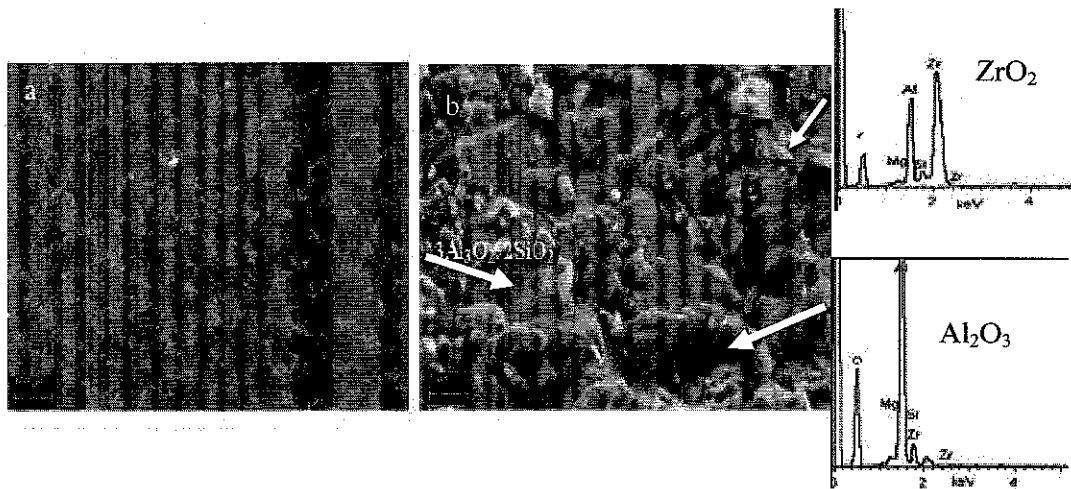


Figure 4.8: FESEM microstructure examination of the sintered sample at different magnification (a). low magnification (b). higher magnification

An attempt to measure the grain size was done by using the AFM. The images produced were shown in Figure 4.9. Length from one end of the grain to another end was taken as grain size. More than 50 grains were measured to estimate the average grain size from each sample. According to the measurement, the average grain size of the alumina ceramic was 0.8 μm , AZ grain size was 0.15 μm and ASZ was 0.056 μm . The grains of each phases in the binary and ternary composites were all equiaxed and similar in size due to the ball milling resulted in mechanical alloying.

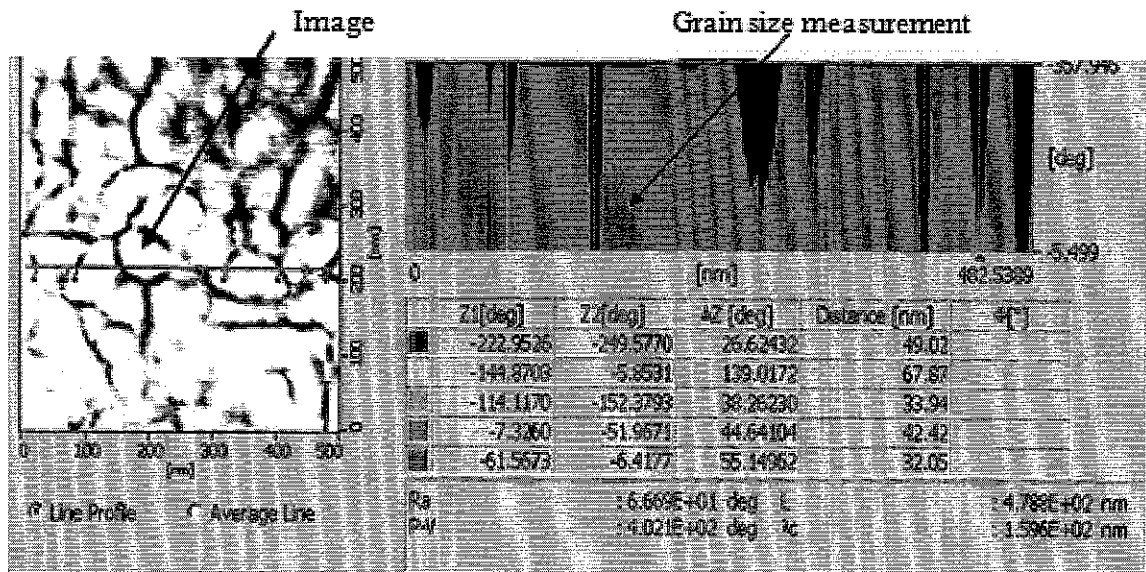
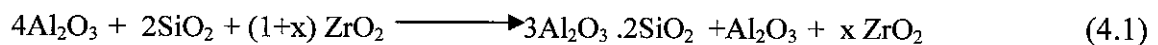


Figure 4.9: AFM micrograph of the ASZ composite and grain size measurement

4.2.2.2 X-Ray Diffraction of the ASZ Composite

The XRD results in Figure 4.10 shows that almost all the sintered samples were composed of Al_2O_3 , ZrO_2 , mullite and some impurities. It was considered that the starting material SiO_2 , and Al_2O_3 , reacted to form mullite (obtained by the reaction between alumina and silica) and other alumina and silica compounds during the sintering process, as shown in the stoichiometric reaction equation below. The XRD pattern shows intense sharp peaks indicating good crystallinity of ASZ based system for all compositions studied. The synthesis reaction in the sintering process was summarized as follows:



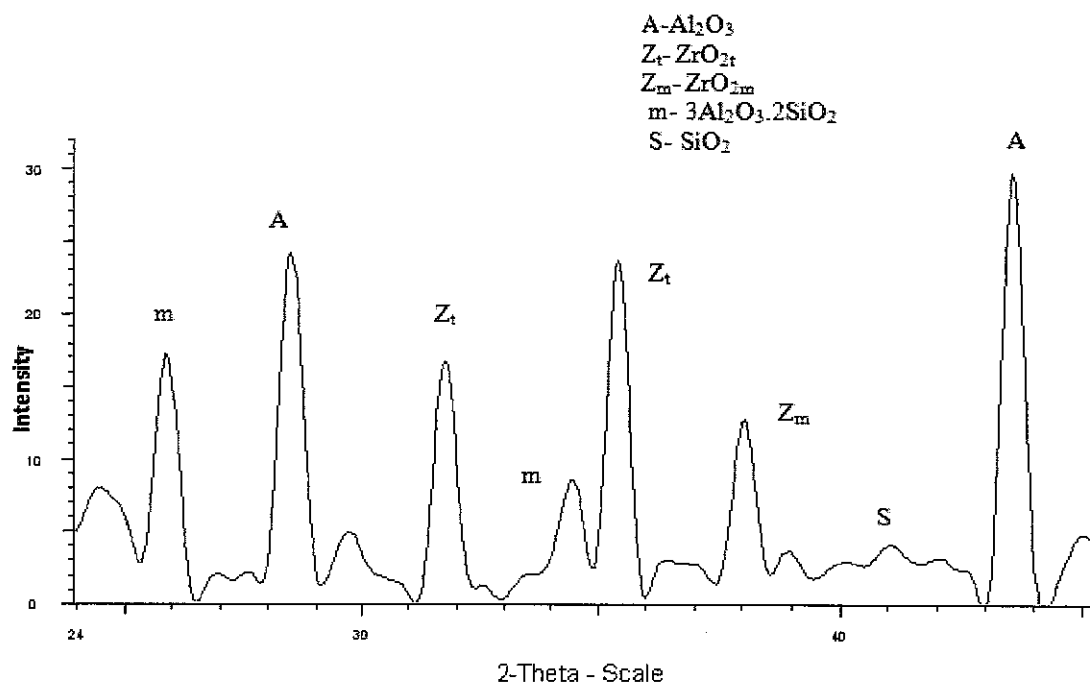


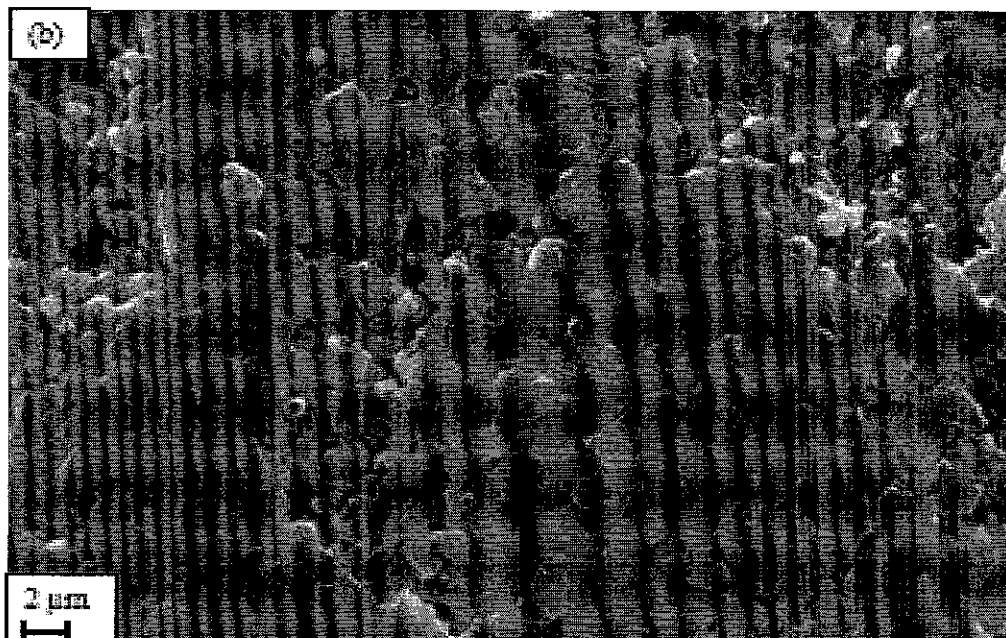
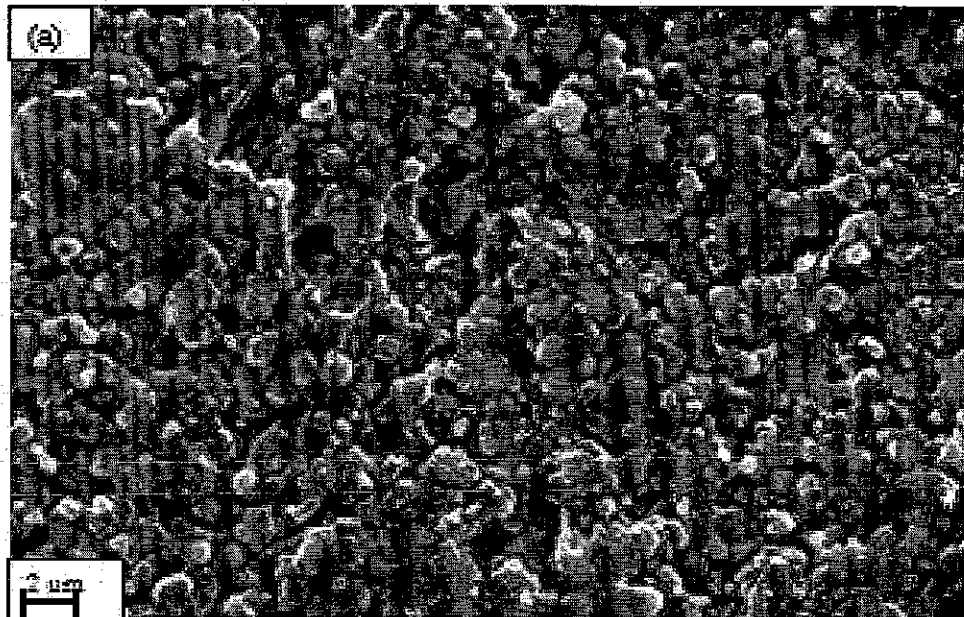
Figure 4.10: X-Ray diffraction pattern of the sintered A-10S-20Z sample

It is shown in Figure 4.10 that mullite and zirconia particles with sub-micrometer in particle size are mainly located at grain boundaries, while finer ones were within matrix grains, inferring that larger mullite and zirconia particles suppress grain boundary movement of alumina matrix. There was a good densification in the composites and a high level of bonding between grains and the matrix and this was considered due to the combination of solid state reaction bonding and liquid phase sintering mechanisms.

4.2.2.3 Effect of Sintering Temperature on the microstructural development of the ASZ Composite

Effect of sintering temperature on the phase change and crystallinity of the ASZ composite was also investigated along the temperature gradient of 1000°C to 1650°C. The FESEM and XRD patterns of the sintered samples were analyzed and summarized in Figures 4.11 and 4.12 respectively. From Figure 4.12, the sample was almost amorphous until the temperature reaches 1000°C. When heated to more than

1000°C, the samples begin to crystallize and t-ZrO₂ forms with a faint spinel-like phase as shown in the FESEM microstructure. With the increase of temperature up to 1200°C the diffraction peaks of t-ZrO₂ and mullite are more evident and traces of spinel crystalline phases were detected in the samples. The spinel was due to the MgO used as stabilizing agent for ZrO₂ in the sintering process. The main crystalline phases are identified as ZrO₂, mullite and cristobalite. This shows that the reaction between alumina and silica transforms to mullite by solid phase reaction.



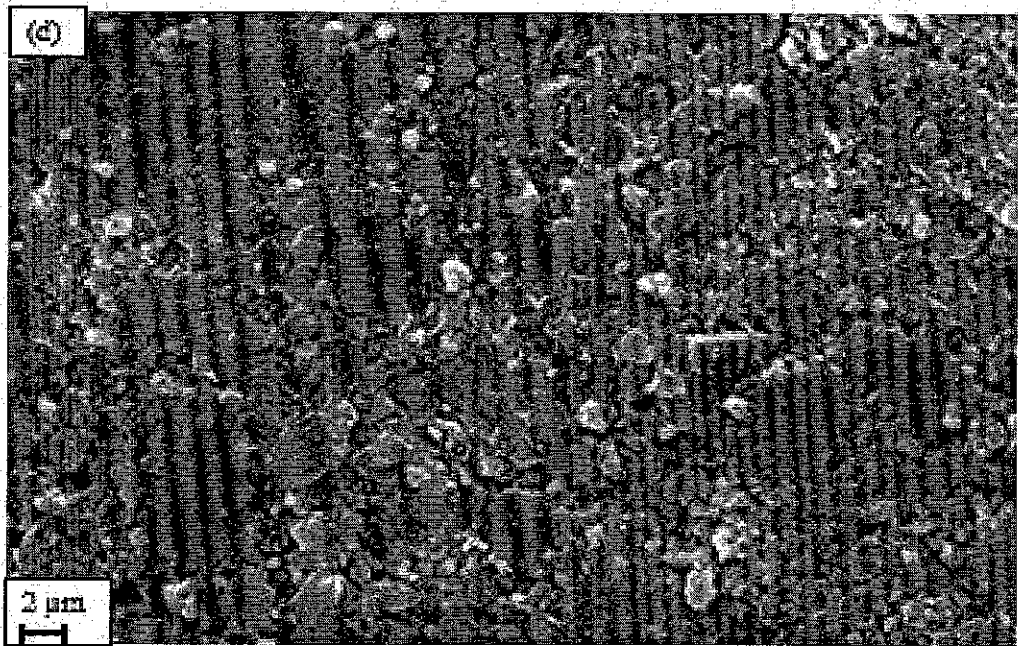
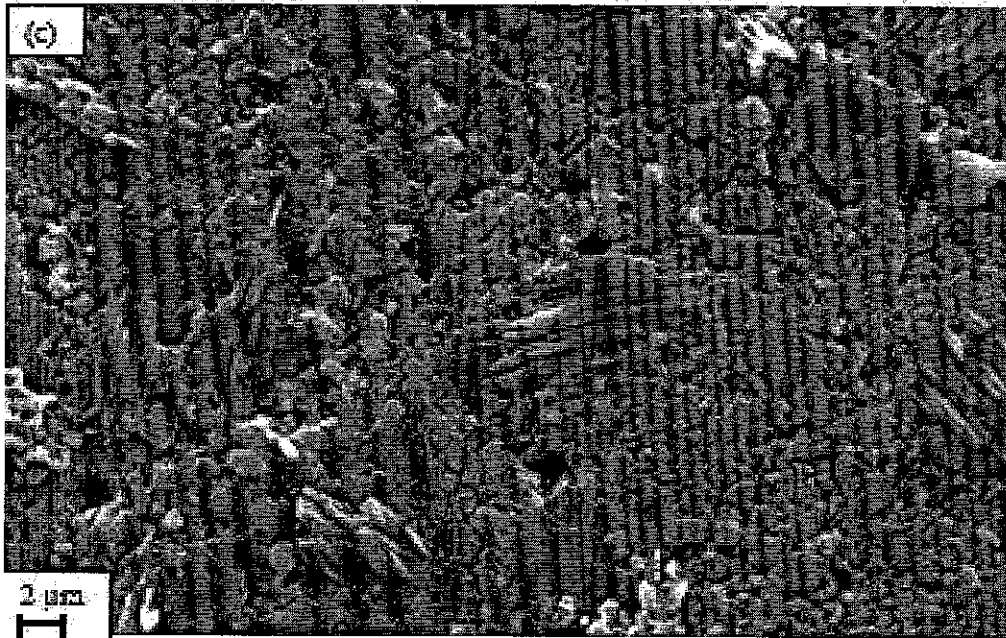


Figure 4.11: FESEM micrograph of the sintered ASZ composite at (a). 1450°C (b). 1300°C (c). 1200°C (d). 1000°C

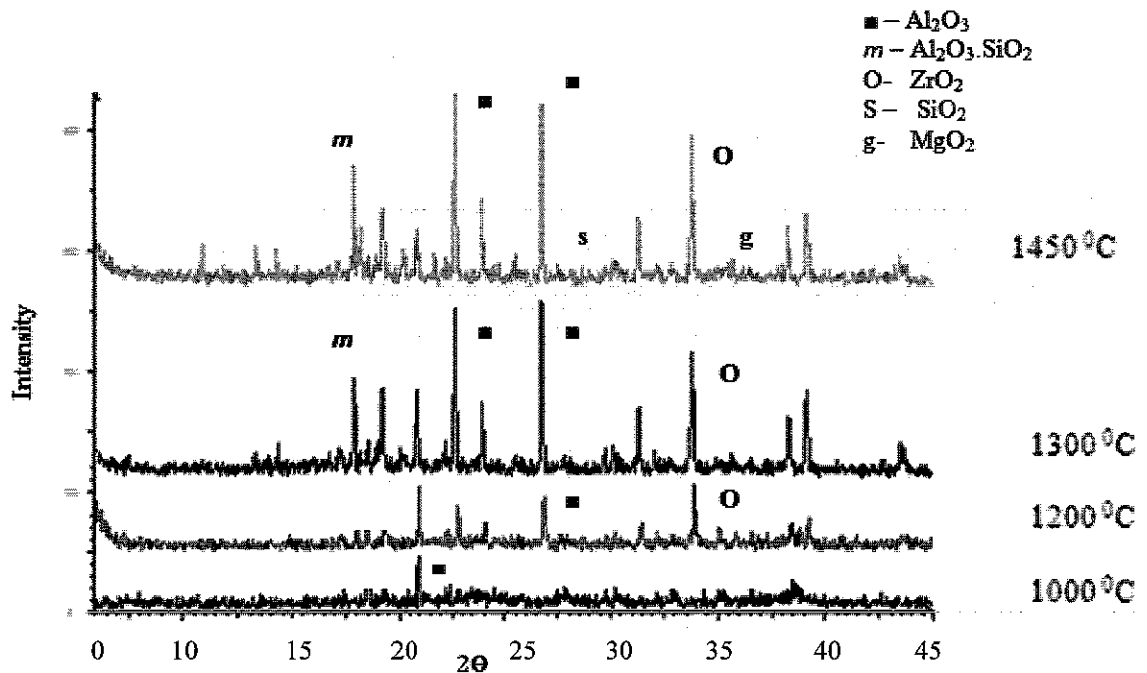


Figure 4.12: X- ray Diffraction pattern of the ASZ sample sintered at different temperatures

Figure 4.12 show the results of the X-ray diffraction analysis of the sintered A-10S-20Z sample at different sintering temperatures. In this figure it can be observed that the reaction of alumina and silica starts at 1300°C. At temperatures at and more than 1450°C, it is observed that a sharp mullite picks appeared. A dense alumina matrix with mullite and zirconia reinforcements with traces of amorphous silica and magnesium oxide are dominants at the sintering temperature of 1450°C.

4.2.2.4 Effect of ZrO_2 on the Mechanical Properties of the sintered Samples

Based on the ceramic powder mix preparation in Table 3.3, the mechanical properties of the Al_2O_3 - SiO_2 - ZrO_2 composite with respect to the weight percentage of the ZrO_2 are shown in Figure 4.13. The results show the mechanical properties of the composite system depend to a great extent on the compositions of zirconia. The experimental results indicated that the increased weight percentage of ZrO_2 , decreased hardness slightly, while the fracture toughness and flexural strength increases

gradually and started to decrease in some point which can be seen in Figure 4.13. Consequently, the ASZ ceramic composite system can be determined with the optimum combination of the three major indexes of mechanical properties. As a result, the most toughened composite system from these experimental measurements show that the Al-10S-20Z is the corresponding composite with the required property. Detailed comparison of mechanical properties of both the monolithic alumina , A-20Z and the A-10S-20Z composite materials is given in section 4.4.

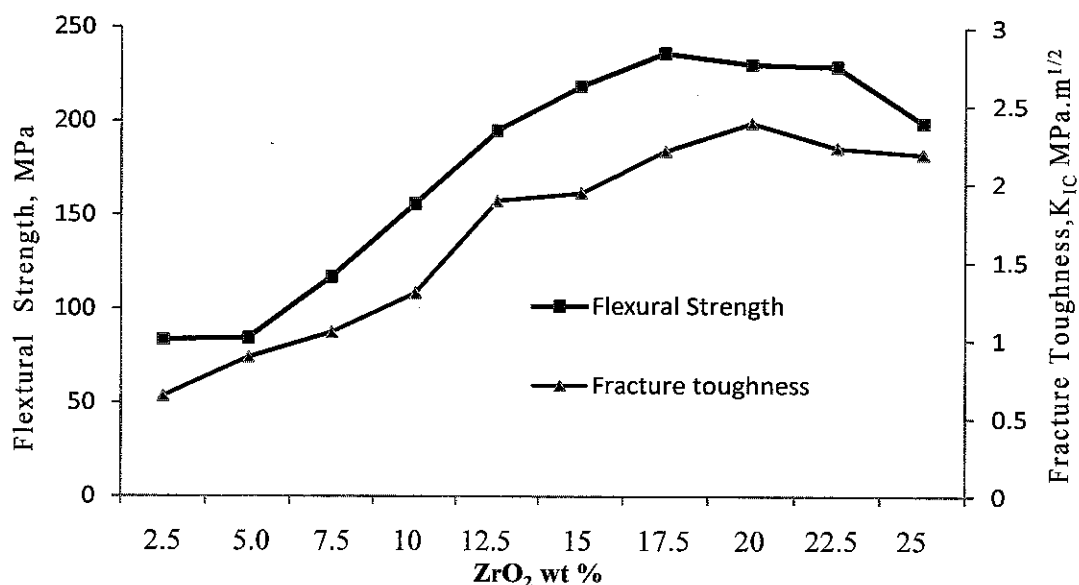


Figure 4.13: Flexural strength and fracture toughness with respect the ZrO₂ composition

From Figures 4.13 and 4.14, hardness and fracture toughness were seen that both values altered in opposite manner. Hardness of the composites dropped but fracture toughness obviously improved. The Vickers hardness was determined using Equation (1) and the calculated range value was from 12.77 GPa to 8.58 GPa, which shows a decreasing value as shown in Figure 4.14. The addition of zirconia and silica in the alumina caused a decrease of the hardness value. This effect can probably be attributed to the lower hardness of the materials included when compared to the monolithic alumina.

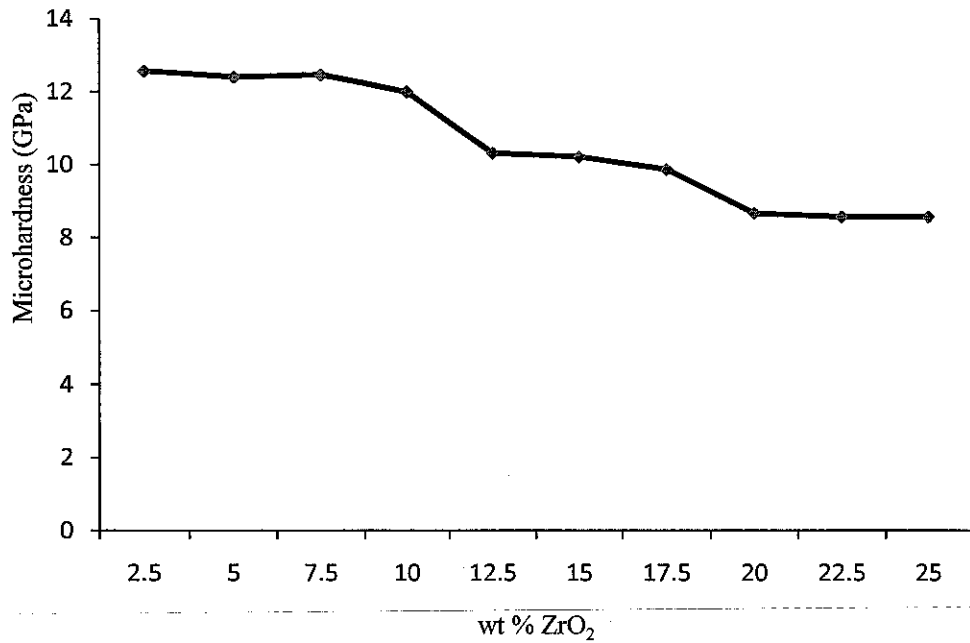


Figure 4.14: Effect of ZrO₂ weight percentage on the micro hardness of the ASZ sample

Summary

From the above results, the following conclusions were drawn out:

- This section was more focused on the optimizing of the operating parameters (compaction pressure, sintering temperature and composition) so that we get the good densification and mechanical properties. The results show that hardness, fracture toughness and flexural strength of the composites are dependent on the composition, compaction pressure and sintering temperature. Systematically, the result show a composition of tri-component composite A-10S-20Z (70% by weight of alumina, 10 % by weight of silica and 20 % by weight of zirconia) will be taken for further mechanical properties investigations. The effect of composition of each component on the hardness, toughness and flexural strength may be associated with the complex residual stress state that develops during cooling from the processing temperature due to the thermal expansion mismatch among the constituent parts of the

composite. The details of the mechanisms which result for such effects are explained in section 4.4.

- Al_2O_3 composites with mullite and ZrO_2 reinforcement was developed using the pressureless sintering technique which is cost effective and most widely used for consolidation.
- Initial materials composition has an influence on the densification of the ternary component composite material. The results show that with varying ZrO_2 content, keeping the silica content constant and the alumina as a matrix, the densification tends to decrease after the concentration of zirconia exceeds 20 wt. % of the composition.
- Hardness value for the A-10S-20Zr was in the range of 12.77 – 8.58 GPa and it shows a decreasing value as the wt % of the ZrO_2 reinforcement increase.

4.3 Dilatometry Study of the ASZ Composite system

4.3.1 Overview

The possibility of using SiO₂ sand as additive for densification of Al₂O₃-SiO₂-ZrO₂ (ASZ) ceramic system was studied. Dilatometry was used to measure the shrinkage behavior of ASZ green bodies under a nitrogen atmosphere from room temperature to 1550°C. The shrinkage started as low as 110°C, resulted in a significant reduction of sintering temperature. It was also indicated that phase transformation occurred during the sintering process had reduced the sintering temperature to 1450°C. Alumina, zirconia and mullite phases were detected and confirmed by the XRD and SEM results. Based on those results it can be concluded that SiO₂ is an effective additive in lowering the sintering temperature of ASZ composites.

4.3.2 Shrinkage and the Phase change Study

The mechanical properties of ceramic based composites for industrial applications are related to the microstructure. Hence, the study of all the aspects that can modify the microstructure of the ceramic composite during sintering is very crucial. Dilatometry is one of the most powerful techniques for the study of solid–solid phase transformations in ceramic sintering, because it permits the real time monitoring of the evolution of transformations in terms of dimensional changes occurring in the sample by application of a thermal cycle [48, 119].

Alumina based composites are relatively low cost, and the ceramic components are manufactured with high output using various ceramic processing such as slip casting, pressing, and injection molding without incorporating expensive equipment such as kilns with special controlled atmosphere. However, the application of alumina based ceramics is still limited due to high cost of additives and high sintering temperatures [28, 29, 47, 120]. Therefore, there is a continuous searching for production process of both low cost alumina starting powder and sintering additives, which are equally inexpensive and enable low sintering temperatures.

Silica sand is the most essential raw material as used by foundries for its thermal resistance and availability. However, its usage in ceramic based composite developments was over looked. The use of oxides such as MgO, CaO, and CrO as a sintering aid is often reported to increase the densification kinetics and to limit the grain growth in ceramic composites [6]. A first approach on the effect of silica addition on the sintering of yttrium aluminum garnet doped by neodymium (Nd:YAG) [30] which was investigated on the basis of microstructural characterizations. However, no work has yet been done on dilatometric study of $\text{Al}_2\text{O}_3\text{-SiO}_2\text{-ZrO}_2$ system to use silica as sintering aid. Thus, the purpose of this section is to investigate the dilatometric behavior of a mixture of $\text{Al}_2\text{O}_3\text{-ZrO}_2$ with SiO_2 addition and to understand the sintering phenomena in the system.

Dilatometric study of sintering process is very useful because it shows the length change of green bodies during heat treatment while the curve shows different phenomena. Figures 4.15, 4.16 and 4.17 show a dilatometric graph of monolithic Al_2O_3 , $\text{Al}_2\text{O}_3+10\text{wt.}\% \text{SiO}_2$ and $\text{Al}_2\text{O}_3+10 \text{ wt.}\% \text{SiO}_2+10\text{wt.}\% \text{ZrO}_2$, respectively. The curves depicted the shrinkage behavior of each of the different samples as the function of temperature. Four samples were studied for the shrinkage behavior which are specified as monolithic Al_2O_3 , $\text{Al}_2\text{O}_3+10\text{wt.}\% \text{SiO}_2$, $\text{Al}_2\text{O}_3+10 \text{ wt.}\% \text{SiO}_2+15\text{wt.}\% \text{ZrO}_2$ and $\text{Al}_2\text{O}_3+10 \text{ wt.}\% \text{SiO}_2+20\text{wt.}\% \text{ZrO}_2$

A representative dilatometric plot of the monolithic alumina is shown in Figure 4.15. Upon heating, change in length (ΔL) was the net result of two opposing mechanisms of linear thermal expansion and pore closing. Up to $\sim 1400^\circ\text{C}$ (region I), the composite expanded due to limited retraction rates characteristic to surface diffusion. This time, the first necks could be observed. As the temperature increased, grain boundary and volumetric diffusion became the dominant mechanisms, as suggested by a significant change in the slope of the plot from region I to region II. The thermal expansion was roughly counterbalanced by the retraction rate. Further heating to around 1600°C was characterized not only by sintering but also homogenization with mutual diffusion of impurities in the system.

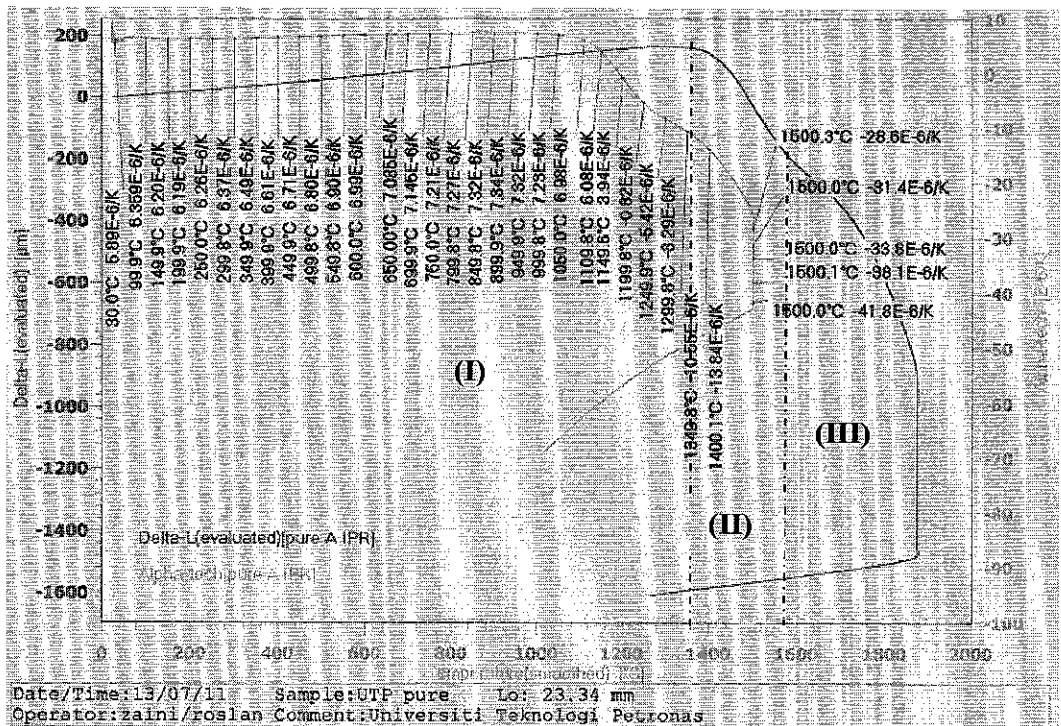


Figure 4.15: Dilatometric plot of monolithic Al₂O₃

In Figure 4.16, as the addition of 10% wt silica to the Al₂O₃-ZrO₂ system, it was observed that the rearrangement of the particles and creation of pores started at lower temperature. The dilatometric behavior of the composite shows, starting from ambient to approximately 880°C, a slight expansion was noticed and ruled by a mechanism similar to that discussed for monolithic Al₂O₃. The slope of the dilatometric plot changed in the range of 880–1200°C, corresponding to the onset of the contraction process. The slope in region II of the plot can be explained by the formation and growth of inter particle necking. Region III, between 1200°C and 1520°C, was characterized by volumetric diffusion and phase transformation. Fast contraction as a result of reaction sintering happened around 1400°C, resulting in rapid contraction.

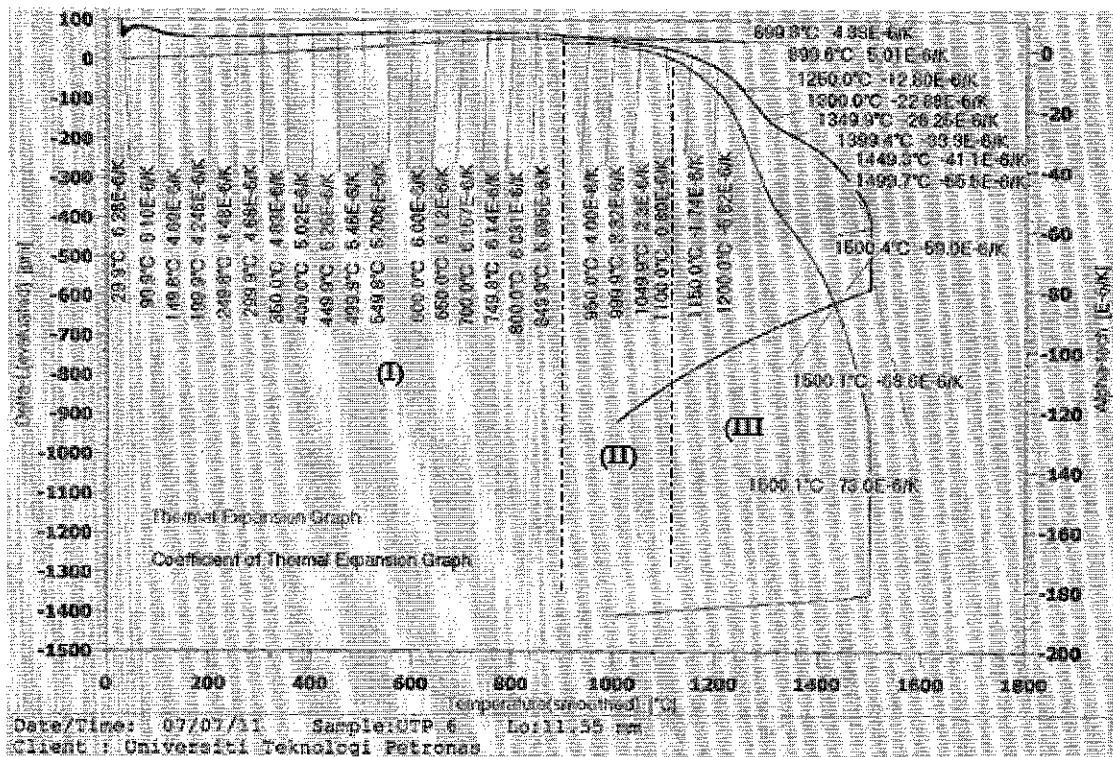


Figure 4.16: Dilatometric plot of sample 2 (10% wt. SiO₂)

The dilatometric plot corresponding to Al₂O₃ + 10% wt SiO₂ + 20% wt ZrO₂ is illustrated in Figure 4.17. The shape of the curve indicated almost similar shrinkage trend as Figure 4.16, even though a 10% wt ZrO₂ was added to it. There were also other dilatometric plots produced with more percentage of zirconia but the shapes of the profile results were similar with Figure 4.17. This implies that the effect of zirconia on the densification of the system is minimal but the exact effect may need further investigation to reach a concrete understanding.

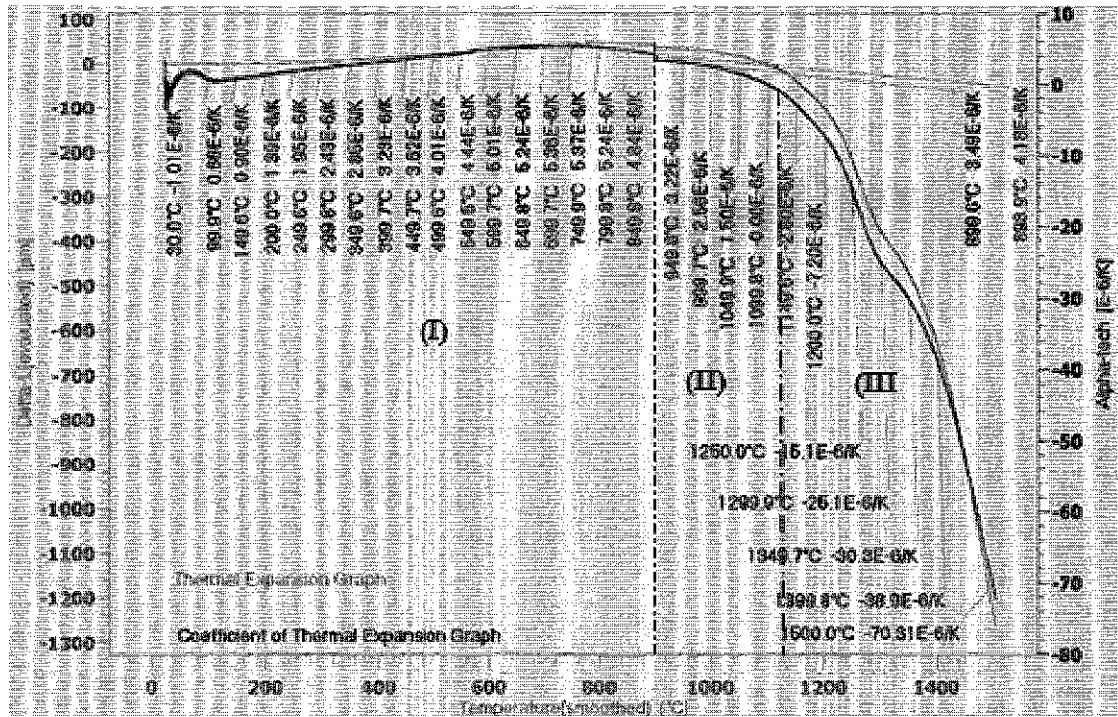


Figure 4.17: Dilatometric plot of sample 3 (10% wt SiO₂ + 10%wt. ZrO₂).

According to the phase diagram of liquidus curve of Al₂O₃-ZrO₂ in Figure 4.18, the lowest eutectic temperature in the system is around 1870 °C [14]. However, the overall liquid forming temperature is lower than the nominal eutectic temperature because of the present of SiO₂ in the liquid phase. This confirms that the Al₂O₃-SiO₂-ZrO₂ acted as a very good solvent for SiO₂, which is also a prerequisite for a good sintering additive.

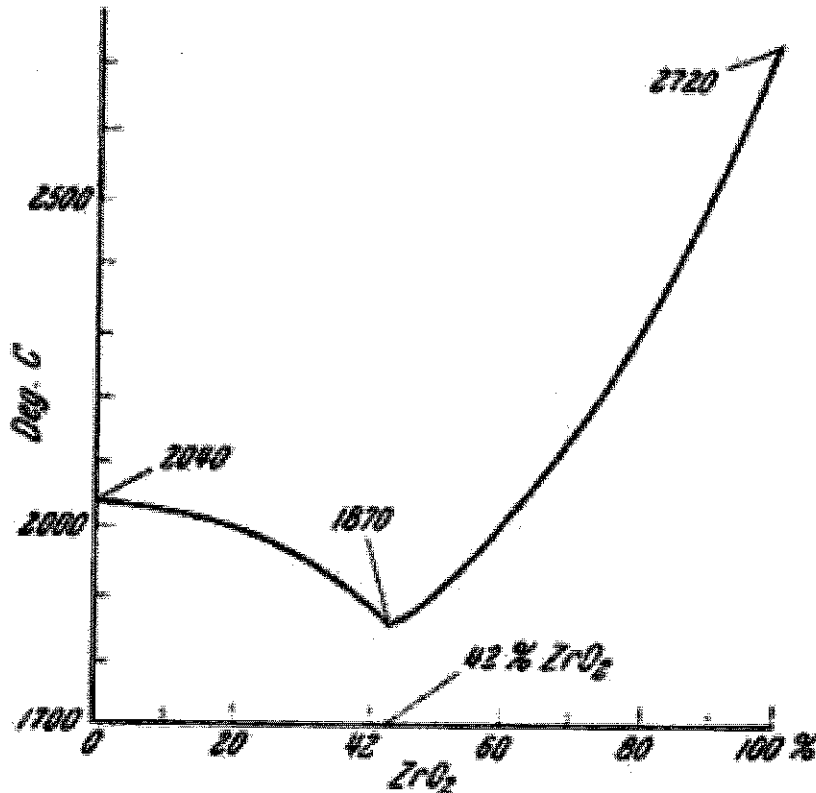


Figure 4.18: Phase diagram for the Alumina- Zirconia system [73].

Due to the occurrence of liquid phase in the pressureless sintering process, it was expected the formation of amorphous glassy phases after cooling. But the XRD pattern in Figure 4.11 shows remarkable increase in the diffraction lines intensities, which can be explained by the increasing of new crystalline phase called mullite. In previous discussions, the sintering of $\text{Al}_2\text{O}_3\text{-}10\text{SiO}_2\text{-}20\text{ZrO}_2$ composite at different temperatures indicates that no significant transformation takes place up to 1000°C . When heated to more than 1000°C , the samples began to crystallize and ZrO_2 phase started to form. With the increase of temperature up to 1200°C the diffraction peaks of $t\text{-ZrO}_2$ and mullite are more evident. These observations agreed with the findings of the dilatometry study discussed above in this section.

Figure 4.19 is the typical SEM image of the $\text{Al}_2\text{O}_3\text{-}10\text{SiO}_2\text{-}10\text{ZrO}_2$ composite which shows the morphologies of zirconia and mullite particles within the alumina matrix. The chemical composition analysis with EDS along the line perpendicular to the $\text{Al}_2\text{O}_3/\text{ZrO}_2/3\text{Al}_2\text{O}_3 \cdot 2\text{SiO}_2$ interface showed that interdiffusion had occurred at the interface zone. Some zirconia was dissolved in the alumina matrix, while some Si

and small amount of Mg were dissolved within the interface of the grain boundary to form Si and Mg oxide solid solution. This implies SiO₂ was also assisting in the sintering of the final composite. The SEM observation of the composite also showed that the distribution of ZrO₂ particles in the Al₂O₃ is uniform except for the small agglomeration in few parts. The interface interdiffusion enhanced the surface adhesion.

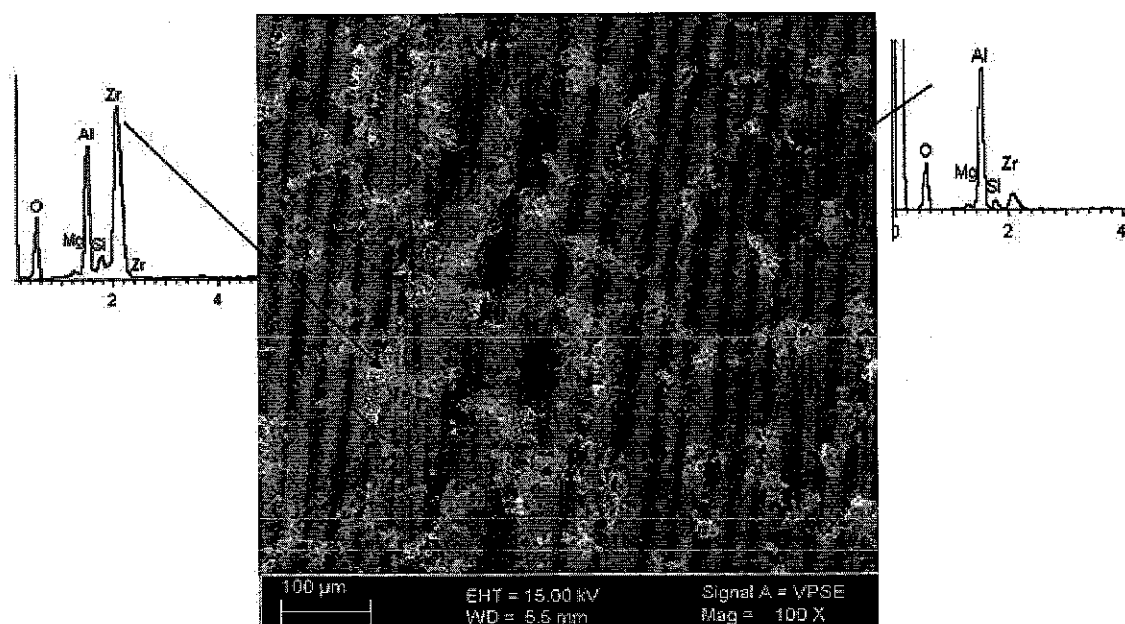


Figure 4.19: SEM + EDS images of the sintered Al₂O₃-10SiO₂-10ZrO₂ composite

It was also found from Figure 4.19 that mullite and zirconia particles were mainly located at grain boundaries of the matrix grains, inferring that mullite and zirconia particles suppress grain boundary movement of alumina matrix. This led to a good densification in the composites and a high level of bonding between grains and the matrix. This was achieved due to the combination of solid state reaction bonding and liquid phase sintering mechanisms as has been analyzed in the dilatometry study.

Summary

In this section, the chemical reactions and phase evolution during pressureless sintering followed by characterization of these phases using SEM, EDS, XRD and dilatometric analysis were done. Results showed that the first liquid forms as low as

1100°C, sharing in a significant reduction of sintering temperature. The final phase composition of the system obtained at 1450°C consists of crystalline alumina, mullite and zirconia phases. The results show that the SiO₂ is a very effective sintering additive for ASZ composites.

4.4 Mechanical Properties Comparison of monolithic Alumina, AZ and ASZ Composites

4.4.1 Overview

In this section, the microstructure and mechanical properties of the three components ASZ composite was analysed. The room temperature mechanical properties of AZ and monolithic Al_2O_3 were compared with ASZ composites. The hardness, flexural strength and toughness were determined and compared of both ceramics. The flexural strength and fracture toughness of the SiO_2 and ZrO_2 reinforced alumina matrix were developed and measured.

4.4.2 Hardness, Fracture Toughness and Flexural Strength of the Sintered ASZ Composites

The hardness was studied by the Vickers micro hardness tester. The indentations were carried out at a load 1 Kgf with 15 sec dwell time. The hardness was determined from the diagonal length using the formula given Equation 3.4. The indent diagonals and the d value were taken from Figure 4.20 as the input for the equation.

Five sintered sample was taken from each type of ceramic composite and average of the result was recorded. The Vickers hardness of the as sintered samples were determined to be 7.91 GPa, 12.86 GPa and 14.35 GPa for Al_2O_3 -10 SiO_2 - 20 ZrO_2 , Al_2O_3 -20 ZrO_2 and alumina monolithic respectively, as shown in Table 4.1.

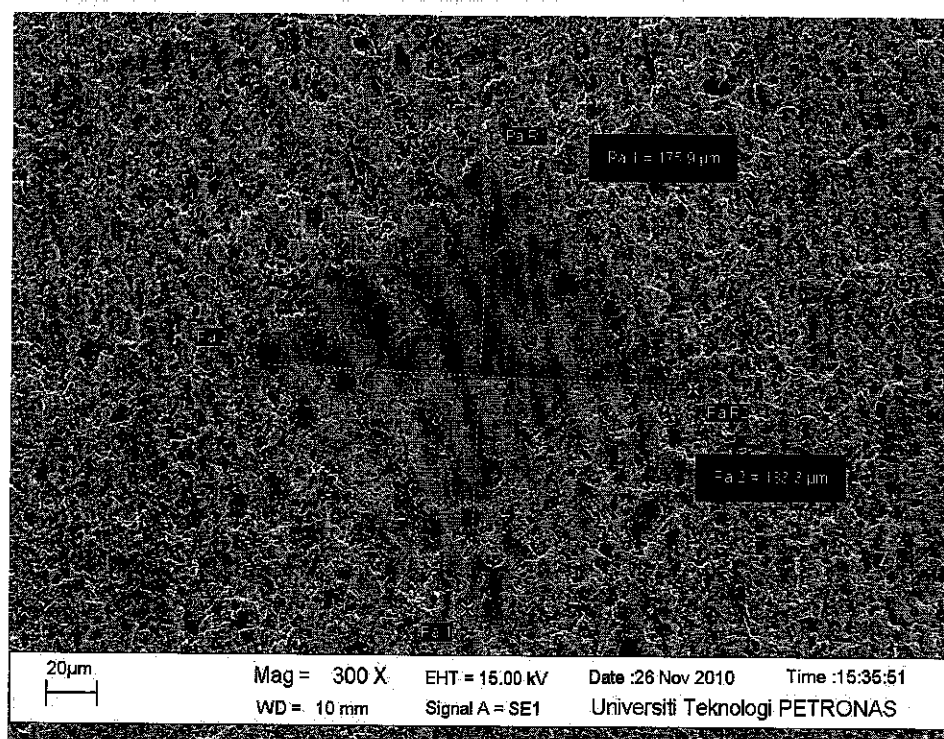


Figure 4.20: Indent to determine the vicker's hardness of the samples

As can be depicted from Table 4.1, the micro hardness value was decreasing as the no of component is increasing. This was evident that as the toughness of material was improved, lower hardness is expected. The second reason may be due to the inclusion of the reinforcement, it becomes less hard as the expense of the other mechanical properties.

The result also showed that the tri-component composite posses the least hardness value attributed to the formation of liquid phase non crystalline SiO_2 along the boundaries. Xu et al. [61] recognized sintering additives such as YO_2 , MgO in the formation of liquid phase during sintering, which on solidification produces more intergranular refractory phase.

Figures 4.21 and 4.26 show that there were micro cracks, deflection, and crack impedances produced in the ASZ composite. The increase in micro cracks easily led to excessive connection of micro cracks, which reduces hardness and strength of the material [62, 117, 118].

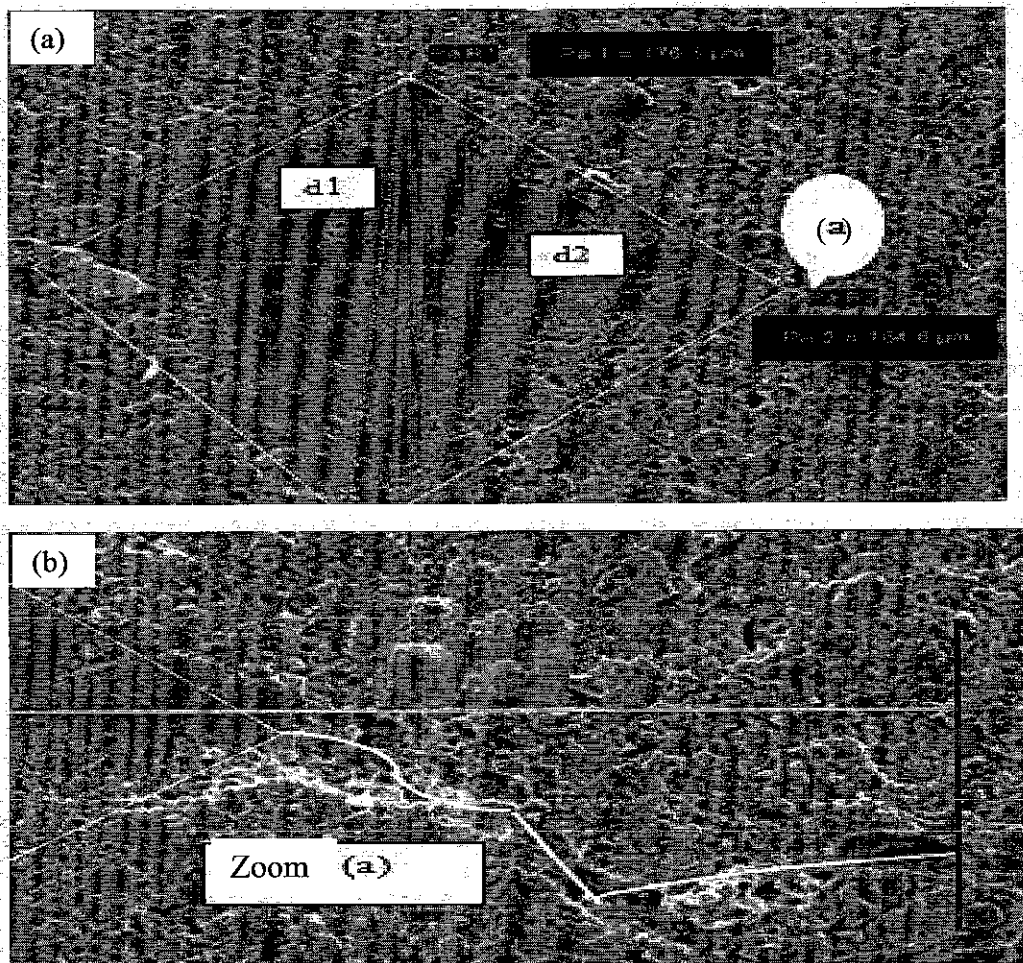


Figure 4.21: Micrograph showing the indentation cracks of the ASZ samples
 (a). the indent (b). high magnification at point a.

Fracture toughness for these ceramics was determined through IF method. It was obtained by measuring crack length at the edges. There are different methods currently used to measure the fracture toughness of ceramic materials. Methods based on the crack-length measurements of cracks introduced into the sample surface by a Vicker's indentation have the advantage of easier to perform. But this method requires careful study of subcritical crack growth and exact length measurement of the cracks. The fracture of brittle ceramics is usually controlled by the fracture toughness of mode I. A simple dimensional analysis of a body containing a crack of length $2C_0$ (see Figure 4.21 zoom) subjected to an applied stress σ showed that the stress intensification at the crack tip K_{IC} is calculated by Equation 3.5 and the Young's

modulus E value calculated for each sample was shown in Table 4.1. For example the calculation used to determine the fracture toughness for one ASZ samples is (refer equations 3.4 and 3.5):

$$K_{IC} = 0.016 \frac{10}{(60.6 \times 10^{-6})^{3/2}} \left[\frac{342 \times 10^9}{7.91 \times 10^9} \right]^{1/2} = 2.04 \text{ MPa.m}^{1/2}$$

Given that $P = 450 \text{ MPa}$, $E = \text{Young's modulus} = 342 \text{ GPa}$ (from table 4.1)

$C_0 = \text{crack extension length} = \text{Figure 421 (b)} = 60.6 \mu\text{m}$

$H = \text{Calculated using the equation } H_V = 1.85 \frac{P}{D^2}$

Based on the results, the tri-component composite possessed the highest fracture toughness value as compared to the other alumina monolithic and A-20Z composites.

Table 4.1: Properties of monolithic Al_2O_3 and $\text{Al}_2\text{O}_3\text{-10SiO}_2\text{-20ZrO}_2$ composite

Properties	Ceramic composites		
	Monolithic alumina	$\text{Al}_2\text{O}_3\text{-20ZrO}_2$	$\text{Al}_2\text{O}_3\text{-10SiO}_2\text{-20ZrO}_2$
Elastic Modulus (E), GPa	380	323.0	342
Flexural Strength (σ), MPa	200	264.71	230.40
Fracture toughness (K_{IC}), $\text{MPa.m}^{1/2}$	0.86	1.75	2.39
Critical Strain energy release rate (G_{IC}), J/m^2 *	2.94	10.48	20.91
Vickers' hardness (GPa)	14.35	12.86	7.91

* $v = 0.21$ is used for the calculation of G_{IC} (Equation 1)

In order to measure the indentation fracture toughness of the composites, five samples have been taken and an average value of $0.8 \text{ MPa.m}^{1/2}$, $1.75 \text{ MPa.m}^{1/2}$, and $2.39 \text{ MPa.m}^{1/2}$ for the AlO_2 , AZ and ASZ composites respectively. A significant

increase in the toughness has been identified by the inclusion of the ZrO_2 and SiO_2 oxides. The judicious inclusion of the reinforcement undergoes phase transformation under stress as well as by making and interlocking tri-component system. It is proposed that the difference in coefficient of thermal expansion may create compressive residual stresses which provide the fracture strength of the composite. It was also observed that the fracture mode was mainly intercrystalline for the sintered AlO_2 and AlO_2-ZrO_2 composite but for the ASZ mainly transcrystalline. It is well discussed in section 4.4.2.3 regarding the toughening mechanisms and fracture behavior of the composite.

Flexural testing was performed to determine the bending strength of the selected composites. An average flexural strength of five samples was determined by using three-point bending testing as per ASTM C1161-90 [121]. Resistance to bending obtained for each monolithic alumina, AZ and ASZ was 200 MPa, 264.71 MPa, 230.40 MPa respectively, as shown in Table. 4.1. This values are comparable to reports in various experimental works for similar refractory obtained by using zircon as raw material [18, 19]. In the latter case, the homogeneous distribution of ZrO_2 throughout the matrix might be responsible for the observed increased in the mechanical properties. It is well known that ceramic materials can show experimental values for their mechanical properties which are lower than the theoretical ones due to the presence of defects caused by porosity, impurities, agglomerates, etc.; which have different sizes, shapes and orientation; and which can act as stress concentration centers [25, 85, 87]. Therefore, two specimens of the same material, identical in principle, may not have an equal distribution of defects, so that their tensile strength and toughness will be different. This could explain the difference observed between the values of the flexural strength determined in this work and that are reported in the literature for similar refractory materials, which could be related to the use of two different raw materials (zirconia vs. zircon) for their synthesis.

It was noted that the fracture toughness of the A-10S-20Z composite was as high as $2.39 \text{ MPa}\cdot\text{m}^{1/2}$ almost 180 and 36.57 percent higher than that of the monolithic Al_2O_3 and AZ respectively, which means that the toughening effect of ZrO_2 and the SiO_2 particles is significant. The critical strain energy rate, G_{IC} , of the A-10S-20Z

composite was 20.91 J/m^2 which is more than six times compared to the monolithic Al_2O_3 , implying that more energy is needed for the crack propagation in the A-10S-20Z composite. The flexural strength of the A-10S-20Z composite was also 230.40 GPa, higher than the flexural strength of the monolithic Al_2O_3 . Meanwhile the elastic modulus of the A-10S-20Z composite is slightly lower than that of monolithic Al_2O_3 , which was attributed to the higher elastic modulus of the matrix Al_2O_3 (380 GPa).

It may be considered that the combination of ZrO_2 with mullite has a better effect for improving the mechanical properties of the material. Effect of combined toughening mechanism is an interesting possibility where investigation of possible synergetic effects may exist. Different toughening mechanisms (transformation toughening, microcrack and crack bridging) combined and the result was very attractive. ASZ composite was very promising, with an improved in fracture toughness as explained above. Each of the second phases contributed, the ZrO_2 reinforcement was paramount. It has been already shown [98, 117] in other tri-phase systems that the combination of ductile phase toughening and transformation toughening to be synergetic in theoretical analysis of microcrystalline system. It was also experimentally shown that the synergetic effect for the combination of fibres toughening and transformation toughening in zirconia composites was significant.

Based on the FESEM observations in the previous sections, it was confirmed that there is no apparent grain growth in the tri-component composite compared to the monolithic and binary. The limited grain growth was due to the tri-component microstructure. Ideally, when three components composite were well mixed, each phase formed was separated by nearby grain from its same phase. Therefore, the diffusion path was increased, thus effectively limiting the grain growth.

FESEM observation in Figure 4.22(a) and (b) showed equiaxed grains in A-20Z and A-10S-20Z materials due to the alumina rich environment. It was interesting to observe that the grain shape of mullite in A-10S-20Z developed an elongated and short fiber like morphology as shown by the arrows in Figure 4.22 (b). The interlock of elongated grains can hinder the grain boundary sliding and so decrease the strain rate. Secondly, tri-component structure limited the grain growth and created new interfaces which did not exist in the binary alumina-zirconia composites. The new

interface may have different grain boundary mobility. Lastly, smaller amount of unreacted silica could remain at the multiple junctions and minimize the stress concentration, thus promoting grain boundary sliding, which increased the fracture toughness of the tri-component composite. These findings were found consistent with other researches [38, 122].

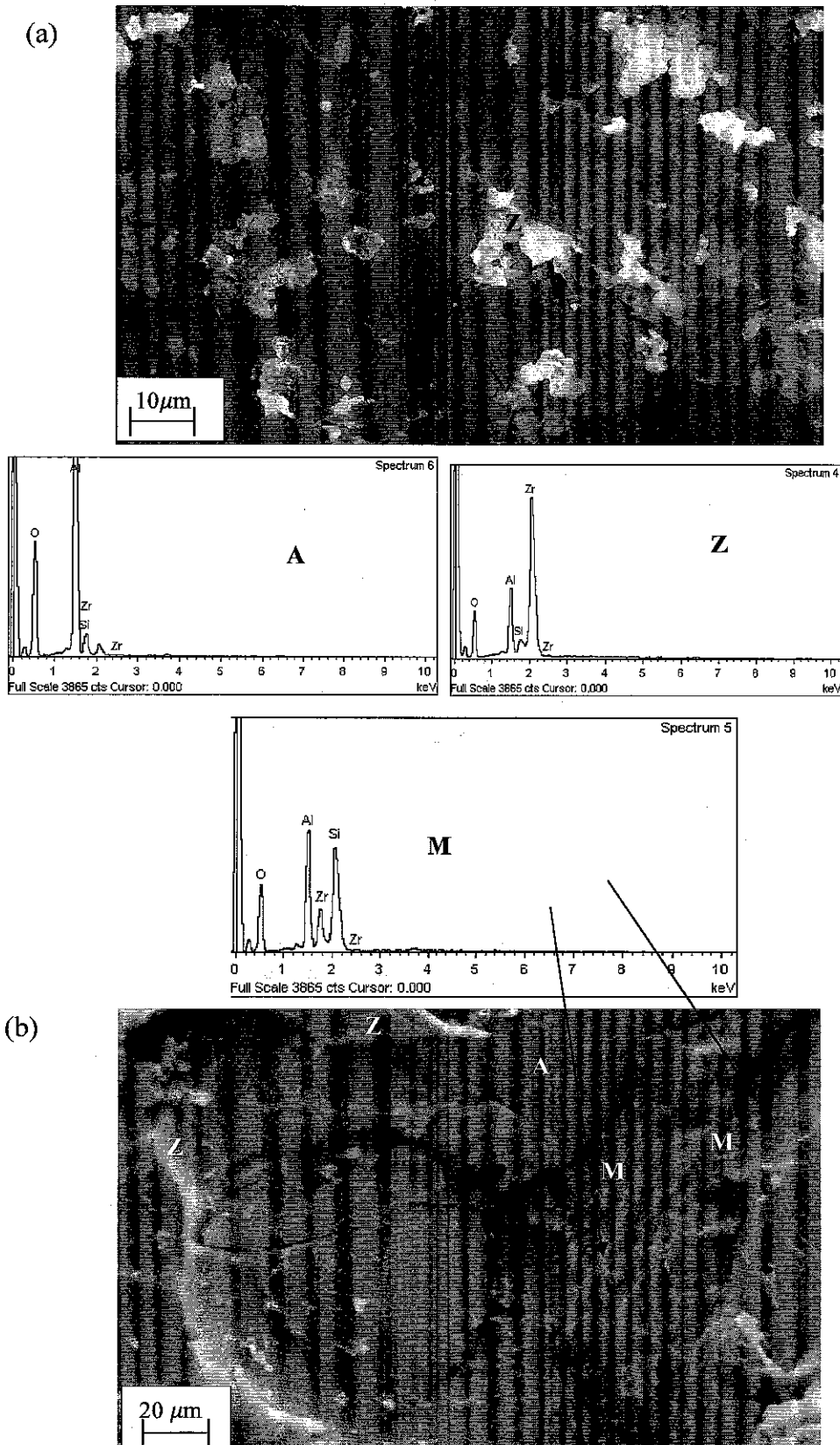


Figure 4.22: FESEM micrographs and EDS spot scan of (a) A-20Z and (b) A-10S-20Z composites

4.4.2.1 Fracture Behavior and Toughening Mechanisms of the ASZ Composite

FESEM micrographs of the surfaces showed distinctive differences in fractured morphology with changes in the material composition. To study the fracture behaviour of the samples, fractographic examination of the fractured surface was performed for possible phase composition. Additional FESEM examination was done by looking at the fractured surface to understand the mode of failure for each composition. The third attempt called Vickers's indentation induced cracks was conducted to determine the crack propagation mechanism in each of the composite. In addition to the microstructural analysis, elemental analysis was carried out by energy dispersive spectrometry (EDS). A detailed FESEM microstructural study on the effect of tri-component for the improved mechanical properties was discussed.

The FESEM micrograph in Figure 4.23 represents the microstructure of sintered ceramic surface for A-10S-20Z. As it has been highlighted in section 4.2, the bright spots on the ceramic surface indicated the area with heavier element like ZrO_2 spectra obtained from Energy Dispersive X-ray Spectroscopy. The line scan across the three component neighboring grains shown in Figure 4.23 indicated that the concentration of ZrO_2 and mullite was increasing towards the grain boundary. This observation proposed that preferential distribution of the phases at grain boundaries was achieved and such microstructures are intended as bases for the formation of toughened boundary that is responsible for the high toughness value.

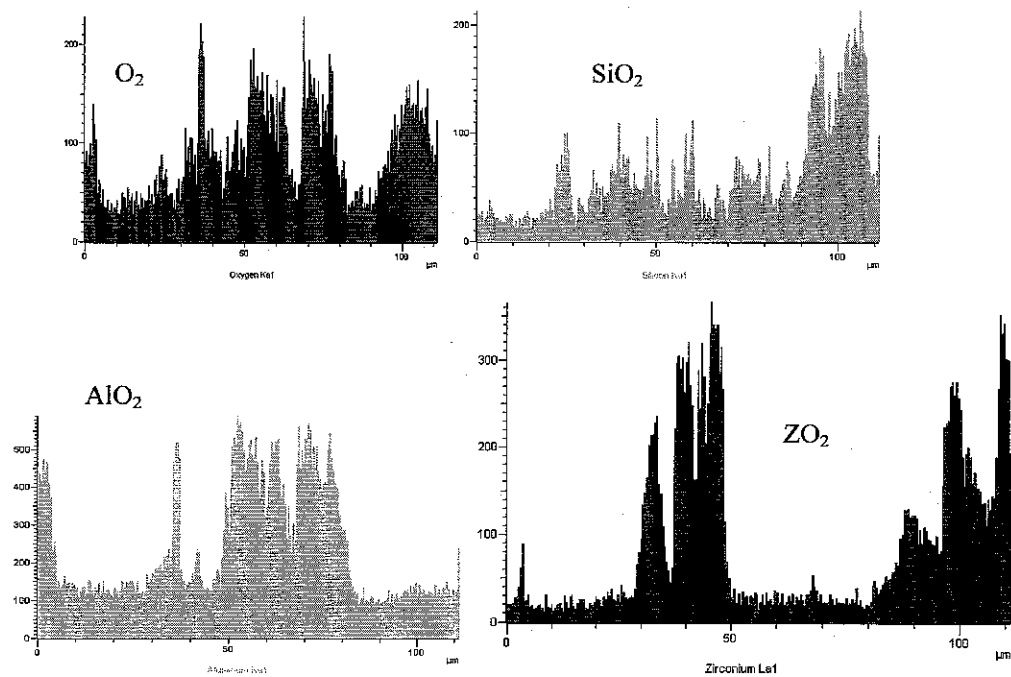


Figure 4.23: FESEM micrograph of the polished surface for the sintered ceramic corresponding EDX line scan across the adjacent grains.

The microstructural observation on cracked and fractured samples showed that three toughening mechanisms, crack deflection, crack bridging and microcracks were

the factors contributing for the high toughness of the matrix and the composite as it would be explained in section 4.4.2.3. Besides, phase transformation toughening and residual stress due to coefficient of thermal expansion difference played a key role for the improved toughness.

4.4.2.2 Cracking behavior of the Monolithic and ASZ composites

The cracking behavior of the three types of composites has been examined by applying a flexural bending load. The surface crack profile and the stress-deflection behavior were studied. Three distinct fracture modes were identified accordingly. A brittle-like structure mode, mixed brittle and ductile modes and mostly ductile failures modes were observed.

Figures 4.24 (a) and (b) showed the load-extension (deflection) curve recorded on a standard sample of the pure Al_2O_3 and A-10S-20Zr composite respectively during three point bending test. The load deflection curve for A-20Z was similar to the A-10S-20Z curve. Figure 4.24(a) showed a sharp decline of the load within the linear elastic behavior showing no residual strength beyond the maximum load, demonstrated by normal brittle materials, and Figure 4.24(b) curve showed an extended feature after the maximum load, differs significantly from the brittle materials property, which gave us a clear indication that plastic deformation has been taken place for the newly developed composite material. The curve is saw-toothed in shape and it was very similar to the AZ obtained by the similar experimental set up. It showed that the crack propagation was very tortuous in the tri-component composite developed.

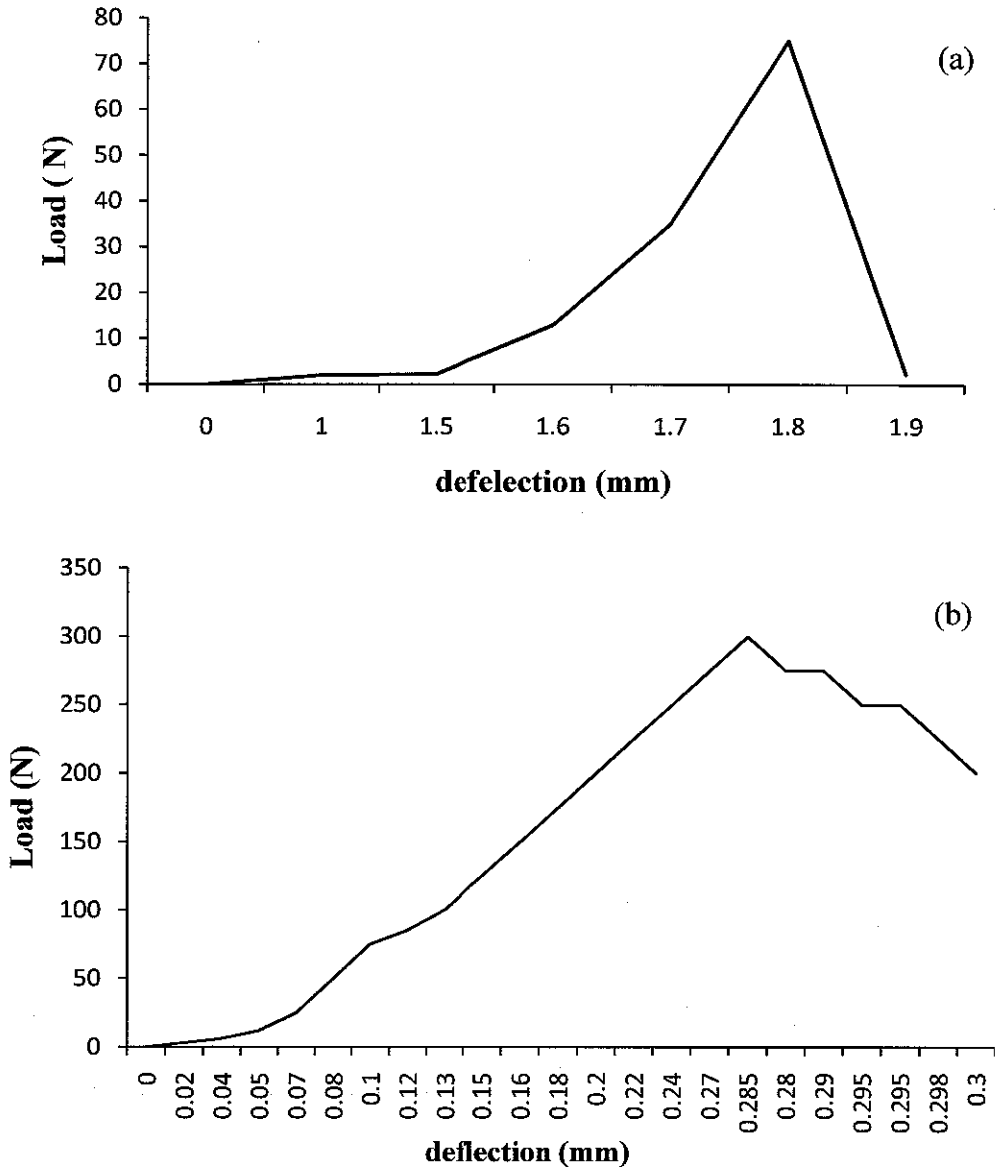


Figure 4.24: Load-displacement curve for (a). monolithic Al_2O_3 and (b). $\text{Al}_2\text{O}_3\text{-SiO}_2\text{-ZrO}_2$ and composites.

The examination of fractured surfaces also revealed information about whether fracture was accompanied by considerable plastic deformation (ductile fracture) or there was almost no plastic deformation (brittle fracture). Figures 4.25 (a)-(c) showed FESEM micrograph on fracture surface of monolithic alumina, AZ and ASZ respectively.

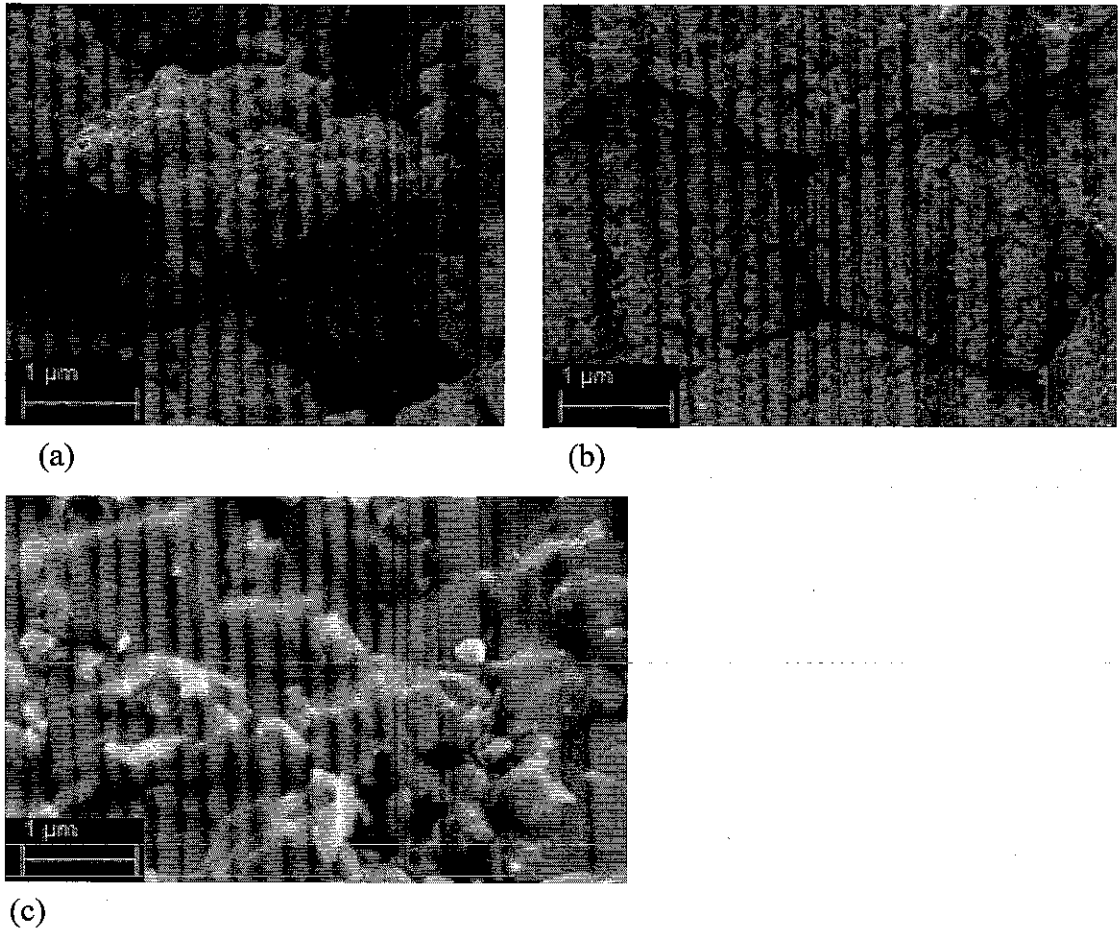


Figure 4.25: FESEM micrographs of the fractured surfaces of (a) monolithic alumina (b) Al₂O₃-ZrO₂ and (c) Al₂O₃-SiO₂-ZrO₂

From Figure 4.25(a), the grain shapes of pure alumina are irregular and there appeared abnormal growth, and the fracture mode was mainly intergranular failure. Meanwhile, from Figures 4.25(b) and 4.24(c) composites with the addition of silica and zirconia, showed a homogeneous distribution of alumina grains but there also appeared abnormal growth. Compared to pure alumina, AZ has uniform size and regular shape of grains, and the fracture mode remained intergranular failure. While in Figure 4.25(c), the addition of zirconia made the microstructures of the composites finer and homogeneous and there was very small trace of grains abnormal growth. Moreover, Figure 4.25(c) showed that there were several “dimples” in fracture surface, which showed tenacious fracture mode and the fracture mode is mainly transgranular failure along with little intergranular failure. A conclusion may be

drawn that the interface between the particle and the matrix was strong. Such an interface ensures the stress to be effectively transferred from the Al_2O_3 matrix to the harder ZrO_2 particles.

4.4.2.3 Toughening Mechanism in the ASZ Composite

In particle reinforced ceramics, residual stress, crack deflection, transformation toughening, microcrack and crack bridging are seen as the main toughening mechanisms. The FESEM micrograph observation and analysis of phases present in A-10S-20Zr composite, the toughening mechanism was likely to be crack bridging, microcracks and these mechanisms were imposed by the lamellar $3\text{Al}_2\text{O}_3 \cdot 2\text{SiO}_2$ (mullite) and zirconia grains. Transformation toughening was also expected to be the main toughening mechanism because high amount of tetragonal and few amount of monoclinic ZrO_2 particles were identified using the EDS in the vicinity of the alumina matrix and along the grain boundaries. The remarkable high toughness than the matrix implies other toughening mechanisms operate in the composite beside the crack bridging toughening mechanisms as indicated above. In this section, the other possible mechanisms were discussed as well.

4.4.2.3.1 Microcracks

Microcrack is one of the toughening mechanisms which are expected to occur in the binary and ternary composites. To investigate this, a fractured surface was analysed using FESEM. Figure 4.26 illustrates the finding of ASZ surface that the zirconia tetragonal-monoclinic transformation occurred during the sintering cooling, producing a concentrated micro cracks in the matrix that may be also responsible for the crack branching as shown by the arrows in Figure 4.26(a) and (b). Such microcrack development was not found during the evaluation of the monolithic alumina sintered samples. The microcracks that surround the grains indicated the branching of the crack actually occurred, which was the source of grain bridging interaction, also enhanced the resistance to fracture.

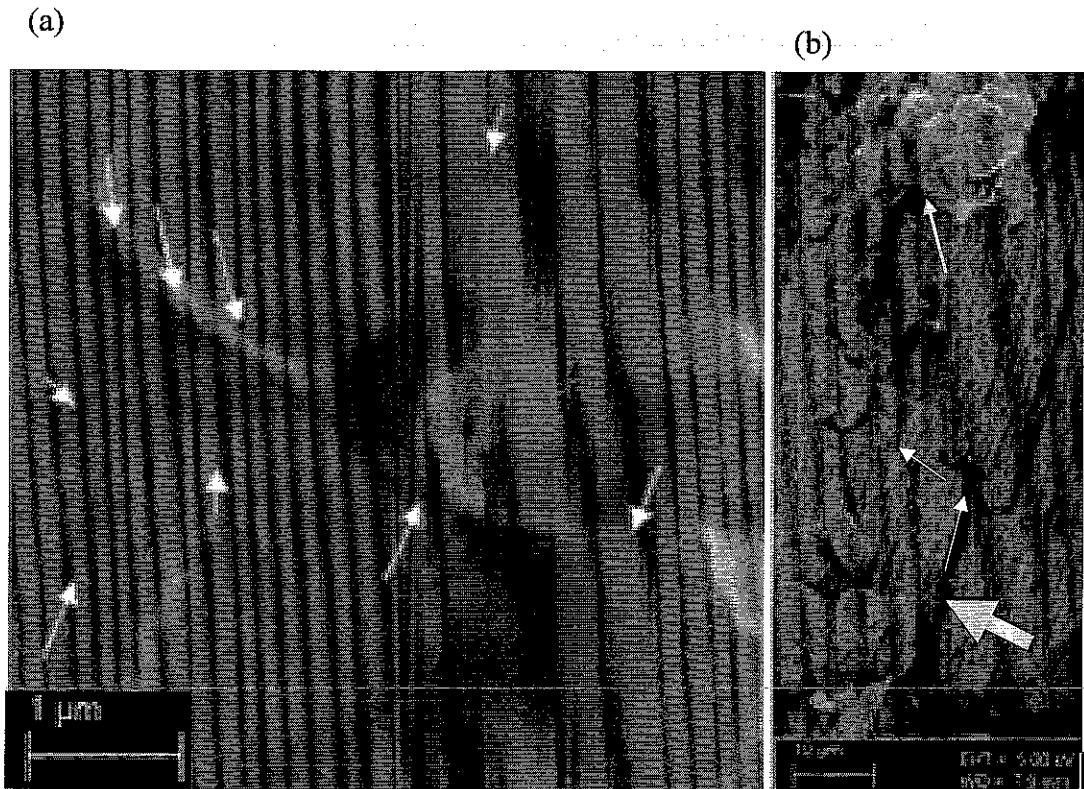


Figure 4.26: FESEM micrograph of the fractured surfaces of ASZ composite (a) microcrack produced by the tetragonal to monoclinic transformation during cooling (b) Note the arrow pointing the microcrack direction and crack bridging

4.4.2.3.2 Crack Deflection and Crack bridging of Fractured surfaces

Crack deflection can take place when there are local areas in ceramics that have lower resistance to crack propagation than the average plane cutting along the tensile stress. Crack deflection can cause partial bridging by grains or second phase particles since the crack may deflect around a grain in its path, leaving the grain bridging the crack. This important toughening mechanism was observed during the fracture surface study in the tri-component ceramic composite (ASZ).

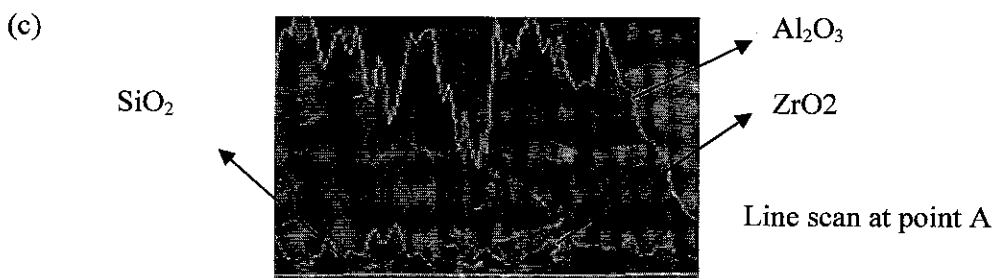
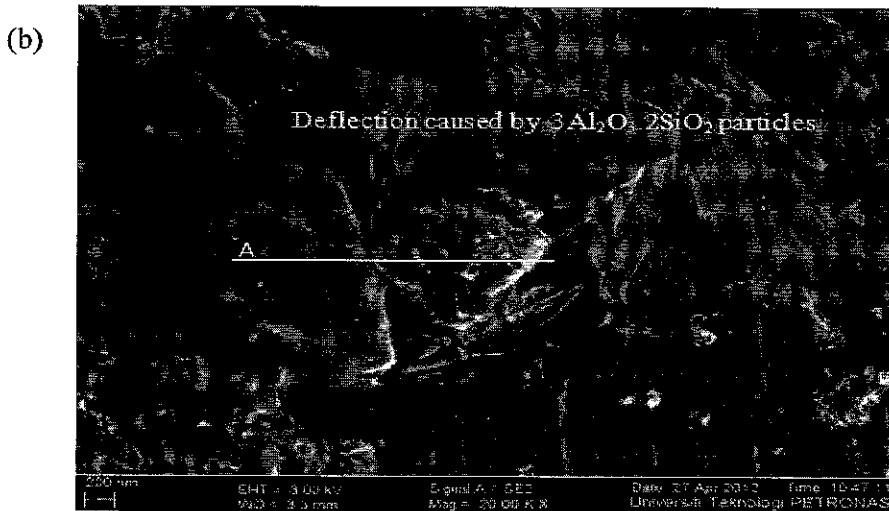
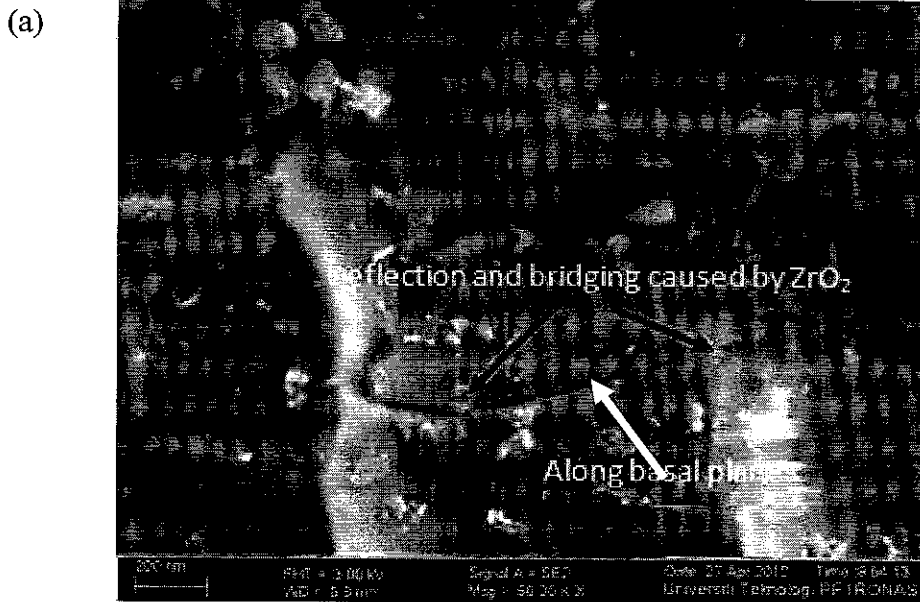


Figure 4.27: FESEM micrographs showing crack deflection and bridging by ZrO_2 and mullite particles in ASZ composite: (a) deflection and bridging by ZrO_2 along basal plane shown by the arrow (b) deflection and bridging by mullite indicated by the arrow (c) EDS line scan at point along A

Figure 4.27 (a) of the ASZ composite surface showed a ZrO_2 phases deflecting the crack propagation as well as bridging at some end. The same was observed in Figure 4.27 (b) that mullet phase was deflecting the crack. Figure 4.27 (c) shows the line scan along the point A on Figure 4.27 (b) which shows the phases available in the cracked surface. The observations of these two phenomenon showed that the interaction between crack deflection and bridging played an important role for the increase in fracture toughness improvement.

4.4.2.3.3 *Vickers Indentation studies*

Cracks were initiated into mirror polished sections of each composite by using a vicker indenter using a load of 1 kg. This load was significant enough to cause crack from the diagonal of pointed edge of the vicker's indenter. The study was performed to gather evidence of energy absorption mechanisms such as crack deflection, crack branching, and microcracking in the ASZ material system. Once indented, specimens were sputter coated using carbon targeted to make them electrically conductive in preparation for the FESEM examination. However, the cracking was not through the thickness, thus, this test was not truly representative of crack propagation through the bulk where material constraint adds another dimension to the propagation modes. It does, however, illustrate the presence of energy absorption mechanisms such as crack deflection, and crack bridging [112, 114].

In the ASZ composite studied, crack propagation occurred via different mechanism depending upon how close was viewed with respect the initial indentation. Near the indentation, crack propagation was marked by significant regions of transgranular fracture and intergranular fracture. This was due to the high driving force in the intermediate vicinity of the vicker's indent. However, at a distance away from the indent it was seen that mostly a form transgranular cracking. Apparently, in all types of cracking a significant amount of crack deflection and grain bridging due to the presence of large grains of zirconia and mullite was observed as shown in Figure 4.21. The crack propagation behavior of the Vickers's indent preferentially along the interface suggested the main toughening mechanism was the crack deflection.

4.4.2.3.4 Transformation Toughening

As discussed in section 4.4.2, where fracture toughness data of the ASZ composite specimens were presented as a function of the total zirconia content, it was clearly observed that the fracture toughness was increasing. Besides that, it was observed in Figure 4.25 that there was micro crack around the grains of zirconia phases. This result suggested that the tetragonal-monoclinic (t-m) transformation potentially contributed to the toughening of ASZ composites. However, increasing the content of zirconia expedites the particle coalescence and coarsening, thereby decreasing the stability of tetragonal phase near room temperature. Therefore, the relative contribution of the t-m transformation toughening is expected to be decreased rapidly with increasing zirconia content. This was observed when the fracture toughness of the composite decreases at 20% by weight along the zirconia axis of the graph of Figure 4.13 in sub section 4.2.2.4.

Because the most important toughening mechanism caused by the monoclinic phase was the microcrack nucleation [62, 89, 92, 103], these results indicated that the toughening by the microcrack nucleation became increasingly important as the total content of zirconia increased. According to the model of transformation toughening proposed by McMeeking and Evans [95], the increment of fracture toughness caused by the transformation toughening was proportional to the volume fraction of tetragonal zirconia particles. Their analysis was based on the reduction in crack-tip stress intensity provided by the transformation-induced stresses. Considering the energy dissipation associated with the transformation toughening, Chen [96] also obtained essentially the same result.

Apart to the transformation toughening, in this research, it was understood that there are other toughening effects which were responsible for the higher toughness of the tri-component than the binary component composite. Because the thermal expansion coefficient of zirconia is significantly larger than that of the alumina matrix and mullite, cooling from processing puts the zirconia particles in tension and the

matrix in hoop compression. Therefore, the crack was not attracted to the dispersed zirconia particles but should deflect around them. Figures 4.26 and 4.27 show typical features of crack propagation in the A-10S-20Z composites containing 10wt% silica and 20 wt% zirconia. A crack propagated straight into the matrix region but deflected around the dispersed zirconia particles.

The difference in thermal and stiffness of the composite components induce residual stress. It was expected that the residual stresses may have been induced due to the thermal expansion misfit between the ZrO_2 , mullite and Al_2O_3 matrix when the composite was cooled down from its sintering temperature. Table 2.1 shows the expansion coefficient of each component used in this research. The interface bonding along the $Al_2O_3/ZrO_2/3Al_2O_3.2SiO_2$ boundaries was improved due to the compressive stress developed, which insured the tough ZrO_2 particles to withstand higher stress loading by effectively transferring load from the matrix to the particles at the interface, and consequently, an effective toughening effect of ZrO_2 on the Al_2O_3 matrix was achieved. A residual tensile stress in the matrix and deflection effect at the phase boundaries might favour the toughening effect of $3Al_2O_3.2SiO_2$ particles.

Summary

This section demonstrates that a strong $Al_2O_3-10SiO_2-20ZrO_2$ (A-10S-20Zr) composite was developed using pressureless sintering route with improved mechanical properties were improved evidently. The flexural strength and fracture toughness of the $SiO_2 - ZrO_2$ reinforced alumina matrix was measured and the value were 230.40 MPa and $2.39 \text{ MPa.m}^{1/2}$, respectively. This demonstrated a significant toughening effect due to the presence of both SiO_2 and ZrO_2 particles. The microstructural observation on cracked and fractured samples showed that three toughening mechanisms, crack deflection, crack bridging and micro cracks were main factors contributing for the high toughness of the matrix and the composite. Besides, phase transformation toughening and residual stress due to coefficient of thermal expansion difference were another contributing factors for the improved toughness of the composite developed.

4.5 The Thermal Shock Resistance of the Al₂O₃-SiO₂-ZrO₂ (ASZ) Composite

4.5.1 Overview

The high temperature properties of the reinforcement are important during service. It was discussed in chapter one that the major attribute of monolithic ceramics was they maintain their properties to high temperatures and this characteristic was only retained in CMCs if the reinforcements also have good high temperature properties. Hence, there is only limited interest in toughening ceramics (mechanical properties) by incorporation of reinforcements of materials, such as ductile metals [25, 106], that lose their strength and stiffness at intermediate temperatures. In this section, the mechanical property and thermal shock behavior of the ASZ composites were investigated. The flexural strength and fracture toughness of ASZ composites were significantly improved when compared with monolithic Al₂O₃ and Al₂O₃-ZrO₂ composites.

4.5.2 Effect of thermal Shock on the Mechanical properties of Al₂O₃-SiO₂-ZrO₂ Composite

Thermal shock happens from two phenomena [105, 106, 123]. Firstly, when the material's uniform thermal expansion is constrained; failure stresses are induced in them. Secondly, internal residual stresses are created when the material is subjected to rapid temperature changes and induce temporary temperature gradients. Because materials do have limited thermal conductivity, thermal shock can be created without external constraints due to temperature gradients. Upon rapid cooling the surface of a high-temperature specimen is accompanied by surface tensile stresses due to the fact that the surface contracts more than the interior where it is still relatively hot. As a consequence, the surface 'pulls' the interior into compression and is itself 'pulled' into tension.

The resistance of ceramics to thermal shock can be characterized using the critical temperature difference (ΔT_c). It is the level of thermal shock resistance characterized the critical temperature required to produce a significant reduction in strength upon cooling or heating.

Figure 4.28 showed the graphs of flexural strength of Al_2O_3 monolith, $\text{Al}_2\text{O}_3\text{-ZrO}_2$, and $\text{Al}_2\text{O}_3\text{-SiO}_2\text{-ZrO}_2$ composites as a function of thermal shock temperature measured after being thermal shocked. The value measured at each of quenching temperature was repeated for 3 times. It can be seen that the flexural (residual) strength of the composites decreased with increasing thermal shock temperature. Similar results have been reported for mullite ceramic [10, 124, 125], ZrC matrix ceramics [126] and nextel or nicalon fiber-reinforced SiC matrix composites [127]. The observation from the curve showed that AZ and ASZ composites increased the thermal shock resistance than monolithic Al_2O_3 as the quenching temperature increased. In the ranges of 0-430 °C, the residual stress was very comparable between the binary ($\text{Al}_2\text{O}_3\text{-ZrO}_2$) and tri component ($\text{Al}_2\text{O}_3\text{-SiO}_2\text{-ZrO}_2$) composites. When the quenching temperature was increased, the residual stress of binary showed a drastic drop while in the ternary system looked moderate, although both composites showed a decreasing trend.

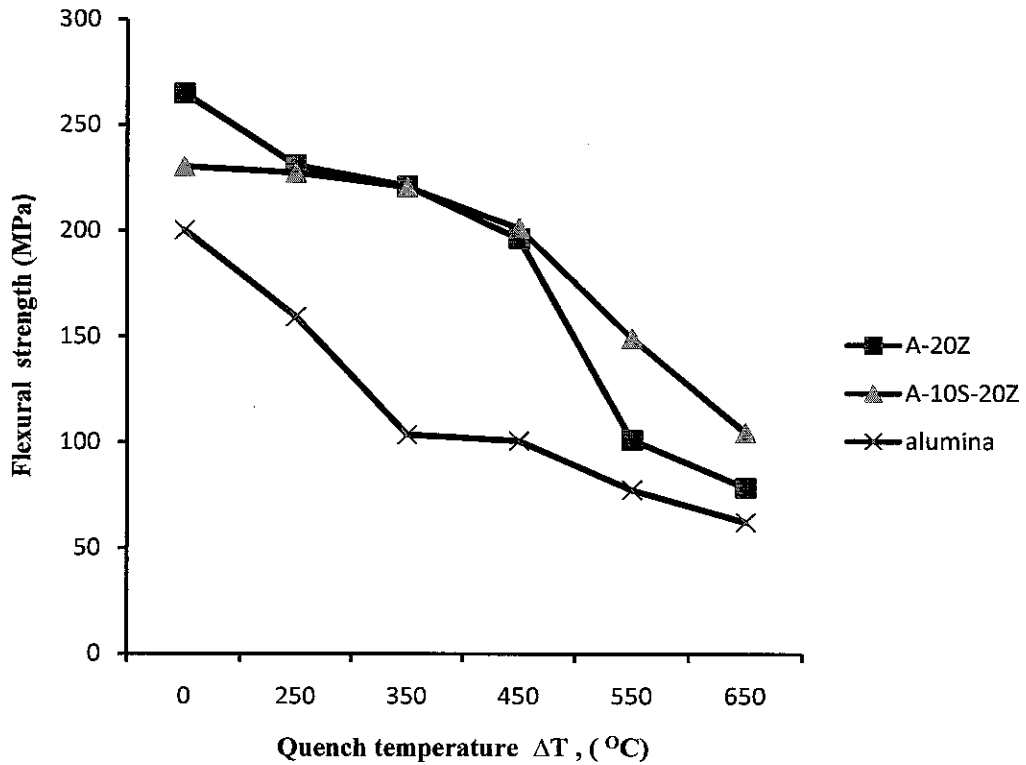


Figure 4.28: Flexural strength versus temperature difference (ΔT) for $\text{Al}_2\text{O}_3 - \text{SiO}_2 - \text{ZrO}_2$, $\text{Al}_2\text{O}_3 - \text{ZrO}_2$ and Al_2O_3 ceramics;

According to ASTM standard, the critical value of the temperature difference (exposure temperature minus the water quench temperature) was determined by a 30% reduction in flexural strength compared to the average flexural strength of the as-received test specimens. And hence, from the experiment, the curve for A10S20Z showed a critical temperature difference of around 430°C and a characteristic drop of flexural strength at that point. This drop was followed by a modest decrease as ΔT increased to 550°C . Further to this temperature, it showed a sharp decline of the flexural strength. The $\text{Al}_2\text{O}_3 - \text{ZrO}_2$ ceramics produced a 30% reduction in strength for a ΔT of 395°C and monolithic AlO_2 around 200°C . These results apparently showed that $\text{Al}_2\text{O}_3 - \text{SiO}_2 - \text{ZrO}_2$ composites had greater resistance to thermal shock. This was attributed to the pinning effect (Zener pinning pressure) of the zirconia oxide and mullite particles positioned at grain boundaries or triple junctions of alumina matrix,

which was one of the well-recognized processes that reduced the driving force for grain growth. The refined grain would play an important role in the improvement of mechanical properties and thermal shock resistance of ASZ composites. Furthermore, the grain size and bulk density would also have an influence on the thermal shock resistance of alumina ceramic. Zhang et al.[128] reported that the thermal shock resistance could be improved by decreasing grain size or increasing the bulk density. It was reported that the thermal shock behavior of pure alumina ceramic with a relative density of 97% has been investigated and reported the improved results. As mentioned before, the presence of ZrO_2 and mullite particles led to a refined alumina matrix grain size and a reduction of porosity. Thus, the combination of them made contribution for improvement of the thermal shock resistance of Al_2O_3 ceramic. Apparently, this composite system was improved in the resistance of thermal shock resistance than the alumina-metallic composites such as alumina-Iron [124], and alumina-copper [129] composite in which the critical temperature difference was reported as 200, and 300°C respectively.

Similarly, as-received and thermally loaded samples after 7 thermal shocks were compared. The fracture toughness as a possible criterion for quantifying microstructural damage caused by the cyclic thermal shock loading was investigated. Indentation method was used to determine the fracture toughness of the composites as shown in Figure 4.29. In order to use the indentation method, the microstructural features of the ceramic materials after thermal shock tests were observed under FESEM. The images obtained at low magnification and high magnification and the resulting shape characteristics (especially the measured indent geometry) were used as input data for fracture toughness calculation.

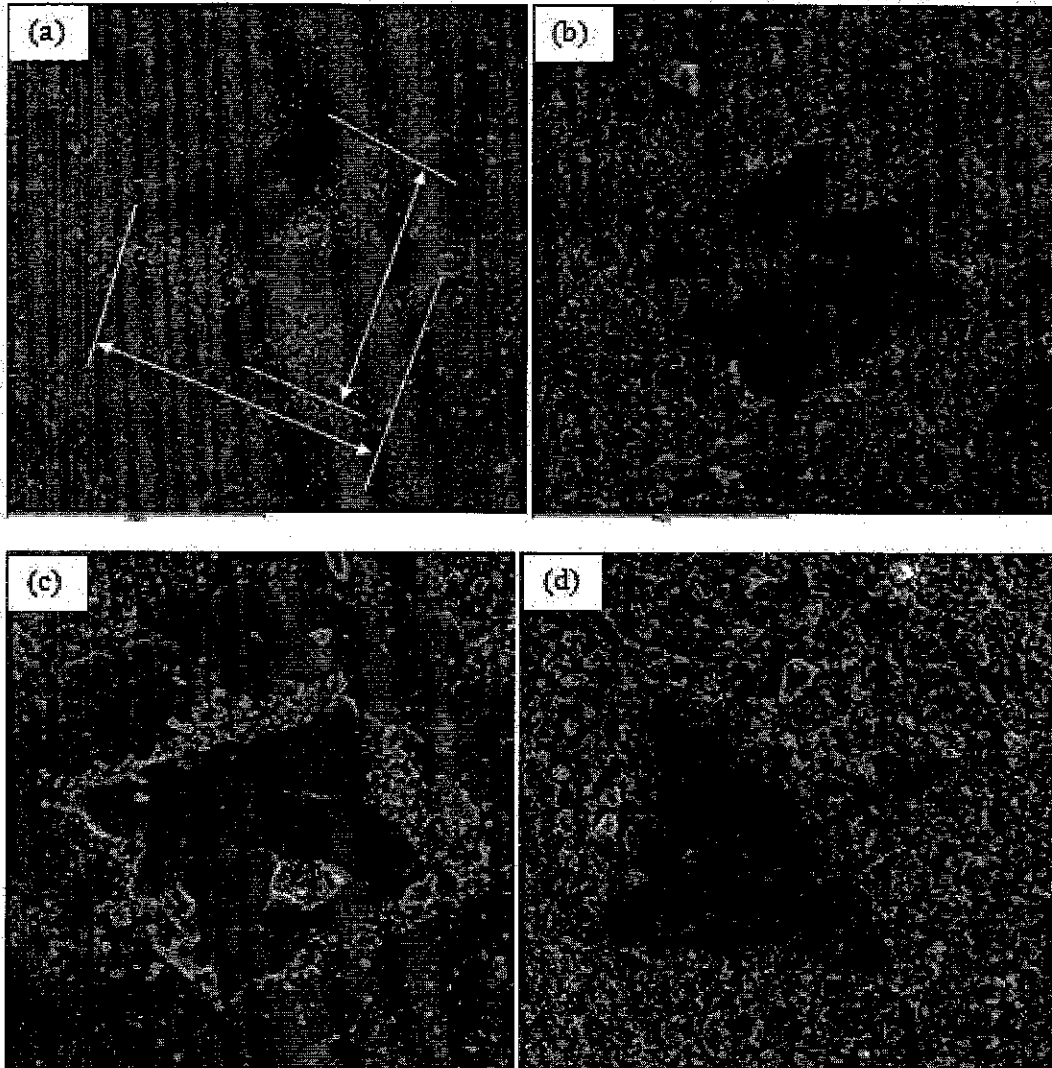


Figure 4.29: Micro indentation of the $\text{Al}_2\text{O}_3\text{-10SiO}_2\text{-20ZrO}_2$ after series of thermal shock cycles (a) 4th cycle (b) 5th cycle (c) 6th cycle (d). 7th cycle

From the previous results in this research, the average fracture toughness value for A-10S-20Z composite in as-received state was $2.39 \text{ MPam}^{1/2}$, for A-20ZrO₂ composite, $1.75 \text{ MPam}^{1/2}$ and for monolithic alumina was $0.8 \text{ MPam}^{1/2}$. After 6 thermal cycles, the Al_2O_3 , AZ and ASZ were tested for fracture toughness. A decrease in fracture toughness by 10.81 % was observed for A-10S-20Z whereas; A-20Z sample exhibits a sharp decline by about 24.65%. This difference in fracture behaviour can be explained by the positive role of the optimum amount of mullites

and silica content in the $\text{Al}_2\text{O}_3\text{-SiO}_2\text{-ZrO}_2$ composite. This was mainly attributed to the improvement of fracture toughness in ASZ composite. It was believed that the grain boundaries were critical to the resistance of crack propagation as much mullite and few amorphous SiO_2 were available. For $\text{Al}_2\text{O}_3\text{-SiO}_2\text{-ZrO}_2$, as mentioned above, the finer grain size due to the tri-component microstructure enhanced fracture toughness by promoting crack bridging and lengthening crack propagation path, which inhibited the propagation of cracks.

4.5.3 Microstructure change during the Thermal shock Test

In the previous sections, the FESEM micrographs of fracture surfaces of sintered monolithic alumina, A-20Z and A-10S-20Z composites before thermal shock experiments were shown. Specifically, it was seen that the mullite and zirconia particles were homogeneously distributed in the alumina matrix and mostly located at grain boundaries. Due to the pinning role of the zirconia and mullite particles, it was also seen that they impeded the growth of grains and led to a refined alumina matrix grain size.

Figures 4.30 (a₁), (a₂), (b) and (c) showed typical FESEM fracture micrographs of a pure Al_2O_3 , AZ and ASZ samples after 6 times of thermal shock tests at 950 °C respectively. It is seen that the fracture surface of pure alumina after thermal shock tests basically exhibited cleavage fracture features (Figure 4.30 (a₁)) and the crack propagation looks straight as the thermal stress too high to resist (Figure 4.30 (b)). With an addition of micro-sized zirconia particles which led to a tougher composite the crack deflection and branching tended to occur frequently, as indicated by arrows in Figure 4.30(b). Most importantly, the ASZ composite was more resistant for thermal shock due to the toughening effect of the zirconia and the shorter length needle-like mullite particles led to some pull-out and crack deflection. It may be also due to the pinning role of the added zirconia and mullite particles that located at grain boundaries or triple junctions of alumina grains as shown in Figure 4.30 c. It indicated that the added micro sized silica and zirconia particles played an important role to improve the thermal shock resistance of alumina ceramic.

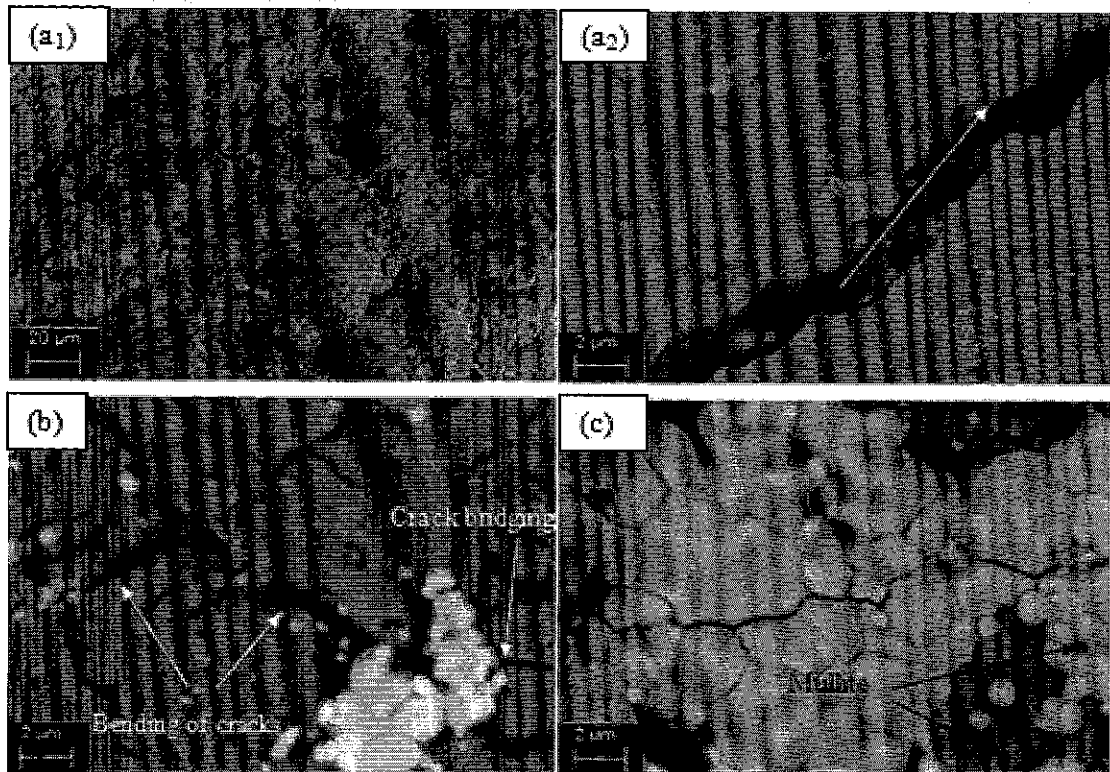


Figure 4.30: FESEM micrographs of thermal shock-induced crack propagation on fractured surfaces at the 6th cycle: (a₁) Al₂O₃ (a₂) Al₂O₃ (b) A-20Z (c). A-10S-20Z

The observation from the FESEM cross sections examination of the AZ and ASZ composites after 6 cycles also showed that more degradation happened in the AZ samples. This degradation can be seen from the zirconia phase scattered and pulled due to the thermal stress. In the ASZ composite, there is still better microstructural integrity where the zirconia can be seen in well stabilized and structured and the cracks were deflected in different direction. This implied shown that the ASZ composite had better fracture toughness than the AZ. The availability of SiO₂ and mullite phases around the grain boundaries could be the main reason for better thermal shock properties [125].

In addition to the above, the improved fracture toughness by tri-component system of the ASZ composite would play an important role in the improvement of thermal shock resistance of alumina ceramic. As Tancret et al. [123] reported, the improvement in the fracture toughness and thermal shock resistance could be

achieved by making composites in which the interfaces between the matrix and particles acted to deflect propagating cracks. Zhao et al. [130] also reported the mechanisms like crack branching and deflection that occurred at the interfaces between the two phases, impeding the crack growth.

The difference in the thermal properties of the SiO₂, ZrO₂ and alumina could also have an effect on the thermal shock behavior of ASZ composite, as indicated in Equation 2.11. The coefficient of thermal expansion of mullite [5] is $5.4 \times 10^{-6}/^{\circ}\text{C}$ which is lower than that of ZrO₂ ($10.3 \times 10^{-6}/^{\circ}\text{C}$). Furthermore, the thermal conductivity of mullite and alumina [5] are $6 \text{ W m}^{-1} \text{ K}^{-1}$ and $18 \text{ W m}^{-1} \text{ K}^{-1}$, respectively. The thermal shock resistance of pure mullite ceramic would thus be better than that of pure alumina ceramic. Many researchers [58, 107, 123, 130] also reported that the thermal properties (i.e., thermal expansively, thermal conductivity, and other properties associated with the use at high temperatures) were important in determining the thermal shock resistance of ceramic composites. Therefore, the improved thermal shock resistance of ASZ composites could also be partly attributed to the superior thermal properties of the added particles.

Summary

The critical temperature difference of thermal shock resistance for Al₂O₃- SiO₂- ZrO₂ was found to be higher than than the monolithic Al₂O₃ and AZ composites. The thermal shock temperature difference (ΔT_c) of the Al₂O₃ monolith was about 200°C, while the ΔT_c of AZ composites was about 395°C and the ΔT_c of ASZ composites was about 430°C. Such superior thermal shock resistance was attributed to the remarkable improvement of the fracture toughness by tri-component composite. The results in this work also indicated that the SiO₂ addition resulted in mullite, contributed for the high resistance to thermal shock.

CHAPTER 5

CONCLUSION AND RECOMMENDATIONS

5.1 Conclusions

The main objective of this experimental research was to develop alumina matrix based ceramic composites, which have improved fracture toughness and resistance to thermal shock. This objective was achieved by a three component Al_2O_3 - SiO_2 - ZrO_2 composite using a pressureless sintering route. The effects of each separate component on the mechanical and thermal properties of ASZ composites were systematically studied. An optimum percentage of SiO_2 and ZrO_2 were added to alumina to determine the right quantity for the improved mechanical properties. Mechanical tests were conducted to determine the flexural and fracture toughness for the monolithic alumina, AZ and ASZ composites. The microstructure of sintered composites, thermal shock and fracture surface states were also investigated using FESEM and AFM. The following conclusions were derived based on the objectives set for this research:

- An appropriate and optimized compositional mix and hence microstructural tailoring, improved mechanical properties in alumina-silica-zirconia composites were achieved. Systematically, the result showed a composition of tri-component composite A-10S-20Z (70% by weight of alumina, 10 % by weight of silica and 20 % by weight of zirconia) was achieved.
- The effect of SiO_2 (Silica sand) addition for the densification of the ASZ composite was studied. Dilatometric study revealed that that the first liquid formed as low as 1100°C , showed a significant reduction of the sintering temperature. The final phase composition of the system was obtained at 1450°C consisted of crystalline alumina, mullite and zirconia phases. The results showed that the SiO_2 is a very effective low-temperature sintering

additive for ASZ composites. This was due to the low viscosities of the silica rich residual phases.

- The $\text{Al}_2\text{O}_3\text{-SiO}_2\text{-ZrO}_2$ composite demonstrated a higher value for fractural toughness. The flexural strength and fracture toughness of the $\text{SiO}_2\text{-ZrO}_2$ reinforced alumina matrix was developed and measured as high as 230.40 MPa and $2.39 \text{ MPa}\cdot\text{m}^{1/2}$, respectively, demonstrating a significant toughening effect due to the presence of both mullite and ZrO_2 phases. The microstructural observation on cracked and fractured samples showed that three toughening mechanisms, crack deflection, crack bridging and micro cracks were the factors accounting for the high toughness of the matrix and the composite. Besides, phase transformation toughening and residual stress due to coefficient of thermal expansion difference were the contributing factors for the improved toughness.
- A standard thermal shock test was done and the critical temperature difference of thermal shock resistance for $\text{Al}_2\text{O}_3\text{-SiO}_2\text{-ZrO}_2$ was found to be higher than the monolithic Al_2O_3 and AZ composites. The thermal shock temperature difference (ΔT_c) of the Al_2O_3 monolith was about 200°C , while the ΔT_c of AZ composites was about 395°C and the ΔT_c of ASZ composites was about 430°C . Such superior thermal shock resistance was attributed to the remarkable improvement of the fracture toughness by three component composite. The results in this work also indicated that, the SiO_2 addition resulted in mullite, contributed for the high resistance to thermal shock.
- The fracture toughness of the thermal shocked composites after 6 thermal cycles were compared and a decrease in fracture toughness by 10.81 % was observed for A-10S-20Z whereas; A-20Z sample exhibited a sharp decline by about 24.65 %. This difference in fracture behaviour can be explained by the positive role of the optimum amount of mullites and silica content in the ASZ composite. This was mainly attributed to the improvement of fracture toughness in ASZ composite. It was believed that the grain boundaries were critical to the resistance of crack propagation as much mullite and few amorphous SiO_2 were available. For $\text{Al}_2\text{O}_3\text{-SiO}_2\text{-ZrO}_2$, due to the tri-component microstructure, it enhanced fracture toughness by promoting crack

bridging and lengthening crack propagation path, which inhibited the propagation of cracks.

5.2 Recommendations

For future consideration and following up of this research, additional work should be done to further investigate and improve the mechanical properties of the composite.

- A separate work for the modelling or analysis or prediction of performance of the composite produced in service may be proposed to compare the results with the experimental work here in this research.
- Recently, the use of alumina based ceramic composites is getting in demand in medical applications such as hip arthroplasty and Orthopedic implants. With this regard, further study may be done in testing the ASZ composite for the application in the medical field.

REFERENCES

- [1] A. Sommers, Q. Wang, X. Han, C. T'Joen, Y. Park, and A. Jacobi, "Ceramics and ceramic matrix composites for heat exchangers in advanced thermal systems" A review," *Applied Thermal Engineering*, vol. 30, pp. 1277-1291, 2010.
- [2] R. W. Bayliss, The sintering, microstructural analysis and mechanical properties of two β' MgSiAlON ceramics: Ph.D dissertation, *University of Warwick*, 1986.
- [3] J. P. B. Singh, Narottam P.; Ustundag, Ersan, *Advances in Ceramic Matrix Composites VI*: John Wiley & Sons Inc, 2000.
- [4] E. Medvedovski, "Alumina-mullite ceramics for structural applications," *Ceramics International*, vol. 32, pp. 369-375, 2006.
- [5] N. Amsc and A. A. Cmps, *Composite Materials Hand Book, Department of Defence*, vol. 5, 2002.
- [6] M. H. Bocanegra-Bernal and S. D. De La Torre, "Phase transitions in zirconium dioxide and related materials for high performance engineering ceramics," *Journal of Materials Science*, vol. 37, pp. 4947-4971, 2002.
- [7] R. Z. C. W.H. Tuan, T.C. Wang, C.H. Cheng, P.S. Kuo, "Mechanical properties of Al_2O_3/ZrO_2 composites," *Journal of the European Ceramic Society*, vol. 22, pp. 2827-2833, 2002.
- [8] C. C. Anya, "Microstructural nature of strengthening and toughening in Al_2O_3-SiC (p) nanocomposites," *Journal of Materials Science*, vol. 34, pp. 5557-5567, 1999.

- [9] H. Kaya, "The application of ceramic-matrix composites to the automotive ceramic gas turbine," *Composites science and technology*, vol. 59, pp. 861-872, 1999.
- [10] C. Aksel, "Mechanical properties and thermal shock behaviour of alumina-mullite-zirconia and alumina-mullite refractory materials by slip casting," *Ceramics International*, vol. 29, pp. 311-316, 2003.
- [11] K. K. Chawla, *Ceramic matrix composites*. New York: Springer, 2003.
- [12] J. S. Moya and M. I. Osendi, "Effect of ZrO_2 (ss) in mullite on the sintering and mechanical properties of mullite/ ZrO_2 composites," *Journal of Materials Science Letters*, vol. 2, pp. 599-601, 1983.
- [13] A. Nevarez-Rascon, A. Aguilar-Elguezabal, E. Orrantia, and M. H. Bocanegra-Bernal, " Al_2O_3 (w)- Al_2O_3 (n)- ZrO_2 (TZ-3Y) n multi-scale nanocomposite: An alternative for different dental applications?," *Acta Biomaterialia*, vol. 6, pp. 563-570, 2009.
- [14] C. Oelgardt, J. Anderson, J. G. Heinrich, and G. L. Messing, "Sintering, microstructure and mechanical properties of Al_2O_3 - Y_2O_3 - ZrO_2 (AYZ) eutectic composition ceramic microcomposites," *Journal of the European Ceramic Society*, vol. 30, pp. 649-656, 2010.
- [15] D. Zhang, L. Zhang, Z. Fu, and J. G. a. W.-H. Tuan, "Differential sintering of Al_2O_3/ZrO_2 -Ni composite,during pulse electric current sintering," *Ceramic international*, Vol. 32, pp. 241-247, 2005.
- [16] K. F. Cai, D. S. McLachlan, N. Axen, and R. Manyatsa, "Preparation, microstructures and properties of Al_2O_3 -TiC composites," *Ceramics International*, vol. 28, pp. 217-222, 2002.
- [17] T. D. Stewart, J. L. Tipper, G. Insley, R. M. Streicher, E. Ingham, and J. Fisher, "Long term wear of ceramic matrix composite materials for hip prostheses under severe swing phase microseparation," *Journal of Biomedical Materials Research Part B: Applied Biomaterials*, vol. 66, pp. 567-573, 2003.

- [18] A. C. Mazzei and J. A. Rodrigues, "Alumina-mullite-zirconia composites obtained by reaction sintering: Part I. Microstructure and mechanical behaviour," *Journal of Materials Science*, vol. 35, pp. 2807-2814, 2000.
- [19] A. C. Mazzei, J. A. Rodrigues, and V. C. Pandolfelli, "Alumina-mullite-zirconia composites obtained by reaction sintering Part II. R-Curve behavior," *Journal of Materials Science*, vol. 35, pp. 2815-2824, 2000.
- [20] R. W. Davidge, *Mechanical behaviour of ceramics*: Cambridge Univ. Pr., 1979.
- [21] M. A. Meyers and K. K. Chawla, "Mechanical Behaviour of Materials, 1999 Prencite-Hall," *Inc., New Jersey*, 1999.
- ~~[22] M. Andre, Krishan Kumar Chawla, "Mechanical Behavior Of Materials, Cambridge: Cambridge University Press, 2008.~~
- [23] C. Santos, R. C. Souza, N. Almeida, F. A. Almeida, R. R. F. Silva, and M. Fernandes, "Toughened ZrO₂ ceramics sintered with a La₂O₃-rich glass as additive," *Journal of Materials Processing Technology*, vol. 200, pp. 126-132, 2008.
- [24] J. A. R. C. R. FERRARI, "Microstructural features of alumina refractories with mullite-zirconia aggregates," *Bol. Soc. Esp. Cerám. Vidrio*, Vol. 42, pp. 15-20 (2003)
- [25] B.-K. Jang, M. Enoki, T. Kishi, and H.-K. Oh, "Effect of second phase on mechanical properties and toughening of Al₂O₃ based ceramic composites," *Composites Engineering*, vol. 5, pp. 1275-1286, 1995.
- [26] J. D. Kuntz, *Processing and properties of ceramic nanocomposites designed for improved fracture toughness*. Davis: University of California, 2005.
- [27] G. Y. Lin and T. C. Lei, "Microstructure, mechanical properties and thermal shock behaviour of Al₂O₃+ZrO₃+SiC composites," *Ceramics International*, vol. 24, pp. 313-326, 1998.

- [28] A. E. Martinelli, D. S. A. Paulo, R. M. Nascimento, M. P. Távora, U. U. Gomes, and C. Alves, "Dilatometric behavior and microstructure of sintered Fe–NbC and Fe–TaC composites," *Journal of Materials Science*, vol. 42, pp. 314-319, 2007.
- [29] B. Matovic, A. Saponjic, M. Posarac, A. Egelja, A. Radosavljevic-Mihajlovic, and S. Boskovic, "Dilatometric study of Si~3N~4-LAS system," *CERAMICS SILIKATY*, vol. 51, p. 210, 2007.
- [30] C. Sallé, A. Maitre, J. F. Baumard, and Y. Rabinovitch, "A first approach of silica effect on the sintering of Nd: YAG," *Optical review*, vol. 14, pp. 169-172, 2007.
- [31] P. Auerkari, Mechanical and physical properties of engineering alumina ceramics: VTT Technical Research Center of Finland, 1996.
- [32] R. Morrell, "Handbook of Properties of Technical and Engineering Ceramics. Part 2: Data Reviews. Section I: High-Alumina Ceramics," *Her Majesty's Stationery Office*, 1987, p. 255, 1987.
- [33] D. W. Richerson, *Modern ceramic engineering: properties, processing, and use in design*. New York: M.Decker, 2006.
- [34] C. B. Carter and M. G. Norton, *Ceramic materials: Science and Engineering*, 1st ed. New York: Springer, 2007.
- [35] L. B. Garrido, E. F. Aglietti, L. Martorello, M. A. Camerucci, and A. L. Cavalieri, "Hardness and fracture toughness of mullite-zirconia composites obtained by slip casting," *Materials Science and Engineering: A*, vol. 419, pp. 290-296, 2006.
- [36] S. Aball, "Effect of TiO₂ doping on microstructural properties of Al₂O₃-based single crystal ceramics," *Journal of Ceramic Processing Research*, vol. 12, pp. 21-25, 2011.

- [37] S. J. Schneider, *Engineered Materials Handbook, Vol. 4: Ceramics and Glasses*. OH: ASM International, Metals Park, 1991.
- [38] T. Chen, "Study and improvement of superplasticity in ceramic composites," in *Dissertation*: University of California, Irvine, 2006.
- [39] M. Awaad, M. F. Zawrah, and N. M. Khalil, "In situ formation of zirconia-alumina-spinel-mullite ceramic composites," *Ceramics International*, vol. 34, pp. 429-434, 2008.
- [40] M. M. Schwartz, *Handbook of structural ceramics*. New York, NY McGraw-Hill, 1991.
- [41] J. S. Reed, *Introduction to the principles of ceramic processing*. New York: Wiley, 1988.
- [42] K. Kendall, "Influence of powder structure on processing and properties of advanced ceramics," *Powder Technology*, vol. 58, pp. 151-161, 1989.
- [43] H. B. Lim, W. S. Cho, and C. Y. Kim, "Effect of Particle Size Distribution of Alumina on Strength of Glass-Infiltrated Alumina," *Ceramics International*, vol. 38, pp. 3067-3074, 2011.
- [44] C. Aksel and F. L. Riley, "Effect of the particle size distribution of spinel on the mechanical properties and thermal shock performance of MgO spinel composites," *Journal of the European Ceramic Society*, vol. 23, pp. 3079-3087, 2003.
- [45] F. Peng, *Pressureless sintering and oxidation resistance of zirconium diboride based ceramic composites*: ProQuest, 2009.
- [46] S. C. Zhang, G. E. Hilmas, and W. G. Fahrenholtz, "Pressureless densification of zirconium diboride with boron carbide additions," *Journal of the American Ceramic Society*, vol. 89, pp. 1544-1550, 2006.

- [47] J. Marchi, J. C. Bressiani, and A. H. A. Bressiani, "Densification studies of silicon carbide-based ceramics with yttria, silica and alumina as sintering additives," *Materials Research*, vol. 4, pp. 231-236, 2001.
- [48] M. C. Garcia, "Dilatometric Study of Ti_3SiC_2 Synthesis from TiC/Si Starting Powders," M.S. thesis, Advanced materials science and engineering, Lulea University of technology, Sweden, 2008.
- [49] M. N. Rahaman, *Ceramic processing and sintering*, 2nd ed. vol. 23. New York: Marcel Dekker, 2003.
- [50] S. Y. Choi and S. J. L. Kang, "Sintering kinetics by structural transition at grain boundaries in barium titanate," *Acta Materialia*, vol. 52, pp. 2937-2943, 2004.
- [51] C. B. Carter and M. G. Norton, *Ceramic materials*: Springer, 2007.
- [52] R. Semp, D. Bourret, T. Woignier, J. Phalippou, and R. Jullien, "Scaling approach to sintering of fractal matter," *Physical review letters*, vol. 71, pp. 3307-3310, 1993.
- [53] M. Braginsky, V. Tikare, and E. Olevsky, "Numerical simulation of solid state sintering," *International journal of solids and structures*, vol. 42, pp. 621-636, 2005.
- [54] R. M. German, *Liquid phase sintering*. New York: Springer, 1985.
- [55] S. C. Lee and K. T. Kim, "Densification behavior of nanocrystalline titania powder under cold compaction," *Powder Technology*, vol. 186, pp. 99-106, 2008.
- [56] Z. Shike, H. Xiaoxian, and G. Jingkun, "The effect of mullite seeding on reaction-sintered mullite-zirconia multiphase ceramic," *Journal of Materials Science Letters*, vol. 19, pp. 707-710, 2000.

- [57] J. Requena, R. Moreno, and J. S. Moya, "Alumina and alumina/zirconia multilayer composites obtained by slip casting," *Journal of the American Ceramic Society*, vol. 72, pp. 1511-1513, 1989.
- [58] V. S. Nagarajan and K. J. Rao, "Thermally induced chemical and structural changes in alumina-zirconia-silica gels during the formation of ceramic composites," *Journal of Solid State Chemistry*, vol. 88, pp. 419-428, 1990.
- [59] C. Zanelli, M. Dondi, M. Raimondo, and G. Guarini, "Phase composition of alumina-mullite-zirconia refractory materials," *Journal of the European Ceramic Society*, vol. 30, pp. 29-35, 2010.
- [60] H. Schneider and K. Okada, *Mullite and mullite ceramics*. Chichester and New York: John Wiley, 1994.
-
- [61] C. Xu, X. Ai, and C. Huang, "Fabrication and performance of an advanced ceramic tool material," *Wear*, vol. 249, pp. 503-508, 2001.
- [62] J. Wang and R. Stevens, "Zirconia-toughened alumina (ZTA) ceramics," *Journal of Materials Science*, vol. 24, pp. 3421-3440, 1989.
- [63] M. D. Sacks, K. Wang, G. W. Scheiffele, and N. Bozkurt, "Effect of Composition on Mullitization Behavior of Alumina/Silica Microcomposite Powders," *Journal of the American Ceramic Society*, vol. 80, pp. 663-672, 1997.
- [64] F. J. Klug, S. Prochazka, and R. H. Doremus, "Alumina-Silica Phase Diagram in the Mullite Region," *Journal of the American Ceramic Society*, vol. 70, pp. 750-759, 1987.
- [65] C. S. Kim, C. W. Kim, and S. N. Chang, "Alumina-silica ceramic," Google Patents, 2003.
- [66] T. S. Jones, S. Kimura, and A. Muan, "Phase Relations in the System FeO-Fe₂O₃-ZrO₂-SiO₂," *Journal of the American Ceramic Society*, vol. 50, pp. 137-142, 1967.

- [67] T. Ahmad and O. Mamat, "The development and characterization of zirconia-silica sand nanoparticles composites," *World*, vol. 1, pp. 7-14, 2011.
- [68] G. Orange, G. Fantozzi, F. Cambier, C. Leblud, M. R. Anseau, and A. Leriche, "High temperature mechanical properties of reaction-sintered mullite/zirconia and mullite/alumina/zirconia composites," *Journal of Materials Science*, vol. 20, pp. 2533-2540, 1985.
- [69] F. Cambier, "Formation of microstructural defects in mullite-zirconia and mullite-alumina-zirconia composites obtained by reaction-sintering of mixed powders," *BR. CERAM. TRANS. J. Br. Ceram. Trans. J.*, vol. 83, p. 196, 1984.
- [70] N. Claussen and J. Jahn, "Mechanical Properties of Sintered, In Situ reacted Mullite-Zirconia Composites," *Journal of the American Ceramic Society*, vol. 63, pp. 228-229, 1980.
- [71] T. Ebadzadeh and W. E. Lee, "Processing-microstructure-property relations in mullite-cordierite composites," *Journal of the European Ceramic Society*, vol. 18, pp. 837-848, 1998.
- [72] R. W. Rice, *Mechanical properties of ceramics and composites: grain and particle effects* vol. 17. New York: Marcel Dekker, 2000.
- [73] M. J. Jackson, *Machining with Abrasives*. New York: Springer 2008.
- [74] X. Zhang, C. Liu, M. Li, and J. Zhang, "Research on toughening mechanisms of alumina matrix ceramic composite materials improved by rare earth additive," *Journal of Rare Earths*, vol. 26, pp. 367-370, 2008.
- [75] T. Chen and M. L. Mecartney, "Superplastic compression, microstructural analysis and mechanical properties of a fine grain three-phase alumina-zirconia-mullite ceramic composite," *Materials Science and Engineering: A*, vol. 410-411, pp. 134-139, 2005.
- [76] R. W. Davidge and T. J. Green, "The strength of two-phase ceramic/glass materials," *Journal of Materials Science*, vol. 3, pp. 629-634, 1968.

- [77] R. W. Davidge, R. J. Brook, F. Cambier, M. Poorteman, A. Leriche, D. O'Sullivan, S. Hampshire, and T. Kennedy, "Fabrication, properties, and modelling of engineering ceramics reinforced with nanoparticles of silicon carbide," *British ceramic transactions*, vol. 96, pp. 121-127, 1997.
- [78] W. J. Clegg, K. Kendall, N. M. N. Alford, T. W. Button, and J. D. Birchall, "A simple way to make tough ceramics," *Nature*, vol. 347, pp. 455-457, 1990.
- [79] K. Hirao, T. Nagaoka, M. E. Brito, and S. Kanzaki, "Microstructure Control of Silicon Nitride by Seeding with Rodlike β -Silicon Nitride Particles," *Journal of the American Ceramic Society*, vol. 77, pp. 1857-1862, 1994.
- [80] R. C. Garvie, R. H. Hannink, and R. T. Pascoe, "Ceramic steel," *Nature International weekly journal of science*, vol. 258, pp. 703-704 1975.
- [81] R. D. Krieg, J. C. Swearingen, and R. W. Rohde, "Physically-based internal variable model for rate-dependent plasticity," Sandia Labs., Albuquerque, N. Mex.(USA) 1978.
- [82] K. Niihara, "New design concept of structural ceramics—ceramic nanocomposites," *Nippon seramikusu kyokai gakujutsu ronbunshi*, vol. 99, pp. 974-982, 1991.
- [83] K. Niihara, A. Nakahira, and T. Sekino, "New nanocomposite structural ceramics," 1993, pp. 405-412.
- [84] T. Ohji, Y. K. Jeong, Y. H. Choa, and K. Niihara, "Strengthening and toughening mechanisms of ceramic nanocomposites," *Journal of the American Ceramic Society*, vol. 81, pp. 1453-1460, 1998.
- [85] I. Levin, W. D. Kaplan, D. G. Brandon, and A. A. Layyous, "Effect of SiC submicrometer particle size and content on fracture toughness of alumina-SiC nanocomposites," *Journal of the American Ceramic Society*, vol. 78, pp. 254-256, 1995.

- [86] H. Tan and W. Yang, "Toughening mechanisms of nano-composite ceramics," *Mechanics of materials*, vol. 30, pp. 111-123, 1998.
- [87] L. Carroll, M. Sternitzke, and B. Derby, "Silicon carbide particle size effects in alumina-based nanocomposites," *Acta Materialia*, vol. 44, pp. 4543-4552, 1996.
- [88] M. Sternitzke, "Structural ceramic nanocomposites," *Journal of the European Ceramic Society*, vol. 17, pp. 1061-1082, 1997.
- [89] D. Singh and D. K. Shetty, "Fracture toughness of polycrystalline ceramics in combined mode I and mode II loading," *Journal of the American Ceramic Society*, vol. 72, pp. 78-84, 1989.
- [90] H. Awaji, S. M. Choi, and E. Yagi, "Mechanisms of toughening and strengthening in ceramic-based nanocomposites," *Mechanics of materials*, vol. 34, pp. 411-422, 2002.
- [91] R. O. Ritchie, "Mechanisms of fatigue crack propagation in metals, ceramics and composites: role of crack tip shielding," *Materials Science and Engineering: A*, vol. 103, pp. 15-28, 1988.
- [92] D. J. Green, R. H. J. Hannink, and M. V. Swain, "Transformation toughening of ceramics," *Nature International weekly journal of science*, 1989.
- [93] K. T. Faber and A. G. Evans, "Crack deflection processes--I. Theory," *Acta Metallurgica*, vol. 31, pp. 565-576, 1983.
- [94] K. T. Faber and A. G. Evans, "Crack deflection processes--II. Experiment," *Acta Metallurgica*, vol. 31, pp. 577-584, 1983.
- [95] A. G. Evans, "Perspective on the Development of Higher Toughness Ceramics," *Journal of the American Ceramic Society*, vol. 73, pp. 187-206, 1990.

- [96] R. Z. Chen, Y. T. Chiu, and W. H. Tuan, "Toughening alumina with both nickel and zirconia inclusions," *Journal of the European Ceramic Society*, vol. 20, pp. 1901-1906, 2000.
- [97] M. A. McCoy and A. H. Heuer, "Microstructural Characterization and Fracture Toughness of Cordierite ZrO₂ Glass Ceramics," *Journal of the American Ceramic Society*, vol. 71, pp. 673-677, 1988.
- [98] W. S. Chang, P. Shen, and S. Chen, "Microstructural development of zirconia-dispersed ceramic in the NiO-Al₂O₃-ZrO₂ system," *Materials Science and Engineering: A*, vol. 148, pp. 145-153, 1991.
- [99] A. H. Aza, J. Chevalier, G. Fantozzi, M. Schehl, and R. Torrecillas, "Slow Crack Growth Behavior of Zirconia Toughened Alumina Ceramics Processed by Different Methods," *Journal of the American Ceramic Society*, vol. 86, pp. 115-120, 2003.
- [100] M. V. Swain and L. R. F. Rose, "Strength Limitations of Transformation Toughened Zirconia Alloys," *Journal of the American Ceramic Society*, vol. 69, pp. 511-518, 1986.
- [101] S. M. Wiederhorn, "Brittle fracture and toughening mechanisms in ceramics," *Annual Review of Materials Science*, vol. 14, pp. 373-403, 1984.
- [102] D. J. Green, "Critical Microstructures for Microcracking in Al₂O₃-ZrO₂ Composites," *Journal of the American Ceramic Society*, vol. 65, pp. 610-614, 1982.
- [103] A. H. Heuer, "Transformation Toughening in ZrO₂ Containing Ceramics," *Journal of the American Ceramic Society*, vol. 70, pp. 689-698, 1987.
- [104] D. J. Green, F. F. Lange, and M. R. James, "Factors Influencing Residual Surface Stresses due to a Stress-Induced Phase Transformation," *Journal of the American Ceramic Society*, vol. 66, pp. 623-629, 1983.

- [105] M. Dimitrijevic, M. Posarac, J. Majstorovic, T. Volkov-Husovic, A. Devecerski, and B. Matovic, "Thermal shock damage characterization of high temperature ceramics by non destructive test methods," *Ceramicsâ€™ SilikãĀity*, vol. 52, pp. 115-119, 2008.
- [106] S. Marenovic, M. Dimitrijevic, T. V. Husovic, and B. Matovic, "Thermal shock damage characterization of refractory composites," *Ceramics International*, vol. 34, pp. 1925-1929, 2008.
- [107] D. P. H. Hasselman, "Unified theory of thermal shock fracture initiation and crack propagation in brittle ceramics," *Journal of the American Ceramic Society*, vol. 52, pp. 600-604, 1969.
- [108] C. Tian and H. Jiang, "Preparation and thermal shock properties of Si₃N₄-WC nanocomposites," 2011, pp. 1482-1486.
- [109] T. Ahmed, O. Mamat, and B. A. Wahjoedi, "Development and Characterization of Alumina-Silica Sand Nanoparticle Composites," *Defect and Diffusion Forum*, vol. 319, pp. 85-94, 2011.
- [110] M. Mujahid, M. I. Qureshi, M. Islam, and A. A. Khan, "Processing and microstructure of alumina-based composites," *Journal of materials engineering and performance*, vol. 8, pp. 496-500, 1999.
- [111] S. Bhaduri, S. B. Bhaduri, and E. Zhou, "Auto ignition synthesis and consolidation of Al₂O₃-ZrO₂ nano/nano composite powders," *J. Mater. Res*, vol. 13, pp. 156-165, 1998.
- [112] P. Chantikul, G. R. Anstis, B. R. Lawn, and D. B. Marshall, "A critical evaluation of indentation techniques for measuring fracture toughness: II, strength method," *Journal of the American Ceramic Society*, vol. 64, pp. 539-543, 1981.
- [113] A. G. Evans, "Fracture toughness: the role of indentation techniques," ASTM International, 1979, p. 112.

- [114] G. R. Anstis, P. Chantikul, B. R. Lawn, and D. B. Marshall, "A critical evaluation of indentation techniques for measuring fracture toughness: I, direct crack measurements," *Journal of the American Ceramic Society*, vol. 64, pp. 533-538, 1981.
- [115] J. B. J. Opfermann, W.-D. Emmerich, "Simulation of the sintering behavior of a ceramic green body using advanced thermokinetic analysis," *Thermochimica Acta*, pp. 213-220, 1998.
- [116] T. American Society for and P. Materials, "Standard Test Method for Quantitatively Measuring the Effect of Thermal Shock and Thermal Cycling on Refractories," 1991.
- [117] Q. Qiang, Z. Xinghong, M. Songhe, H. Wenbo, H. Changqing, and H. Jiecai, "Reactive hot pressing and sintering characterization of ZrB₂-SiC-ZrC composites," *Materials Science and Engineering: A*, vol. 491, pp. 117-123, 2008.
- [118] G. Magnani and A. Brillante, "Effect of the composition and sintering process on mechanical properties and residual stresses in zirconia-alumina composites," *Journal of the European Ceramic Society*, vol. 25, pp. 3383-3392, 2005.
- [119] M. Castrillon Garcia, "Dilatometric study of Ti₃SiC₂ synthesis from TiC/Si starting powders," Lulea Tekniska University, Sweden, 2008.
- [120] M. D. Sacks and H. W. Lee, "Alumina-or alumina/zirconia-silicon carbide whisker ceramic composites and methods of manufacture," Google Patents, 1991.
- [121] C. R. Brinkman and G. D. Quinn, "Standardization of Mechanical Properties Tests for Advanced Ceramics," *Mechanical Testing Methodology for Ceramic Design and Reliability*, pp. 353-386, 1998.

- [122] T. Chen, F. A. Mohamed, and M. L. McCartney, "Threshold stress superplastic behavior and dislocation activity in a three-phase alumina-zirconia-mullite composite," *Acta Materialia*, vol. 54, pp. 4415-4426, 2006.
- [123] F. Tancret, I. Monot, and F. Osterstock, "Toughness and thermal shock resistance of $\text{YBa}_2\text{Cu}_3\text{O}_{7-x}$ composite superconductors containing Y_2BaCuO_5 or Ag particles," *Materials Science and Engineering: A*, pp. 268–283, 16 May 2000.
- [124] E. S. S. Mm, X. Sun, and L. Zuo, "Thermal Shock Behaviour of Alumina-Iron Composites," *J. Mater. Sci. Technol*, vol. 18, p. 347, 2002.
- [125] M. Hamidouche, N. Bouaouadja, C. Olagnon, and G. Fantozzi, "Thermal shock behaviour of mullite ceramic," *Ceramics International*, vol. 29, pp. 599-609, 2003.
- [126] Z. Wang, C. Hong, X. Zhang, X. Sun, and J. Han, "Microstructure and thermal shock behavior of ZrB_2 -SiC-graphite composite," *Materials Chemistry and Physics*, vol. 113, pp. 338-341, 2009.
- [127] H. Wang, R. N. Singh, and R. A. Lowden, "Thermal Shock Behavior of Continuous Fiber Ceramic Composites (CFCCs)," 1994, pp. 292-302.
- [128] H. B. Zhang, Y. C. Zhou, Y. W. Bao, and M. S. Li, "Abnormal thermal shock behavior of Ti_3SiC_2 and Ti_3AlC_2 ," *Journal of materials research*, vol. 21, pp. 2401-2407, 2006.
- [129] L. Wang, J. L. Shi, M. T. Lin, H. R. Chen, and D. S. Yan, "The thermal shock behavior of alumina-copper composite," *Materials research bulletin*, vol. 36, pp. 925-932, 2001.
- [130] X. J. Zhao, H. Q. Ru, D. L. Chen, N. Zhang, and B. Liang, "Thermal shock behavior of nano-sized SiC particulate reinforced AlON composites," *Materials Science and Engineering: B*, 2012.

PUBLICATIONS DURING THE RESEARCH WORK

1. Processing and characterization of $\text{Al}_2\text{O}_3\text{-SiO}_2\text{-ZrO}_2$ composite material: Int. J. Microstructure and Materials Properties, Vol. 7 (64-760), Inderscience Publishers, UK, (2012).
2. Pressureless Sintering and Characterization of $\text{Al}_2\text{O}_3\text{-SiO}_2\text{-ZrO}_2$ Composite, Defect and Diffusion Forum, Vol. 329, (113-128), Trans tech Publication, Switzerland, (2012).
3. Toughening mechanisms of $\text{Al}_2\text{O}_3\text{-SiO}_2\text{-ZrO}_2$ composite materials Journal Ceramics-Silikáty, Czech Republic.
4. Journal of ceramic processing research (JCPR), South Korea. Investigation on the effect of silica sand addition in densification of $\text{Al}_2\text{O}_3\text{-SiO}_2\text{-ZrO}_2$ composite
5. ICMET 2012 International Conference on Materials Engineering and Technology, WASET (Oral presentation) on 19-20 Feb. 2012.
6. Fracture behavior of a pressureless sintered $\text{Al}_2\text{O}_3\text{-SiO}_2\text{-ZrO}_2$ composite: The International Conference on Production, Energy and Reliability (ICPER2012), ESTCON2012.
7. 29th Science and Engineering design exhibition presentation, Universiti Teknologi PETRONAS (UTP), Silver Medal, 17-18 April 2012